MINERAL PARAGENESIS AND CONTACT METAMORPHISM IN THE JARILLA MOUNTAINS, OROGRANDE, NEW MEXICO

by

Mark S. Bloom

Submitted in Partial Fulfillment
of the Requirements of the Degree of
Master of Science in Geology

New Mexico Institute of Mining and Technology

Socorro, New Mexico

September, 1975

TABLE OF CONTENTS

This thesis is accepted on behalf of the faculty of the Institute by the following committee:

Richard E Blane

Date 12 July, 1976

LIST OF FIGURES

LIST OF PLATES

LIST OF TABLES

ABSTRACT

Compositional variation in an aqueous phase under constraints of isothermal, isobaric conditions is in part responsible for pyrometasomatic mineral assemblages in the system $CaO-Fe_2O_3-Al_2O_3-SiO_2-CO_2-H_2O$; the sequence in which minerals appear as stable phases during a progressive compositional change may be interpreted as the mineral zonation in a system in which a large volume of a mobile aqueous phase, undersaturated with respect to CO_2, flows through carbonate wallrock. Calc-silicate phases in the Jarilla Mountains show well-developed zonation of characteristic mineral assemblages systematically arranged radially away from intrusive contacts; these assemblages are clinozoisite-epidote-calcite± idocrase±actinolite±plagioclase, andradite-grossularite-calcite±quartz± hematite, and wollastonite-calcite±hedenbergite moving progressively away from the intrusive contact.

Calc-silicate phase equilibria in compositional space is documented employing conventional triangular composition diagrams and an isothermal, isobaric chemical potential diagram in the system $CaO-Al_2O_3-SiO_2-CO_2-H_2O$. Chemical reactions occurring among calc-silicate phases in carbonate wallrock are balanced conserving CaO. The geometry of the chemical potential diagram is compatible with an aqueous phase which emanates from relatively low μCaO space (intrusive monzonite) and saturates with respect to calcite in relatively high μCaO space (carbonate wallrock). The tentative reaction path is suggested as a first approximation to progressive metasomatism in the system $CaO-Fe_2O_3-Al_2O_3-SiO_2-CO_2-H_2O$; a series of generalized reactions (below) representing the reaction path is

proposed to replace, in part, the traditional series of decarbonation reactions empirically determined by early investigators:

$$2CaAl_2Si_2O_8 + H_2O \rightleftarrows Ca_2Al_3Si_3O_{12}(OH) + Al_2O_3 + SiO_2$$

$$(3-x)CaAl_2Si_2O_8 + (x+1)CaO + (x)Fe_2O_3 + (2x)SiO_2 + H_2O \rightleftarrows$$
$$(2-2x)Ca_2Al_3Si_3O_{12}(OH) + (2x)Ca_2Al_2FeSi_3O_{12}(OH) \quad \text{where } 0 \leq x \leq 1$$

$$3CaCO_3 + (x)Fe_2O_3 + (1-x)Al_2O_3 + SiO_2 \rightleftarrows$$
$$(x)Ca_3Fe_2Si_3O_{12} + (1-x)Ca_3Al_2Si_3O_{12} + 3CO_2 \quad \text{where } 0 \leq x \leq 1.$$

ACKNOWLEDGEMENTS

The author wishes to express his gratitude to his advisor, Dr. R.E. Beane, for his guidance during the research and writing of this thesis, and for his stimulating lectures and encouragement throughout the author's attendance at the New Mexico Institute of Mining and Technology. Acknowledgement is also due to the other members of the thesis committee, Professors A.J. Budding and C.E. Chapin, whose suggestions and critical reading of this manuscript were invaluable.

Special thanks is extended to the staff of the New Mexico Bureau of Mines and Mineral Resources for providing field transportation, preparation of thin sections, and the use of analytical equipment and X-ray fluorescence standards.

The New Mexico Geological Society, the Society of Sigma Xi, and the Geoscience Department of the New Mexico Institute of Mining and Technology are to be thanked, for without their financial support completion of this project would not have been possible.

INTRODUCTION

Purpose

The purpose of this study is to determine and evaluate the mineral paragenesis within calc-silicate skarns adjacent to multiple monzonite intrusives in the Jarilla Mountains of south-central New Mexico. Particular emphasis is given to the temporal and spacial relationships between intrusive bodies and structure, alteration, and fluid flow, and to the genesis of the calc-silicate zonation in view of mass balance and mass transfer.

Methods of Investigation

Field work in the area was primarily devoted to sampling of the intrusive and calc-silicate rocks for subsequent whole-rock geochemical and petrographic analysis. Detailed geologic mapping at the scale of 1:4000 in order to demonstrate the areal distribution of the various rock types and to establish field relationships among the rock and mineral types with the structure was performed by plane table traverse to supplement existing geologic maps (Seager, 1961; Schmidt, 1962; Schmidt and Craddock, 1965).

Laboratory investigations included petrographic examination of forty thin sections in order to determine paragenetic relationships among the mineral phases, and major element whole-rock analysis of forty-five samples. Quantitative determination of SiO_2, TiO_2, Al_2O_3, Fe_2O_3, MgO, CaO, Na_2O, and K_2O were made using non-destructive X-ray fluorescence (Appendix B); wet chemical techniques were used for analysis of twenty calc-silicate assemblages (Appendix D). The results of the wet chemical analyses (reported in weight percent) are distributed among the phases observed in thin section, and quantitative calculations of mass transfer are demonstrated. Schematic chemical potential diagrams are then employed to define calc-silicate zonation based upon observed mineral assemblages.

Previous Investigations

Geologic inquiry concerning the Jarilla Mountains was initiated in 1893 when Hidden reported turquoise deposits in the area. A limited amount of geologic work was reported in four subsequent publications, all of them brief and in relation to the ore deposits. A condensed summary of the gold and copper operations appeared in Lindgren, Graton, and Gordon (1910), followed by a statistical report on metal production in the district (Lasky and Wooton, 1933). A more detailed account of ferrous metal production including geologic summaries of the larger mines was presented by Kelly (1949).

The next significant mention of the Jarilla Mountains was in the five-year period from 1959 to 1963. Reynolds and Craddock (1959) published a reconaissance map and preliminary summary of the geology. More recently, Seager (1961) and Schmidt (1962) have prepared general descriptions of the geology of the entire mountain range. Schmidt and Craddock (1963) culminated a study sponsored by the New Mexico Bureau of Mines and Mineral Resources primarily concerned with providing a reconaissance geologic map, measured sections, lithologic descriptions, and regional correlations of the sedimentary rock units. Only cursory descriptions of the mineral deposits were provided; no mapping on a scale of less than 1" = 10000", petrographic or chemical analysis, or interpretation of these data were attempted. Jaramillo (1973) reported on the igneous petrology, hydrothermal alteration, and mineralization with emphasis on the alteration zoning present within the hornblende monzonite intrusive and the related skarns and disseminated copper mineralization in Sections 34 and 35, T.21S., R.8E immediately to the north of the area of this investigation. His study recognized local potassic, phyllic, and argillic-propylitic hypogene hydrothermal alteration with superimposed supergene alteration and accompanying sulfide mineralization.

Geographic Setting

The Jarilla Mountains are located approximately midway between El Paso, Texas, and Alamogordo, New Mexico in T.21 and 22 S., R.8E (Figure 1). U.S. Highway 54 lies along the eastern boundary between Alamogordo and Orogrande, New Mexico; numerous secondary roads provide ample access to the range. The specific area under investigation, including most of Section 3, T.22S, R.8E., may be reached by traveling north-northwest from the unincorporated settlement of Orogrande at the southern end of the range.

Geologic Setting

The Jarilla Mountains are near the southern end of a group of mid-Tertiary intrusives aligned in a north-south direction, and very near to the intersection of this intrusive series with the Texas lineament

Figure 1. Location map of New Mexico showing the location of Otero County and the Jarilla Mountains.

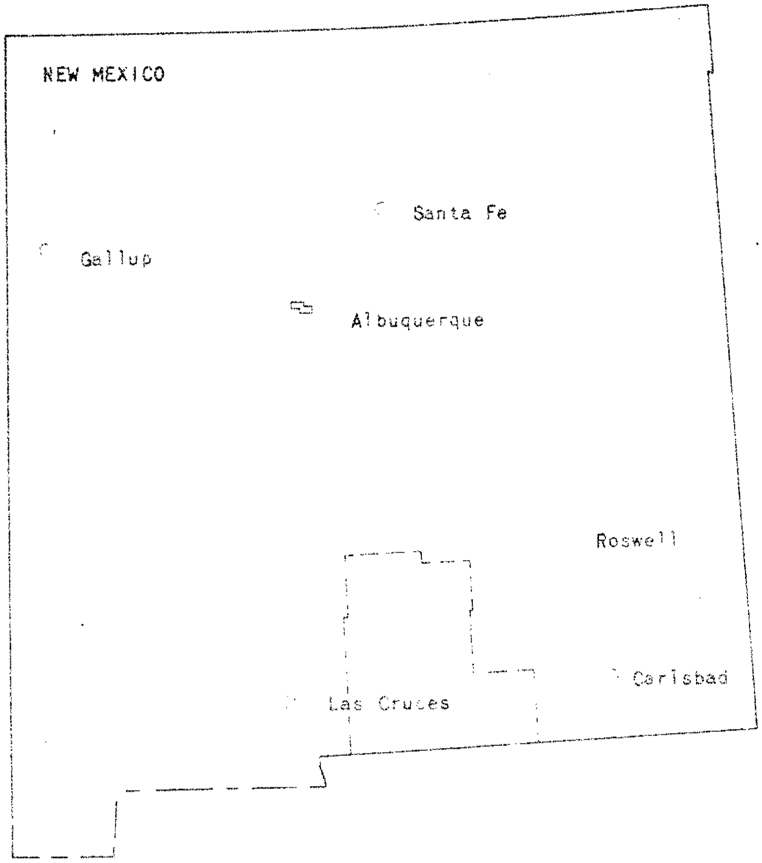
NEW MEXICO
Santa Fe
Gallup
Albuquerque
Roswell
Carlsbad
Las Cruces

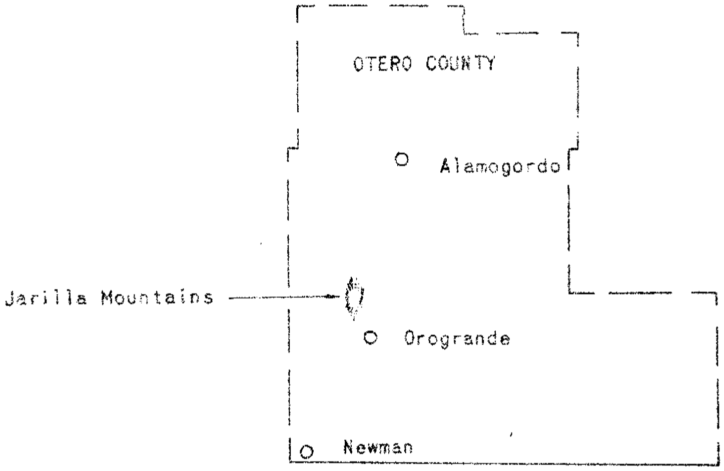
OTERO COUNTY
Alamogordo
Jarilla Mountains
Orogrande
Newman

proposed by Schmitt (1965). The range is surrounded on all sides by the Tularosa Basin, a graben bounded on the west by the Franklin-Organ-San Andres uplift belt and on the east by the Hueco, Sacramento, and Sierra Blanca escarpments. The Jarilla Mountains are an up-faulted block in the center of the basin. The range is approximately four miles wide from east to west and ten miles long in a north-south direction. Maximum relief is approximately 1200 feet and averages about 600 feet. Steep and rugged slopes, not uncommon near the outer perimeter, encompass a drainage basin bordered by extensive alluvial fans and pediment surfaces.

INTRUSIVE ROCKS

Intrusive rocks in the south-central Jarilla Mountains may be divided into four types based upon texture and modal percentages of the primary minerals plagioclase, orthoclase, and quartz. These are 1) granodiorite, 2) quartz latite, 3) monzonite, and 4) andesite. The intrusive rocks were classified according to the generally accepted conventions for naming rocks on the basis of mineralogy and texture (Travis, 1955). The textural terminology is the standard nomenclature as used by Williams, Turner, and Gilbert (1954).

Distribution and Field Relations

Granodiorite occurs both in the central and extreme northwest corner of the Jarilla Mountains. Intrusive quartz latite occurs along the southeastern margin of the mountain range. Direct geologic relationships from which the relative ages of the granodiorite and quartz latite may be ascribed were not observed during the course of the field work. Rocks of monzonitic composition are the most abundant intrusives in the southern Jarilla Mountains. A hornblende-rich monzonite facies occurs in large masses approximately five miles in north-south length and about four miles in east-west width. The monzonite intrudes both granodiorite and quartz latite; it shows typical contact relations including chilled margins, sheeting parallel to the contact, and apophyses into the intruded material.

Granodiorite

The granodiorite crops out immediately north of the area of investigation. It is a dark-gray, massive, fine- to medium-grained rock consisting of 40 to 60 percent plagioclase, 10 to 30 percent orthoclase, 5 to 15 percent biotite, 4 to 8 percent hornblende, 5 to 20 percent quartz, a few percent augite, plus accessory magnetite, pyrite, epidote, apatite, and sphene (Jaramillo, 1973). The texture in hand specimen is typically phaneritic equigranular.

Monzonite

Monzonite is the most abundant igneous rock type in the southern Jarilla Mountains, and comprises approximately sixty percent of the intrusive exposures. Compositional variation with areal distribution is typical of the monzonite. Individual facies may be distinguished on the basis of the proportions of mafic minerals and quartz content, the proportion of phenocrysts to groundmass, and grain size. The monzonite is characterized by a facies of medium-gray color with phenocrysts of plagioclase and hornblende four to eight millimeters in length set in a fine-grained groundmass. Outcrops weather to slabby, slightly rounded boulders. Additional facies characterized by a pronounced phaneritic porphyritic texture may be identified on the basis of abundant biotite and quartz phenocrysts. Biotite-hornblende monzonite may consist of as much as five percent primary igneous biotite occurring as hexagonal plates two to eight millimeters in diameter in addition to the prismatic phenocrysts of hornblende. Quartz monzonite is characterized by euhedral to embayed anhedral quartz phenocrysts one to five millimeters in diameter. No attempt was made during the course of the field work to differentiate the monzonite facies; detailed geologic mapping of the monzonites is recommended to determine whether the variation in primary composition reflects a multiple-phase intrusive, contamination by assimilation of carbonate wallrocks, or mass transfer of components during deuteric or hypogene hydrothermal alteration.

Monzonite phases intrude quartz latite and are cut by andesite dikes. The quartz latite is slightly brecciated along the contact with monzonite, numerous fragments of quartz latite are suspended in a thin chilled margin of monzonite, and dikes and sills of monzonite intrude fractures in the quartz latite (Plate 1). Nowhere in the area under consideration is granodiorite observed in contact with the monzonite; however, Jaramillo (1973) reports that monzonite dikes and apohpyses cut the granodiorite, and numerous granodiorite fragments are suspended in monzonite along the contact.

Quartz Latite

Quartz latite is the only other intrusive phase with significant exposure in the area under consideration; it crops out in the extreme northeast and as isolated outliers in the alluvium. Exposures of quartz latite occur as low hills covered with small angular fragments which are generally yellowish-white; fresh surfaces are white to pale yellowish-pink in color. The quartz latite is almost entirely aphanitic, although locally white plagioclase phenocrysts as much as 3 millimeters in length and anhedral quartz phenocrysts approximately 2 millimeters in diameter may be observed set in the aphanitic groundmass. There is a conspicuous absence of mafic minerals. Disseminated pyrite, largely altered to jarosite and goethite, is common. No contacts of quartz latite with

Plate 1   Hornblende monzonite intruding quartz latite

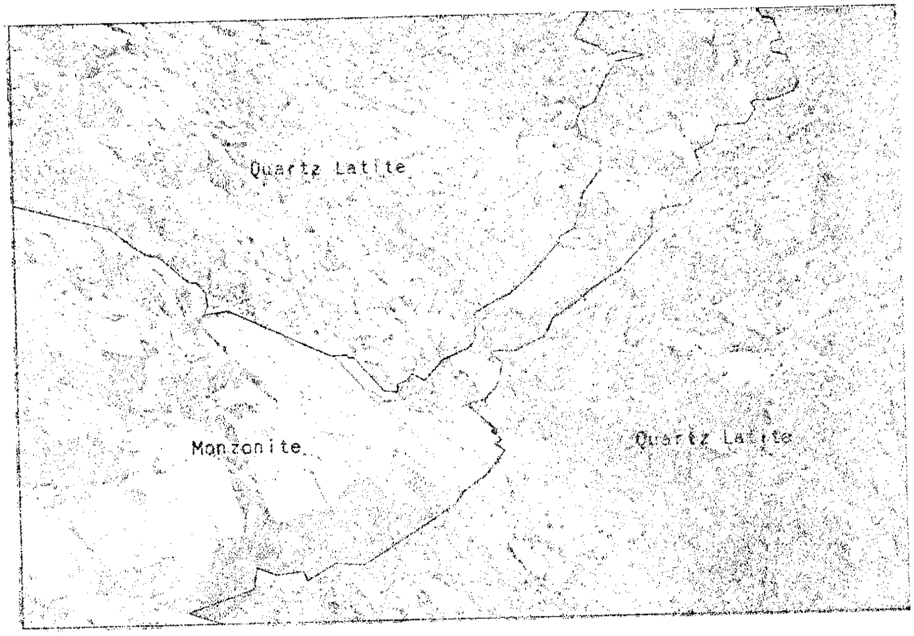
Quartz Latite
Monzonite
Quartz Latite

granodiorite have been reported by previous workers; the contact with monzonite demonstrates that the quartz latite predates the monzonite.

Andesite

Several dikes of andesitic composition cut both monzonite and quartz latite (Plate 2). Fresh surfaces are dark-greenish-gray, weathering to olive-gray. Hand specimens are generally fine-grained and equigranular; occasional plagioclase phenocrysts are set in a groundmass consisting mostly of chlorite and micro-laths of plagioclase. The term andesite will be used in this report to indicate both unaltered andesite and the propylitically altered equivalent. Andesite dikes are generally confined to the peripheral areas of the intrusives which they cut, and appear to be intruded along pre-existing zones of weakness (i.e., fractures, etc.).

Igneous Petrology

Special emphasis must be given to the essential igneous mineral phases for which a precise compositional determination by optical techniques can be made, for from these data tentative suggestions may be proposed with respect to genetic relationships and external sources of components introduced into carbonate wallrock during the course of pyrometasomatic alteration. Twenty-four thin sections of monzonite were studied in detail for this purpose; concise but comprehensive documentation of the results may be found in Appendix A.

The essential mineral phases are plagioclase, quartz, and orthoclase. Plagioclase and quartz may be observed occurring both as phenocrysts and in the groundmass, whereas the latter is restricted to the matrix

Plate 2A Postmineral andesitic dike intruding monzonite

Plate 2B Postmineral andesitic dike intruding quartz latite

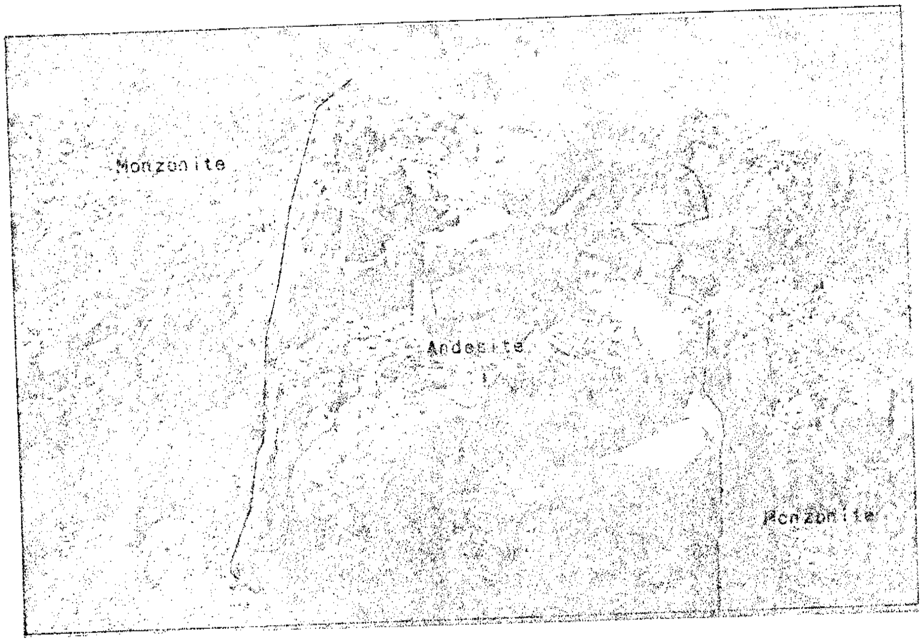
Monzonite
Andesite
Monzonite

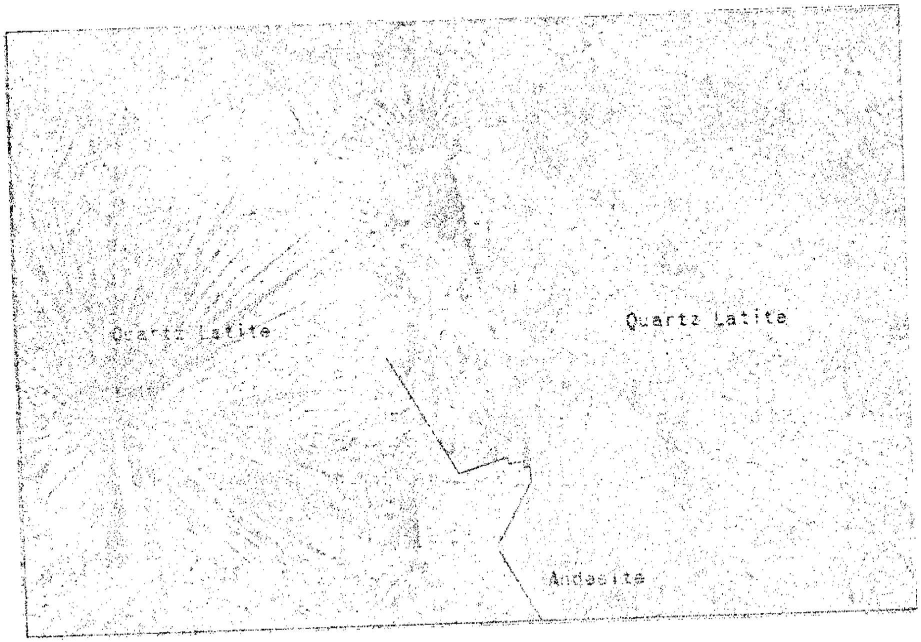
Quartz Latite
Quartz Latite
Andesite

Characterizing accessory minerals are hornblende and biotite, both of which occur as phenocrysts in the monzonite. Apatite, magnetite, and sphene are minor accessory minerals disseminated throughout the phenocrysts and groundmass.

Hypogene Hydrothermal Alteration

Several types of hypogene alteration have been recognized in igneous rocks of the south-central Jarilla Mountains, each characteristic of certain areas and rock types. Those recognized include potassic, phyllic/argillic, and propylitic. The hypogene hydrothermal alteration assemblages in the area of investigation are similar to those associated with porphyry copper deposits (cf. Lowell and Guilbert, 1970). The generalized model of alteration was not established; an outline of alteration areas in the intrusive rocks was beyond the scope of this report. Assemblages representing the traditional porphyry copper zonation will be considered below.

Propylitic

The epidote-calcite-chlorite assemblage characteristically encountered in the propylitic zone as defined by Lowell and Guilbert (1970) is the most widespread alteration type. Incipient alteration of calcic plagioclase to epidote (saussuritization) ranges from 1 to 5 percent, and averages 3 percent. Epidote also replaces hornblende in small amounts. Calcite replaces plagioclase and ranges from 2 to 6 percent; it is present in all thin sections of the monzonite which were investigated. Chlorite replaces hornblende and biotite, and comprises as much as 4 percent of a representative monzonite; total propylitic alteration ranges from 10 to

30 percent.

Phyllic

Pervasive sericitization of all silicates except quartz, characteristic of phyllic alteration, was not observed in thin sections of the monzonite. Sericite locally replaces plagioclase as much as 2 percent but generally occurs only in trace amounts oriented parallel to cleavage or twin planes. Incipient sericitization of this nature favors more calcic plagioclase; the boundary between rim and core in zoned phenocrysts may often be perceived by this selective sericitization.

The stable alteration assemblage characteristic of the quartz latite is sericite-quartz. Plagioclase phenocrysts demonstrate from moderate to pervasive sericitization; often all that may be observed in thin section are remnant sericite pseudomorphs replacing plagioclase. Many fractures are coated with as much as two millimeters of sericite. Strong quartz veining may be observed. Pyrite mineralization is considered characteristic of the phyllic alteration assemblage (Lowell and Guilbert, 1970); the quartz latite locally contains as much as 2 volume percent pyrite, largely altered to jarosite and goethite in ratios of approximately 2:8.

Potassic

Potassic alteration characterized by the pervasive replacement of primary minerals by secondary biotite, potash feldspar, and quartz was not consistantly encountered during the course of the petrographic investigation. Localized areas occasionally contain small anhedral biotite crystals concentrated along microfractures or biotite clusters replacing hornblende in addition to minor quartz - potash feldspar veining. Jaramillo (1973) recognized isolated exposures of potassic alteration elsewhere in the Jarilla Mountains; however, additional petrographic investigation supplemented by detailed geologic mapping of the multiple monzonite intrusive is necessary to document persistent potassic alteration zones within the area of this investigation.

Supergene Argillic Alteration

Diffractometer patterns of feldspar phenocrysts indicate that mixtures of kaolinite and/or montmorillonite replace plagioclase to some degree in all thin sections. Clays replace from 2 to 20 percent of the plagioclase in a representative monzonite; total argillization effects from 6 to 25 percent of a typical monzonite. Because clays are universally present in all sections studied regardless of the hypogene assemblage recognized, it is the opinion of this author that supergene argillic alteration has been superimposed upon the hypogene hydrothermal assemblages.

Intrusive Affinities

Geologic information permits relative and absolute temporal and genetic relationships among the granodiorite, quartz latite, and monzonite to be established which are not immediately apparent with respect to the pyrometasomatic alteration extensively developed adjacent to the intrusive contacts. Because the extent of pyrometasomatic alteration is directly related to the causitive intrusive, it is desirable to define these temporal and genetic relationships. Several approaches are amenable to establishing the affinities between the quartz latite and monzonite in this area and in the granodiorite immediately to the north. Relative age relationships, analysis of fracture orientations, and petrogenesis in the system $NaAlSi_3O_8$-$KAlSi_3O_8$-$CaAl_2Si_2O_8$-SiO_2-H_2O will be considered in this discussion.

Temporal Relationships

Direct contact relationships do not permit relative age relationships to be established among all the intrusive rocks of the Jarilla Mountains. The granodiorite is intruded by the monzonite to the north, and quartz latite shows similar relationships in the study area. Direct geologic relations between the granodiorite and the quartz latite have not been observed in the course of the field work. Dikes of andesitic composition cut the larger intrusive masses as well as the altered sedimentary rocks throughout the mountain range and constitute a post-mineral intrusive event.

Absolute ages of monzonites, similar to those in the Jarilla Mountains and of the granodiorite from the northern end of the range, have recently been determined by K-Ar dating techniques. Monzonitic rocks of the Organ Mountains to the west show a significant resemblance in composition and in sequence of intrusion to those in the area of investigation. Seager (1961) therefore concludes that the intrusives of monzonitic composition in the Organ and Jarilla Mountains are temporally and spacially related. Although a reliable date for the Jarilla monzonites is not currently available, the similar monzonitic intrusives in the Organ Mountains have recently been dated at 32 million years (C.E. Chapin, written communication; August, 1975).

Biotite concentrates from the granodiorite immediately to the north of the area of investigation have been dated at 47.1 ± 1.8 million years

(C.E. Chapin, written communication; June, 1975). This age corresponds with determinations of 48.8 ± 2.6 million years (biotite concentrate) for the Cuchillo Mountain Stock in Hidalgo County and 49.0 ± 2.6 million years (hornblende concentrate) for the Tres Hermanes Stock in Luna County (C.E. Chapin, written communication; August, 1975). Similar granodiorite and porphyritic monzonite to quartz monzonite intrusives elsewhere in Southwest New Mexico have been dated at 56.2 ± 1.7 million years (biotite concentrate from Tyrone Stock), 58.0 to 58.4 ± 1.8 million years (biotite and hornblende concentrates, respectively, from the Hanover-Fierro Stock), and 59.0 ± 3.5 million years (biotite concentrate from the Chino Stock). The time and space distribution of the presently dated intrusives suggests a northwest-southeast trending front of magmatic emplacement which migrated eastward during the Laramide intrusive episode (Anderson and Silver, 1974). The ages systematically decrease from 56-59 million years in southwest New Mexico to 47-49 million years in south-central New Mexico. Similar trends have been documented in Sonora, Mexico (Anderson and Silver, 1974) and the southern basin and range province (Livingston, 1973). These trends lend credence to a proposal that the Jarilla granodiorite may be a more easterly and younger but related intrusive to the easterly-migrating linear source of magmatic activity.

Structural Relationships

Two distinctly different fracture orientations are exhibited by intrusive rocks in the Jarilla Mountains. Both the granodiorite and the quartz latite are dominated by similar steeply-dipping fractures; however, the monzonite is characterized by a near-vertical joint set of different orientation. Figure 2A is a rose diagram to 75 fracture sets

Figure 2A Rose diagram to 75 characteristic fracture orientations in quartz latite

Figure 2B Rose diagram to 150 characteristic fracture orientations in hornblende monzonite; dark stippling illustrates trends inherited from late Laramide intrusive, and light stippling illustrates trends from the mid-Tertiary intrusive

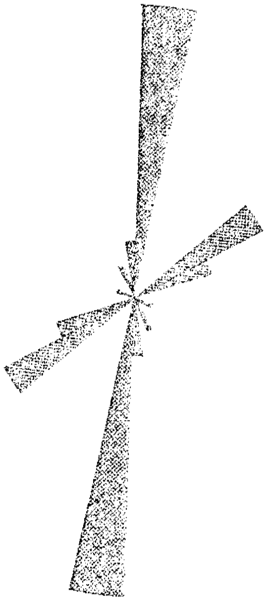


N

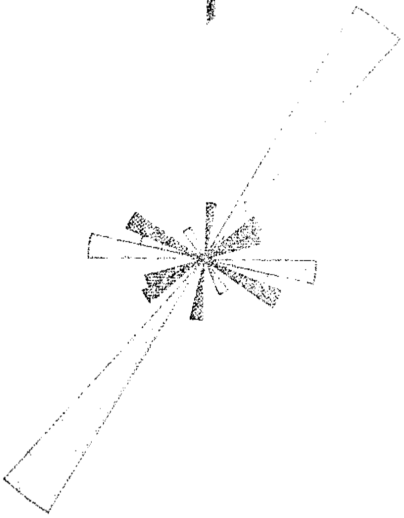

in the quartz latite. The primary fracture direction is oriented N5°E with the conjugate set at N55°E. This is identical to the fracture pattern of the granodiorite determined by Jaramillo (1973). Figure 2B is a rose diagram to 150 fracture sets in the monzonite. The primary fracture direction is N34°E; conjugate sets are oriented at S85°E. Superimposed on the monzonite fracture patterns are relic patterns from the granodiorite or quartz latite.

In the field, predominantly northeast-trending fractures in the monzonite change abruptly to north-south trending fractures in the quartz latite. This difference in fracture orientations is occasionally reflected by late andesite dikes which change strike at contacts between the monzonite and quartz latite. The major north- and northeast-trending fractures were important in controlling emplacement of these dikes. Fractures may generally be traced for distances of as much as 50 meters on the surface in areas of good exposure; however, talus and landslide debris often obscure the regional pattern. The fractures are generally vertical or dipping very steeply. Systematic fracturing of this nature is generally at approximately right angles to both the upper and lower surfaces of the rock unit in which it is present. This may be interpreted as indicating that the monzonite may not be a rooted intrusive in the area of investigation, but instead is the surface expression of a thick sill. In the immediate vicinity of xenoliths or roof pendants the regional pattern is interrupted by parallel sheeting conformable to the strike and dip of the contacts. Secondary minerals of pyrometasomatic or hypogene hydrothermal origin (particularly the epidote, quartz-sericite, and orthoclase-quartz-biotite assemblages) pervasively effect the wall rocks of major fractures. Argillic alteration of supergene origin is also much more evident along fractures. There is little or no evidence of displacement either along the strike or dip of the fractures; however, in many cases there must have been a slight amount of movement normal to the fracture surface to open the fractures.

Figures 3 and 4 are point density plots to fracture poles in the quartz latite and monzonite. Uniformity in strike of the fractures is evident from these diagrams; moreover, the point density plots emphasize that nearly all the fractures are vertical or dip very steeply. Similar fracture patterns in the granodiorite and quartz latite imply approximate time-coincidence of intrusion; the monzonite, however, has a different fracture pattern and probably differs in age.

Petrogenesis

Tentative suggestions may be proposed regarding intrusive affinities by means of normative mineral compositions. Laboratory petrographic investigations in addition to whole-rock major element analysis of 20 granodiorite samples, 40 monzonite samples, and 5 quartz latite samples were used to calculate mesonorms in terms of the primary mineral phases corundum, quartz, orthoclase, albite, anorthite, and Fe-Mg biotite. Quantitative determination of the major oxide components was made using non-destructive X-ray fluorescence (Appendix A). The normative compositions were calculated using a computor program designed for this purpose and provided by Dr. K. C. Condie, New Mexico Institute of Mining and Technology.

Figure 5 is the generalized compositional tetrahedron in the system $KAlSi_3O_8$-$NaAlSi_3O_8$-SiO_2; Figure 6 shows the projection of the mesonorm compositions through the anorthite corner of the normative tetrahedron onto the quartz-albite-orthoclase base. The schematic eutectic line

Figure 3 Point density plot of poles to 75 fracture sets in quartz latite; contours at 5 percent (light stippling), 10 percent (cross-hatching), and 15 percent (dark stippling)

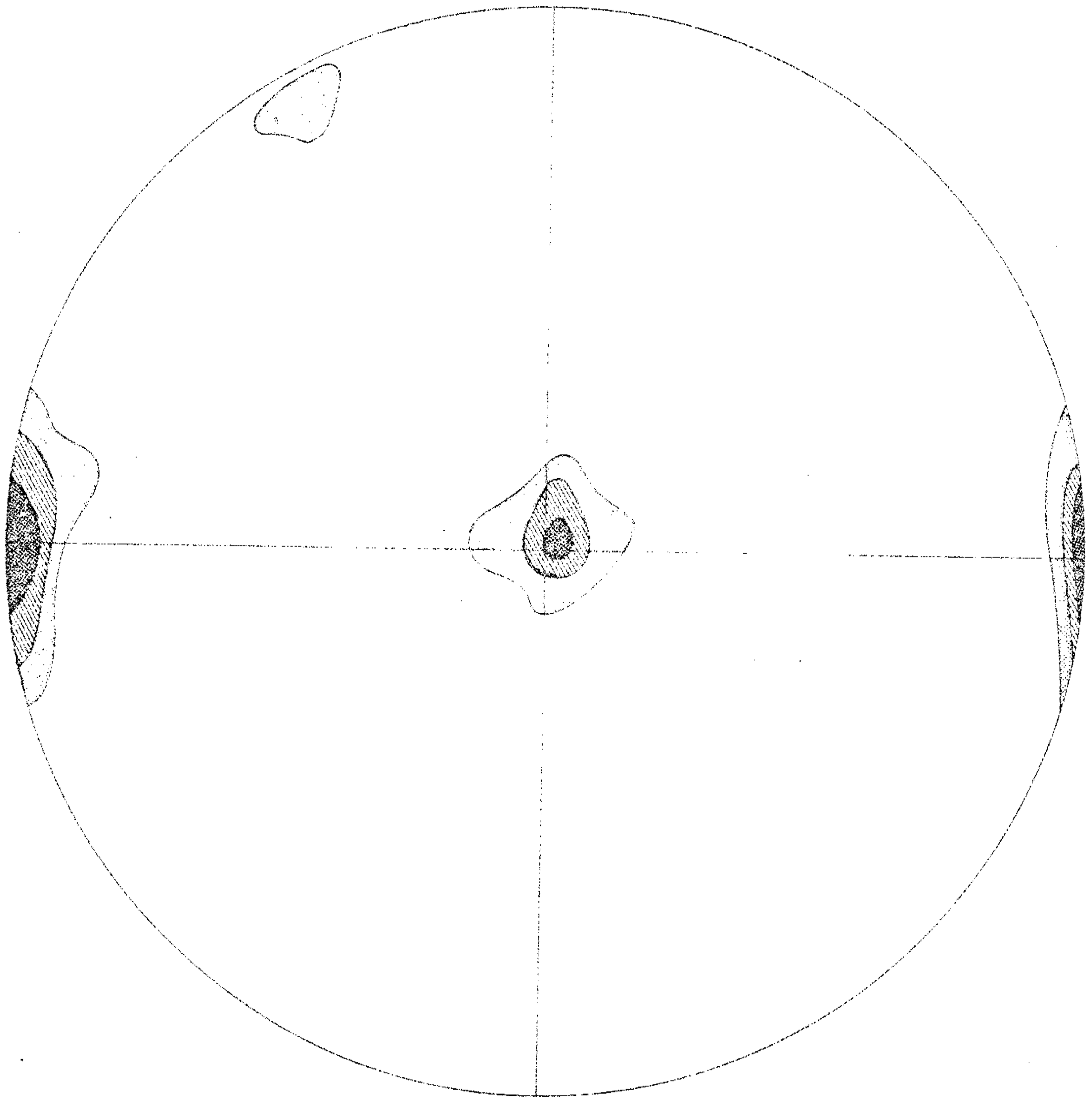

Figure 4 Point density plot of poles to 150 fracture sets in monzonite; contours at 5 percent (light stippling), 10 percent (cross-hatching), and 15 percent (dark stippling)

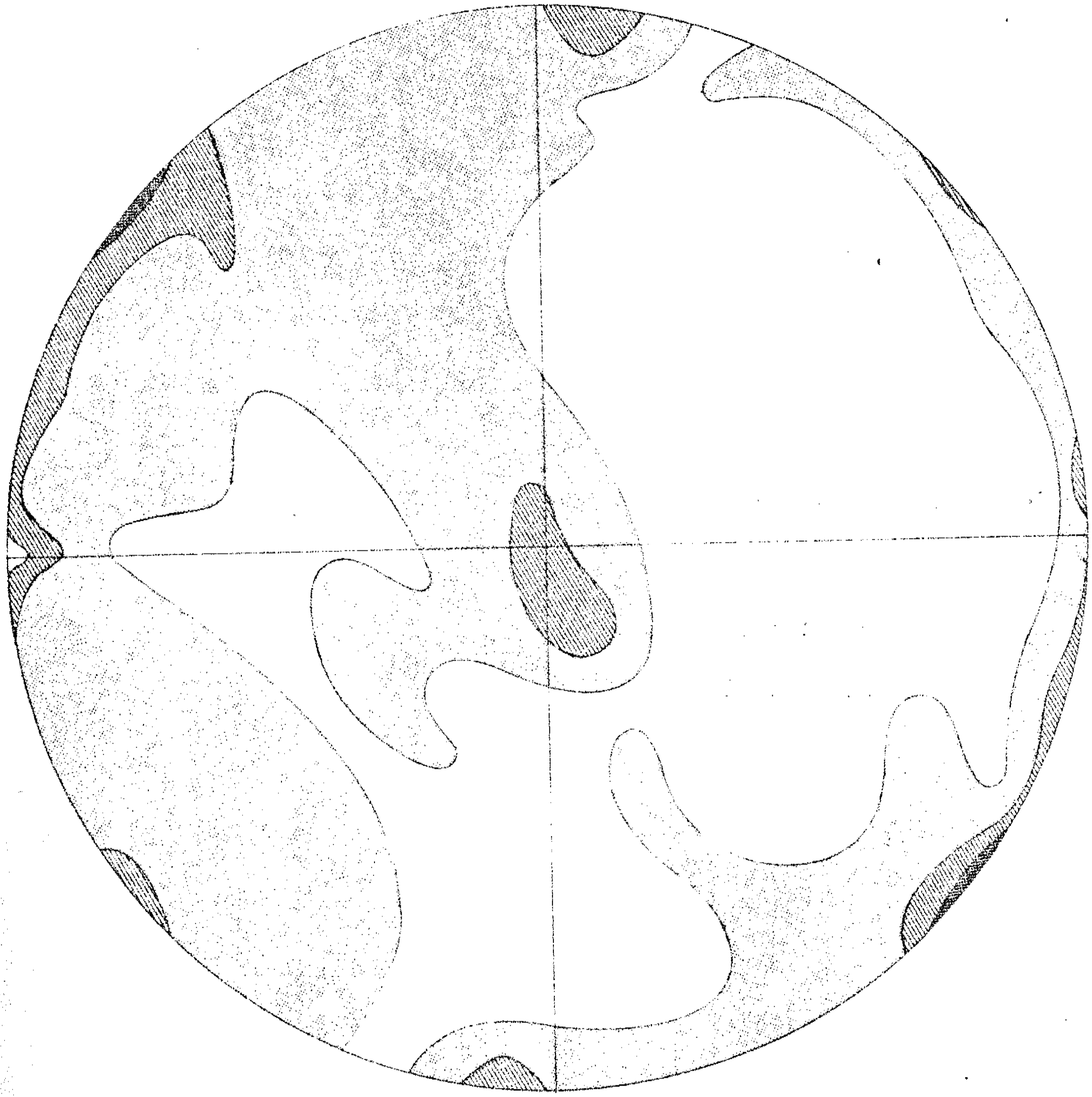

Figure 5 Compositional tetrahedron illustrating generalized phase relations in the system $KAlSi_3O_8$-$CaAl_2Si_2O_8$-$NaAlSi_3O_8$-SiO_2 (modified after Ehlers, 1972)

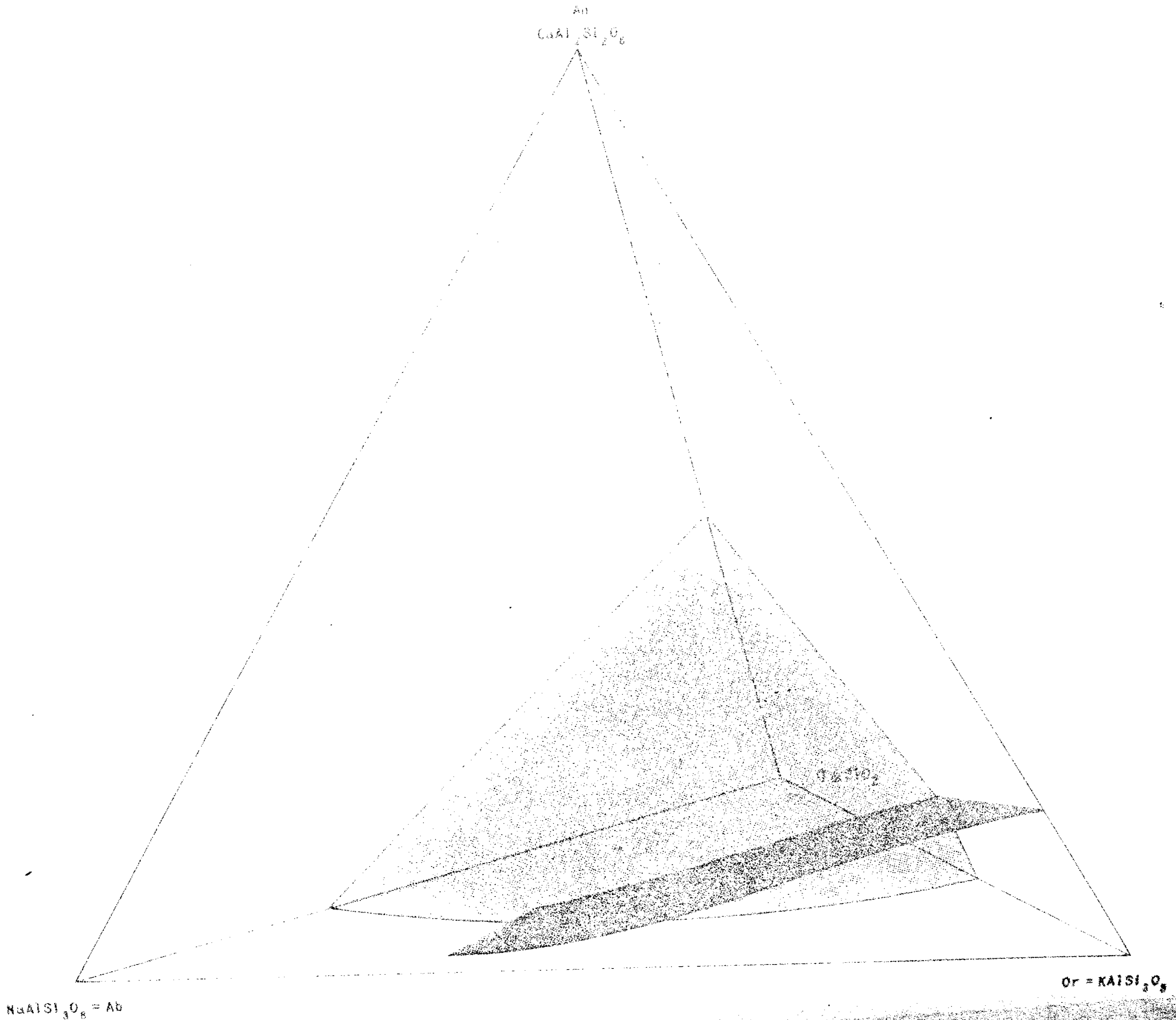
An
$CaAl_2Si_2O_8$
Q = SiO_2
$NaAlSi_3O_8$ = Ab
Or = $KAlSi_3O_8$

Figure 6 Compositional triangle illustrating whole-rock intrusive compositions and generalized eutectic lines in the system $KAlSi_3O_8$-$NaAlSi_3O_8$-SiO_2

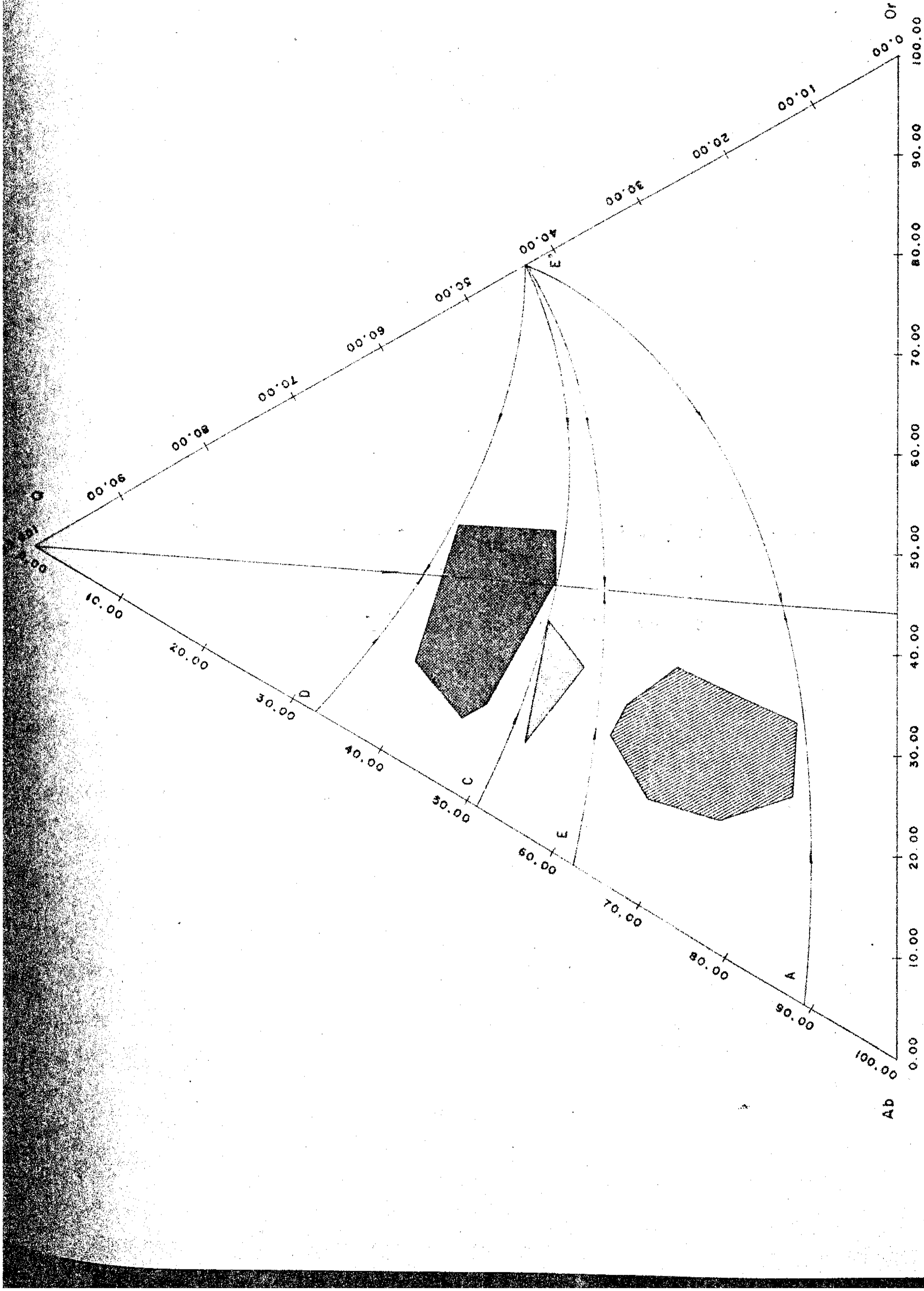
Q
Or
Ab
A
C
D
E
E'
0.00
10.00
20.00
30.00
40.00
50.00
60.00
70.00
80.00
90.00
100.00

(E-E') divides the composition triangle into two areas: quartz crystallizes as a primary phase in the silica-rich region (quartz-E-E'), and alkali feldspar precipitates in the silica-poor region (albite-E-E'-orthoclase). The actual position of the eutectic line shifts as a function of pressure and plagioclase composition, moving in the direction of the albite apex with increasing P_{H_2O} and albite content of the Na-Ca feldspar. Crystallization paths on the compositional tetrahedron move either from the quartz apex or the albite-orthoclase edge toward the eutectic line.

The four possible positions of the eutectic line which are of interest in defining the relative ages of the intrusives in the Jarilla Mountains are illustrated in Figure 6. All three intrusive types could be derived from the same magmatic source, with granodiorite intruding both the quartz latite and monzonite; the crystallization path would move from the albite-orthoclase edge toward the eutectic line at position D-E' giving the sequence monzonite → quartz latite → granodiorite. The eutectic line occurring at position C-E' indicates two source magmas, one from which the granodiorite was generated, and the other which gave rise to early monzonite followed by quartz latite; granodiorite could be either earlier than or later than both the monzonite and quartz latite. The possible sequences are granodiorite → monzonite → quartz latite or monzonite → quartz latite → granodiorite. Two source magmas are also indicated in the third alternative (E-E') in which the granodiorite and quartz latite are cogenetic and the monzonite is of independent origin; the monzonite must preceed or follow both the quartz latite and granodiorite; the alternatives are monzonite → granodiorite → quartz latite or granodiorite → quartz latite → monzonite. In the fourth option the three intrusive types could be derived from the same magmatic source with the monzonite intruding both the granodiorite and the quartz latite (A-E') giving the sequence granodiorite → quartz latite → monzonite.

Only the third and fourth alternatives are compatible with field observations (monzonite intrudes both granodiorite and quartz latite). The third option is compatible only if monzonite postdates the quartz latite. The position of the eutectic line A-E' allows the three intrusive types to be cogenetic only if the plagioclase in the late monzonite contained very little of the anorthite component and/or the confining pressure was geologically unreasonable; the fourth option can therefore be eliminated because neither of these requirements are in agreement with petrographic or geologic observations. Consequently, this suggests that the granodiorite and quartz latite are genetically and chronologically related, the quartz latite being a possible late differentiate of the granodiorite; the monzonite intrudes both of these rock types and was generated from a separate magma. These data support the earlier interpretation of igneous intrusive affinities, i.e., the granodiorite and quartz latite are genetically related, and the monzonite postdates both.

SEDIMENTARY AND METAMORPHIC ROCKS

The Jarilla Mountains are an asymmetrical domal uplift with an axial core occupied by monzonite and granodiorite; the axial zone is flanked by radially-tilted sequences of Upper Paleozoic strata. The forceful intrusion of magmas along the north- to south-trending axial zone caused the sedimentary pile to break; dikes and sills of monzonitic rock separate roof pendants and xenoliths -- the only sedimentary units exposed within the area of investigation. The absense of key marker horizons, the lithologic similarities of the sedimentary units and their metamorphic equivalents, and small-scale faulting associated with the igneous intrusives render precise correlations with the measured type sections of questionable validity.

Stratigraphy and Lithology of Sediments

The Pennsylvanian section has been subdivided into three major rock units--the Gobbler, Beeman, and Holder Formations. A distinctive facies termed the Bug Scuffle Limestone is recognized as a member of the Gobbler Formation. Previous workers are not in accord regarding the precise terminology of lower Permian rock units in the Jarilla Mountains; Panther Seep (Seager, 1961) and Laborcita (Schmidt, 1962) have both been proposed as the rock-stratigraphic equivalents of the units cropping out in the area of investigation. Pray (1959) and Kottlowski (1963) have reported a maximum total composite thickness of approximately three thousand feet. Figure 7 is an east-west cross section of Pennsylvanian and lower Permian strata from the southern San Andres

Figure 7 Composite stratigraphic section between the San Andres uplift and the Sacramento escarpment (after Pray, 1959)

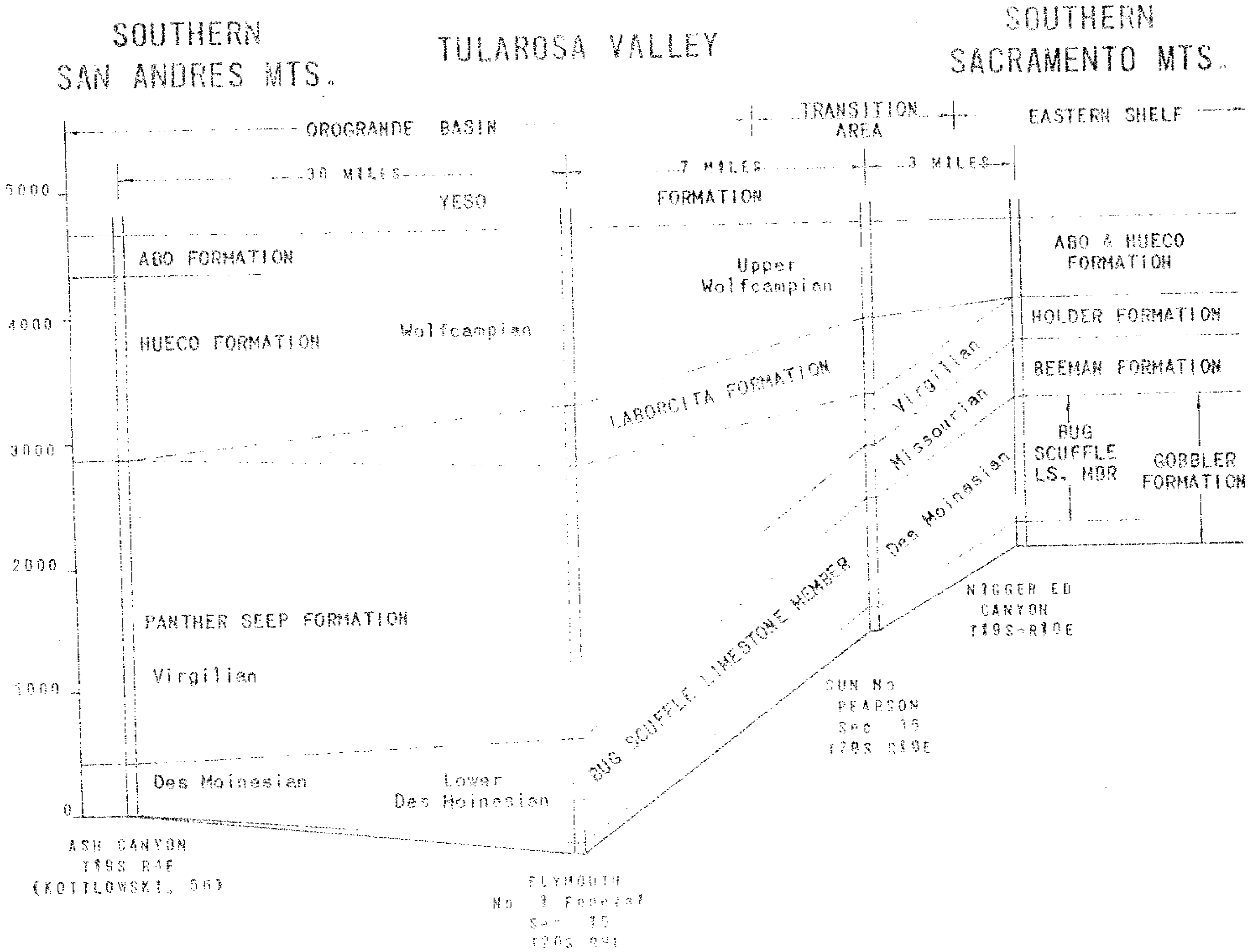
SOUTHERN
SAN ANDRES MTS.
TULAROSA VALLEY
SOUTHERN
SACRAMENTO MTS.
OROGRANDE BASIN
TRANSITION AREA
EASTERN SHELF
30 MILES
7 MILES
3 MILES
5000
4000
3000
2000
1000
0
YESO
FORMATION
ABO FORMATION
HUECO FORMATION
Wolfcampian
Upper Wolfcampian
ABO & HUECO FORMATION
HOLDER FORMATION
BEEMAN FORMATION
LABORCITA FORMATION
Virgilian
Missourian
Des Moinesian
BUG SCUFFLE LS. MBR
GOBBLER FORMATION
PANTHER SEEP FORMATION
Virgilian
BUG SCUFFLE LIMESTONE MEMBER
Des Moinesian
Lower Des Moinesian
ASH CANYON
T19S R4E
(KOTTLOWSKI, 56)
PLYMOUTH
No 1 Federal
Sec 15
T20S R9E
SUN No
PEARSON
Sec 16
T20S R10E
NIGGER ED
CANYON
T19S-R10E

Mountains to the southern Sacramento Mountains illustrating the time-stratigraphic relationships. Seager (1961) and Schmidt (1962) have adequately described the general occurrence, outcrop, and location of the strata of interest, and the following summary of the stratigraphy and lithology of the sedimentary rocks in the area of investigation is in large part derived from their work. Detailed descriptions of these rocks will not be presented in this report; however, a brief summary is necessary for clarity in reviewing the discussion to follow involving controls of pyrometasomatic alteration.

Des Moinesian Series

The base of the Pennsylvanian section is represented by an 822-foot sequence of predominantly massive- to thin-bedded, locally cherty, coarse crinoidal limestone which is correlative with the Bug Scuffle Limestone Member of the Gobbler Formation in the Sacramento Mountains (Pray, 1959). The basal 50 feet of the Gobbler Formation consist of coarse, cross-bedded, arkosic siltstones and sandstones with minor interbedded limestone (Schmidt and Craddock, 1964). The upper part of the formation contains a few thin shales and is gradational into sedimentary units of the Missourian-Virgilian Series.

Missourian-Virgilian Series

Although all upper Pennsylvanian/lower Permian rock units overlying he Bug Scuffle Limestone Member of the Gobbler Formation have been dentified as Permian Laborcita by Schmidt and Craddock (1964), ithologically the lower members more closely resemble the Missourian nd Virgilian Beeman, Holder, and Panther Seep Formations of the acramento (Pray, 1959) and San Andres (Kottlowski, 1959) Mountains.

The lowest unit consists of calcareous shales, argillaceous limestones, and limestone grading upwards into interbedded coarse, dark, argillaceous sandstone and shale. This unit is tentatively correlated with the Missourian Beeman Formation of the Sacramento Mountains (Pray, 1959). Overlying the clastic sediments is massive- to thin-bedded, white, coarse limestones containing chert layers and nodules, and abundant solitary corals. These units may be correlative with the algae reef-bearing Virgilian strata of the Sacramento (Holder Formation) and San Andres (Panther Seep Formation) Mountains recognized by Pray (1959) and Kottlowski (1963), respectively. Above the limestones a thick sequence of calcareous siltstones and shales with minor sandstone and limestone dips beneath the Quaternary sedimentary deposits along the margins of the Jarilla Mountains; these units might actually be correlative with the Laborcita Formation (Schmidt, 1962). Schmidt and Craddock (1964) have measured a minimum composite thickness of 1234 feet for the Laborcita (?) Formation exposed extensively to the north of the study area. Evidence for exposures of the sedimentary units above the Laborcita (?) and Gobbler Formations was not observed in the area of investigation; detailed descriptions of these rocks have been given by Pray (1959).

Distribution and Field Relations of Pyrometasomatic Alteration

Carbonate sediments spatially related to intrusive monzonite demonstrate a systematic and well-developed zonation of calc-silicate minerals radially away from the intrusive. Titley (1973) suggests that such zonation in a carbonate wall rock is the manifestation of processes similar to those which result in hypogene hydrothermal assemblages in an igneous wall rock, and proposes that pyrometasomatic alteration is the extension of the alteration process. Special emphasis is given to pyrometasomatic alteration in this report; however, the irregular and gradational nature of pyrometasomatic contacts allows only a schematic illustration of calc-silicate zonation on the geologic map (Figure 15).

The zones are divided into two major catagories bearing a spatial relation to each other: endoskarn formed by the alteration of monzonite, and exoskarn formed by the alteration of carbonate sediments (Zharikov, 1970). The metasomatic effects appear to be restricted to the immediate vicinity of the intrusive contact. There is a general tendency for the zones to be segregated into characteristic assemblages arranged radially away from the intrusive contact. The zones are idealized for the purposes of this study. They are not monomineralic, but usually contain significant proportions of accessory minerals and grade both laterally and vertically into adjacent zones. Moving progressively away from the intrusive the calc-silicate zones are 1) epidote solid solution-calcite±plagioclase-amphibole-idocrase, 2) garnet solid solution-calcite±quartz± hematite, 3) pyroxene-calcite, and 4) marble. Additional or missing zones are locally common, particularly on a small scale. Figure 8 schematically illustrates the idealized calc-silicate zonation; Plate 3 demonstrates how this zonation may be exposed in the field.

Clinozoisite-Epidote-Calcite Zone

The endoskarn consists entirely of the clinozoisite, epidote, and calcite and for convenience is hereafter referred to as the epidote zone. The color of freshly broken surfaces is dark-green to dark-yellowish-green. Exposures are grayish-olive to olive-black and are more susceptable to weathering than either garnet or monzonite. The texture in hand specimen

Figure 8 Schematic section illustrating the position of calc-silicate zones in the idealized metasomatic zonation (scale = 1:1000)

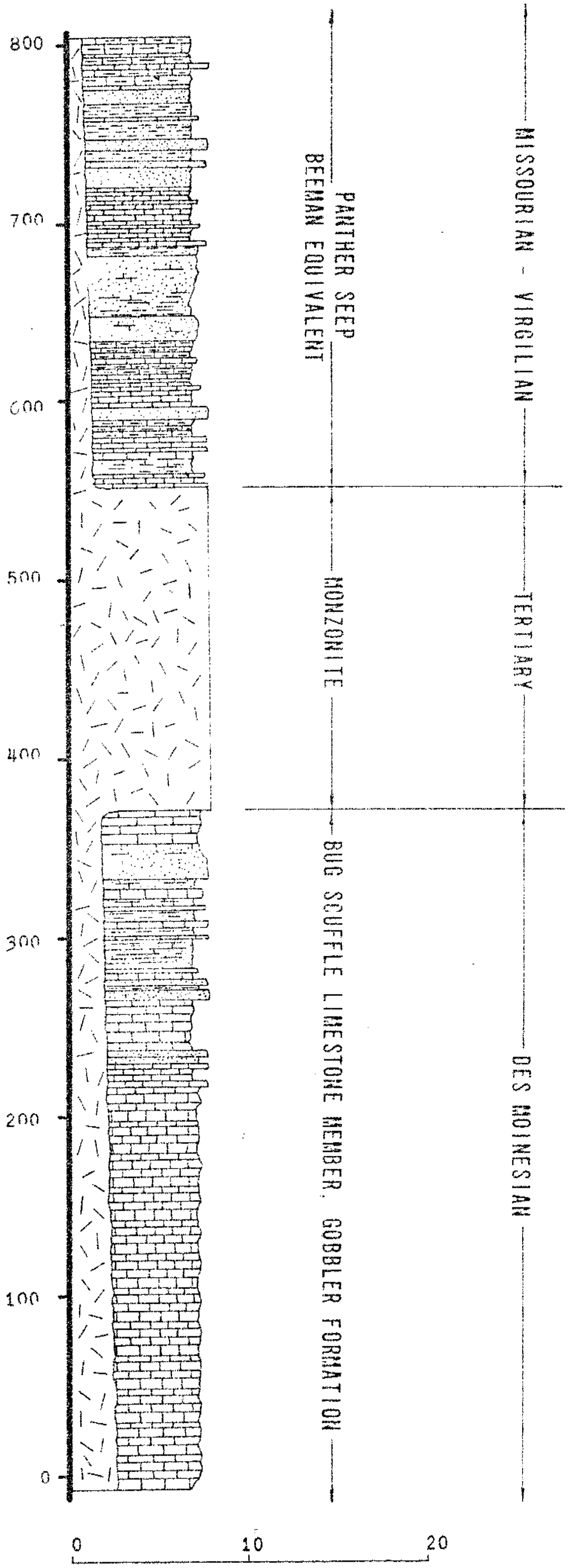
800
700
600
500
400
300
200
100
0
0
10
20
MISSOURIAN - VIRGILIAN
TERTIARY
DES MOINESIAN
PANTHER SEEP
BEEMAN EQUIVALENT
MONZONITE
BUG SCUFFLE LIMESTONE MEMBER, GOBBLER FORMATION

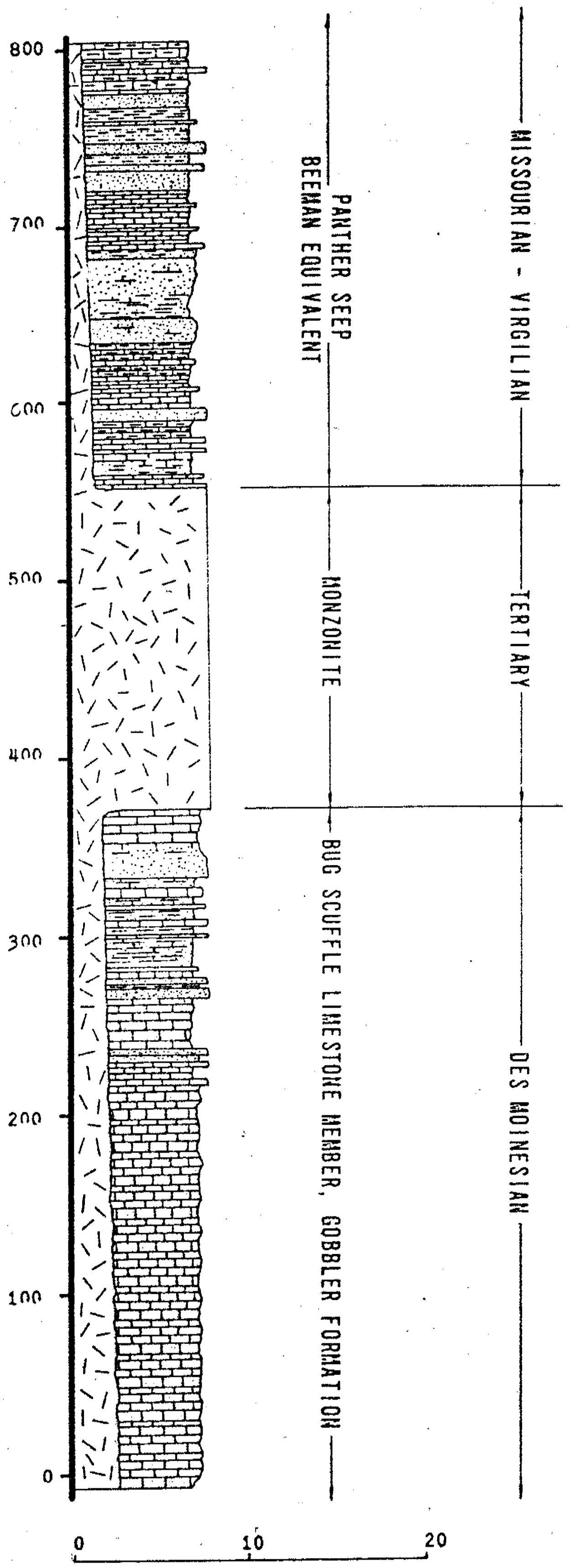
800
700
600
500
400
300
200
100
0
0
10
20
PANTHER SEEP
BEEMAN EQUIVALENT
MONZONITE
BUG SCUFFLE LIMESTONE MEMBER, GOBBLER FORMATION
MISSOURIAN - VIRGILIAN
TERTIARY
DES MOINESIAN

PYROMETASOMATIC ALTERATION OVERLAY: MAGNETITE REPLACEMENTS

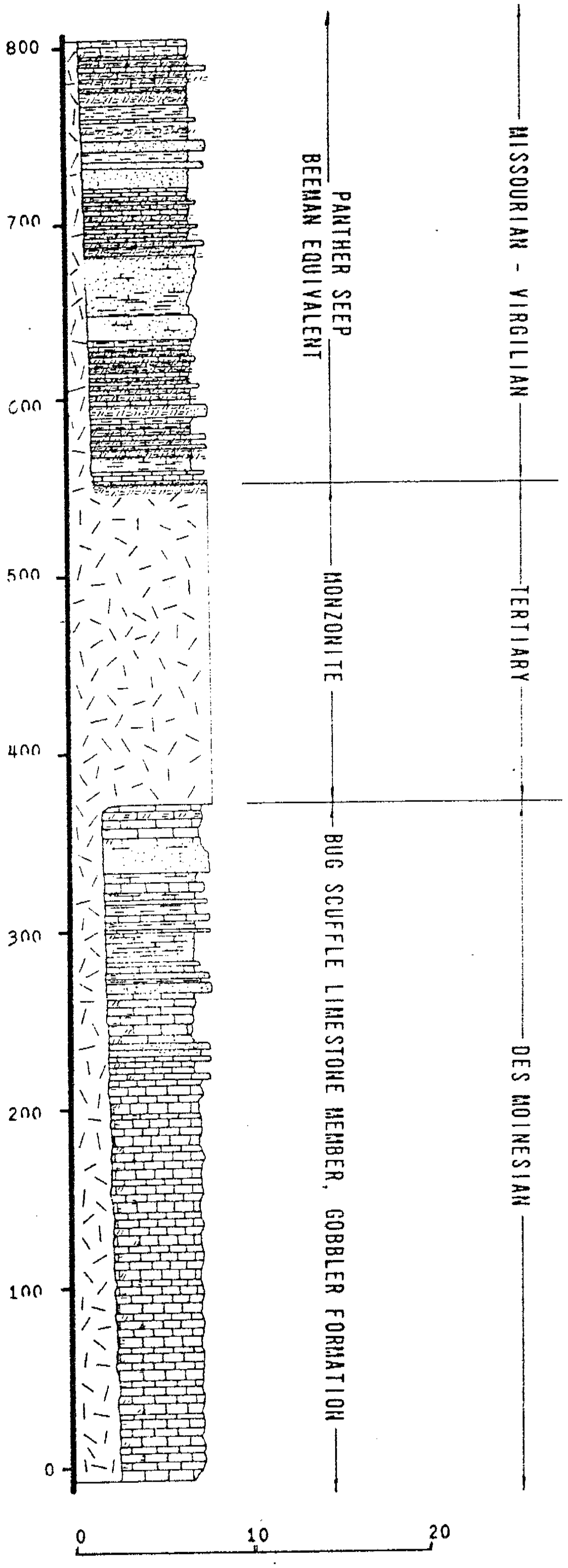

PYROMETASOMATIC ALTERATION OVERLAY CLINOZOISITE-EPIDOTE ZONE

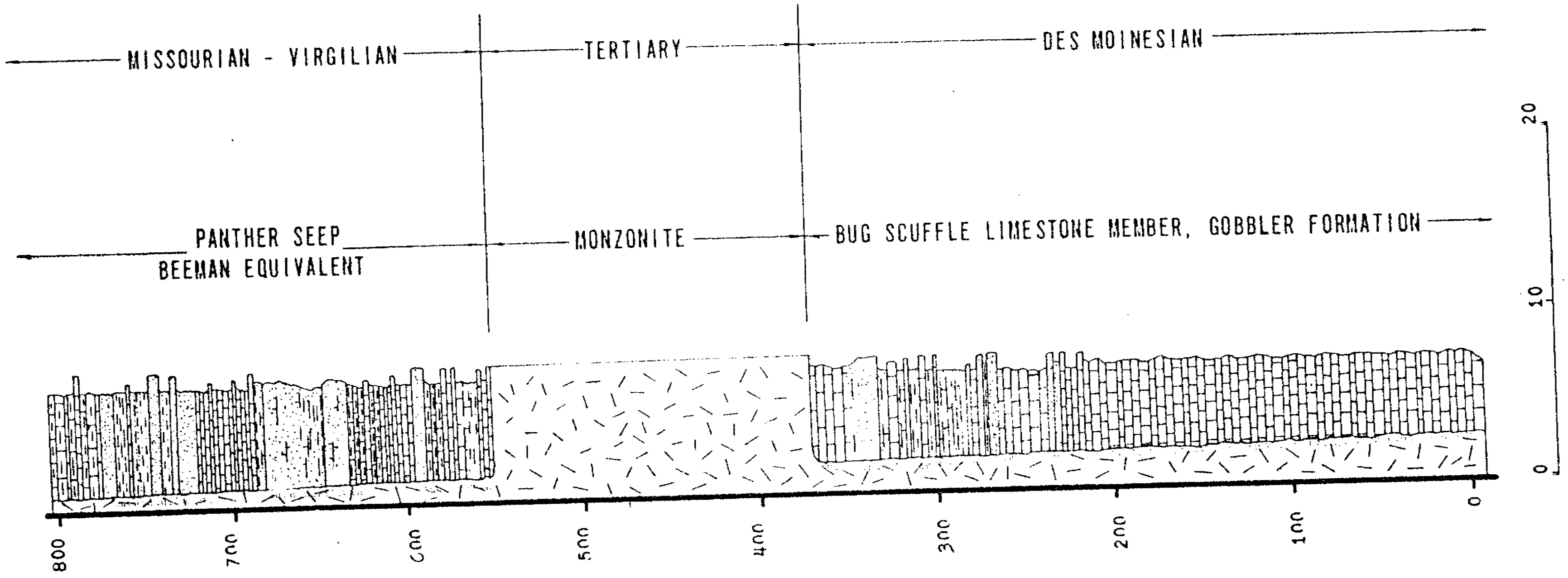

Plate 3 Exposures illustrating observed metasomatic zonation in carbonate wallrock

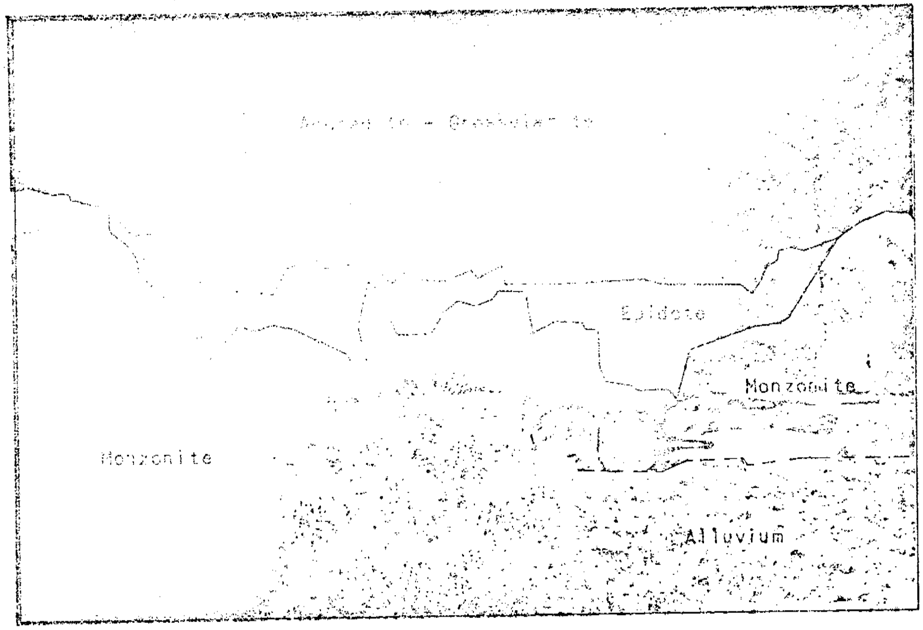
Andradite - Grossularite
Epidote
Monzonite
Monzonite
Alluvium

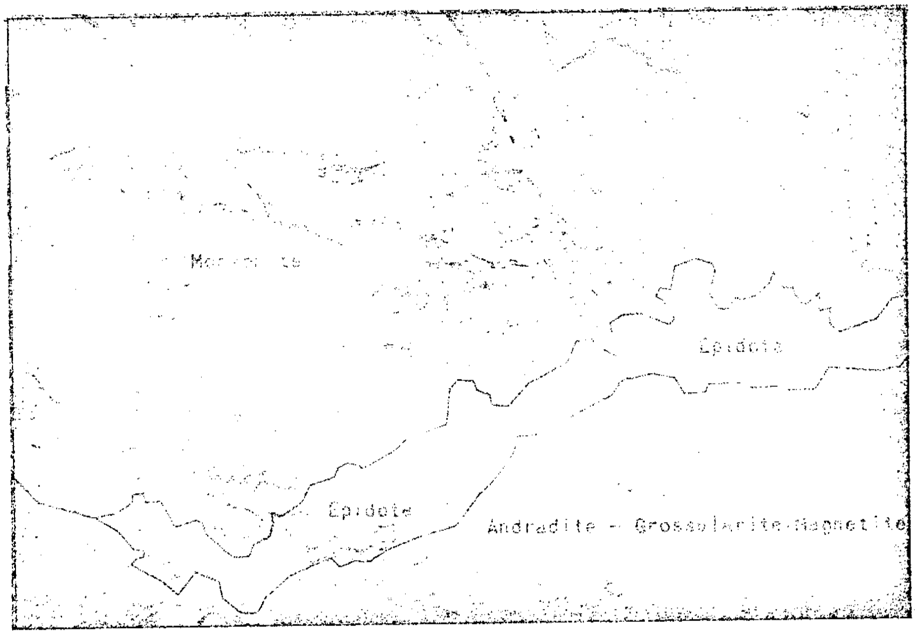
Monzonite
Epidote
Epidote
Andradite - Grossularite-Magnetite

is granoblastic, consisting of a mosaic of equidimensional, unoriented grains of green clinozoisite-epidote as much as 2 millimeters in diameter with colorless to white rhombs of interstitial calcite which may exceed several centimeters in their largest dimension. Greenish-gray amphibole needles as much as 5 millimeters in length and an occasional engulfed quartz or garnet grain 1 to 5 millimeters in diameter may be locally present.

The monzonite/epidote zone contact is gradational; epidote progressively decreases moving into fresher intrusive normal to the contact and extends proportionally greater distances into the intrusive along major fractures. Epidote also grades into the first zone of the exoskarn; a bimineralic zone of coexisting garnet and epidote may locally be observed.

Andradite-Grossularite-Calcite Zone

The garnet (andradite-grossularite-calcite) zone is the most extensively exposed calc-silicate assemblage. The garnet zone varies from a dense, resinous, brown to green hornfels to friable masses of euhedral to subhedral crystals as much as one centimeter in diameter. Pure garnet is especially resistant to physical weathering. There are substantial accessory minerals, and the garnet is usually brecciated and vuggy. Hematite is the most common characterizing accessory mineral and occurs as radiating blades. Interstial calcite, and locally, quartz are also present in significant amounts. Lenses and thin beds of fine-grained pyroxene (wollastonite-diopside) and epidote hornfels are intercalated with the garnet; these are the metamorphic equivalents of interbedded siliceous, dolomitic limestones and calcareous shales, respectively.

The garnet zone and garnet porphyroblasts within it often demonstrate zonation. Garnets rich in the grossularite end member generally occur immediately adjacent to the endoskarn. Andradite-rich garnets are relatively more abundant in the exoskarn at greater distances from the intrusive contact. This generalized zonation in areal distribution does not preclude isolated grossularite porphyroblasts or horizons occurring within the exoskarn; the position of high-aluminum garnet is dependent either upon the components available from the original lithology or enrichment of aluminum from an external source. Garnet porphyroblasts are also strongly zoned, although no consistent relationship among the zones was observed during the petrographic investigation. This zoning is a response of the system to variable thermochemical parameters; these parameters may be defined in terms of temperature, pressure, and chemical composition. It is reasonable to assume a temperature gradient in time and space; this gradient, however has not been documented in this report. Variation in total pressure is a reasonable response to variation in P_{H_2O} through influx of H_2O from intrusive pulses, differentiation, venting, hydrofracing, etc. An aqueous phase of variable composition, under isothermal and isobaric restraints, in equilibrium with the garnets, and flowing through an open system would result in similar effects. The garnet zoning is certainly the response to a combination of these variations in thermochemical parameters.

The garnet zone is transitional into marble, or locally the pyroxene zone, at distances not exceeding forty feet from the intrusive contact. The transition is not a sharp line but is marked by inclusions of marble in garnet, alternating strata of marble and garnet, and by porphyroblasts of garnet in marble.

Pyroxene Zone

Between the garnet and marble zones there may exist an irregular zone of lenses and disseminated crystals of wollastonite-diopside. The disseminated pyroxenes occur as fine needles averaging about 0.02 millimeters in length set in white to dark-gray marble. The isolated lenses of pyroxenes tend to replace former chert nodules in the limestone. Schmidt (1962) reports nodules as much as six inches in diameter in which residual chert is surrounded by a reaction aureole consisting of wollastonite and minor veinlets of diopside.

Marble Zone

The garnet or pyroxene zones pass into marble at still greater distances from the intrusive contact; Schmidt (1962) reports this transition occurring from forty to sixty feet normal to the contact. The marble is characteristically medium-grained and varies in color from white to dark gray. It is granoblastic, consisting mainly of a mosaic of equant calcite grains ranging from 1/2 to 2 millimeters in diameter. The marble zone passes into unaltered limestone within sixty feet from the calc-silicate zones, measured normal to the contact in the same stratigraphic horizon (Schmidt, 1962).

Controls of Pyrometasomatic Alteration

The most important controls governing pyrometasomatic alteration are lithology and structure. The contrasting lithologies of the Gobbler and Panther Seep equivalents each appear to have their own unique alteration assemblages. Structure is a major control when the favorable host rocks have been domed, faulted, and fractured by the force of the intrusion.

Lithology

The most abundant type of pyrometasomatic alteration in the area of investigation is the assemblage of the garnet zone which replaces calcareous beds of the Bug Scuffle Limestone Member of the Gobbler Formation. Monzonite sills intruding limestones of this unit produce calc-silicate zonation on a small scale (Plate 4) which is identical to the generalized zonation previously discussed. The Panther Seep Formation, consisting of interbedded argillaceous limestones and calcareous shales, produces metamorphic equivalents which do not closely resemble those of the Bug Scuffle Limestone. The relatively impure interbedded limestones are replaced by massive magnetite with accessory pyroxene of the diopside-hedenbergite series. The general model of calc-silicate zonation proposed herein for metamorphic equivalents of the Bug Scuffle Limestone is not everywhere consistent with field observations; massive magnetite is often in direct contact with monzonite without the formation of an epidote endoskarn (Plate 5). The more characteristic calcareous shales of the Panther Seep Formation alter to dense, greenish-gray clinopyroxene-epidote-quartz hornfels characterized by conchoidal fracture and disseminated pyrite; very fine granular texture is typical with the most common minerals being epidote and quartz. The metamorphic equivalent of Panther Seep is often alternating intervals of massive magnetite and clinopyroxene-garnet hornfels (Plate 6).

Composition of the causative intrusive rock is also of significant influence. The most intense degree of pyrometasomatic alteration is associated with intrusive rocks of monzonitic composition intruded into calcareous wallrock of the Bug Scuffle Limestone. Alternately, monzonite

Plate 4 Monzonite sill intruding the Bug Scuffle Limestone Member of the Gobbler Formation illustrating the observed metasomatic zonation

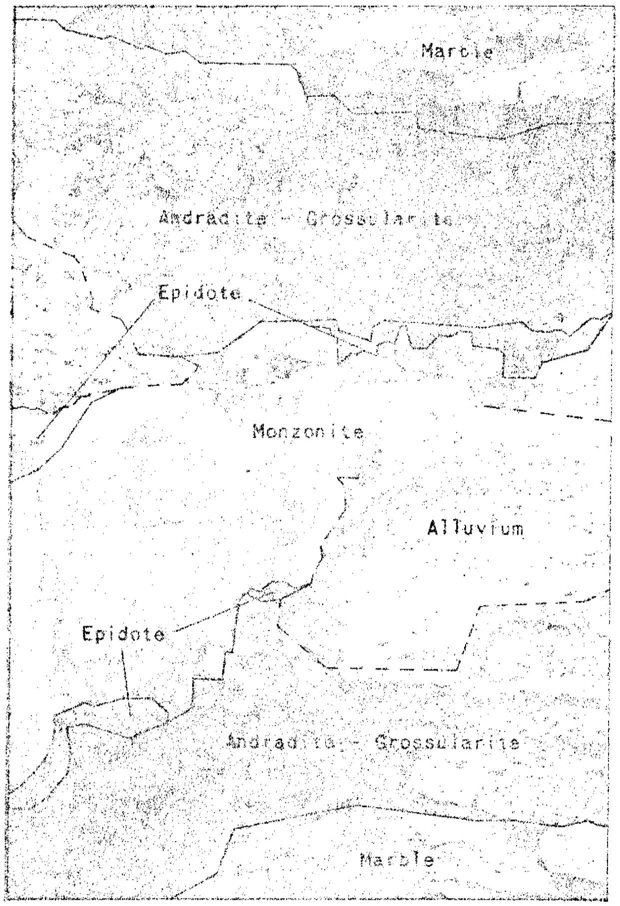
Marble
Andradite - Grossularite
Epidote
Monzonite
Alluvium
Epidote
Andradite - Grossularite
Marble

Plate 5 Massive magnetite (replacing carbonate units in the Panther Seep equivalent) without an endoskarn in contact with monzonite

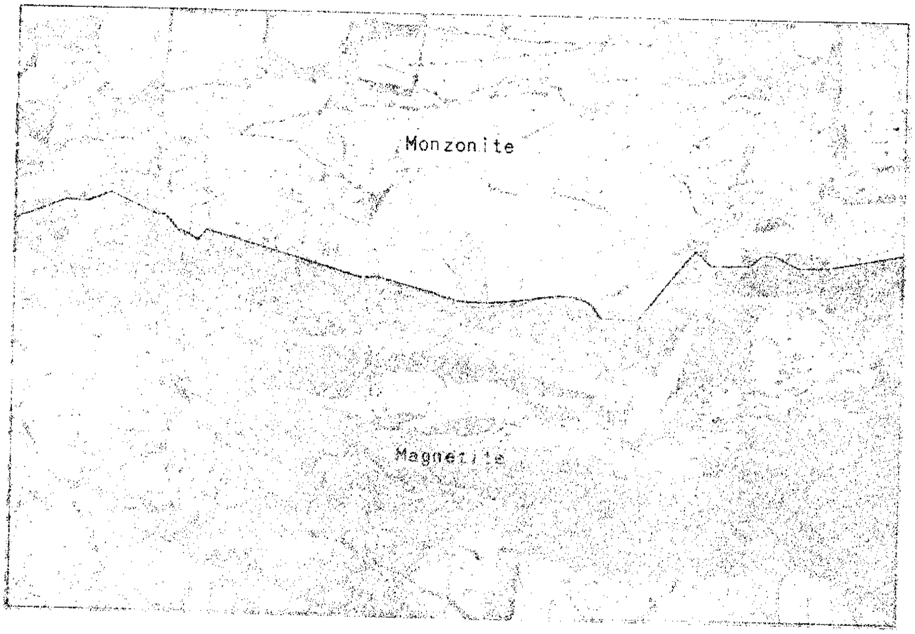
Monzonite
Magnetite

Plate 6 Alternating massive magnetite replacements and clinopyroxene-garnet hornfels in the Panther Seep equivalent

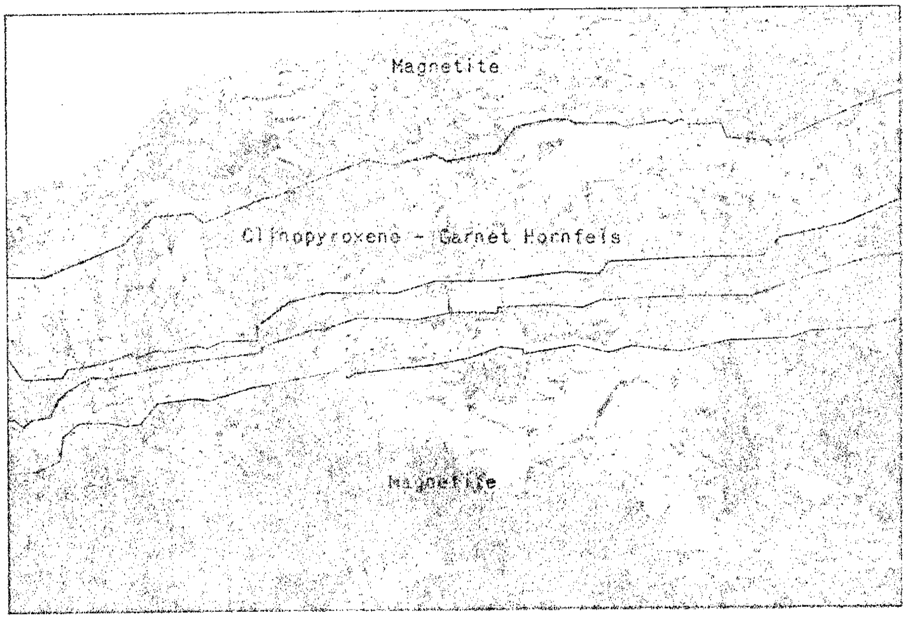
Magnetite
Clinopyroxene - Garnet Hornfels
Magnetite

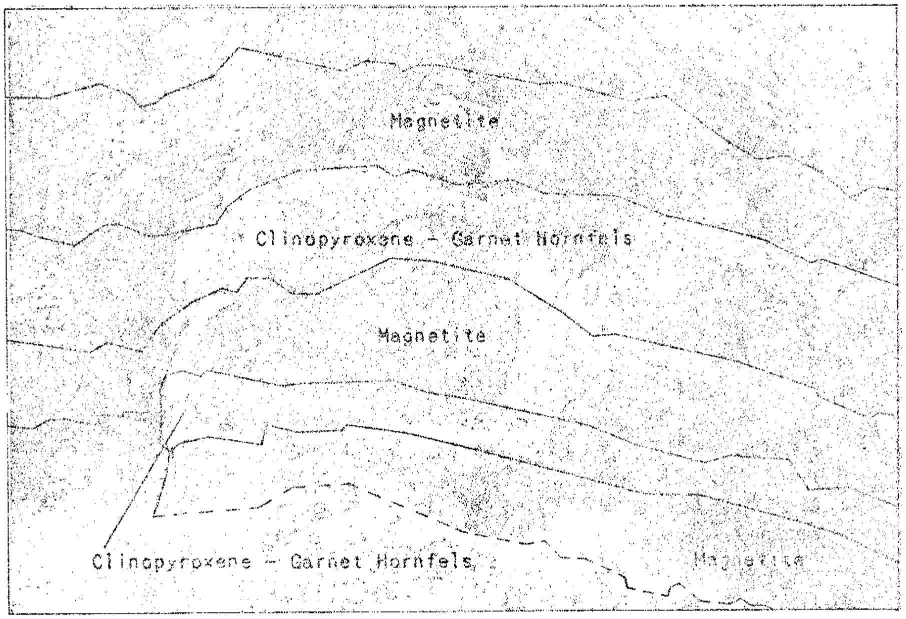
Magnetite
Clinopyroxene - Garnet Hornfels
Magnetite
Clinopyroxene - Garnet Hornfels
Magnetite

in contact with shales of the Panther Seep Formation produces approximately 8 to 12 inches of calc-silicate alteration (generally epidote), and quartz latite in contact with shales of the Panther Seep Formation produces an approximate 4 to 6 inches "baked" zone without calc-silicates (Plate 7).

Structure

When the favorable strata have undergone intense faulting, fracturing, and brecciation in response to intrusive emplacement, calc-silicates are often located along fractures which acted as channelways for hydrothermal fluids. Thermal disequilibrium, causing recrystallization involving relatively immobile components, merges with, and is often eclipsed by, pyrometasomatic alteration which involves the introduction or removal of mobile components.

Calc-silicate phases in the area of this investigation and the area immediately to the north demonstrate pronounced asymmetry with respect to areal distribution. Carbonate wallrock and its metamorphic equivalents are exposed in a ring (enveloping north-central Section 3, T.22S., R.8E.) bounded by two concentric circles. The systematic calc-silicate zonation occurs along the inner circle. Asymmetry and systematic zoning suggest fluid movement from the center to the edge of this ring and normal to the intrusive contacts. Possible sources and the direction of flow will be the topic of a subsequent discussion which considers pyrometasomatic alteration as the product of an aqueous phase entering carbonate wallrock with which it is not in equilibrium.

Plate 7 Quartz latite intruding Panther Seep equivalent

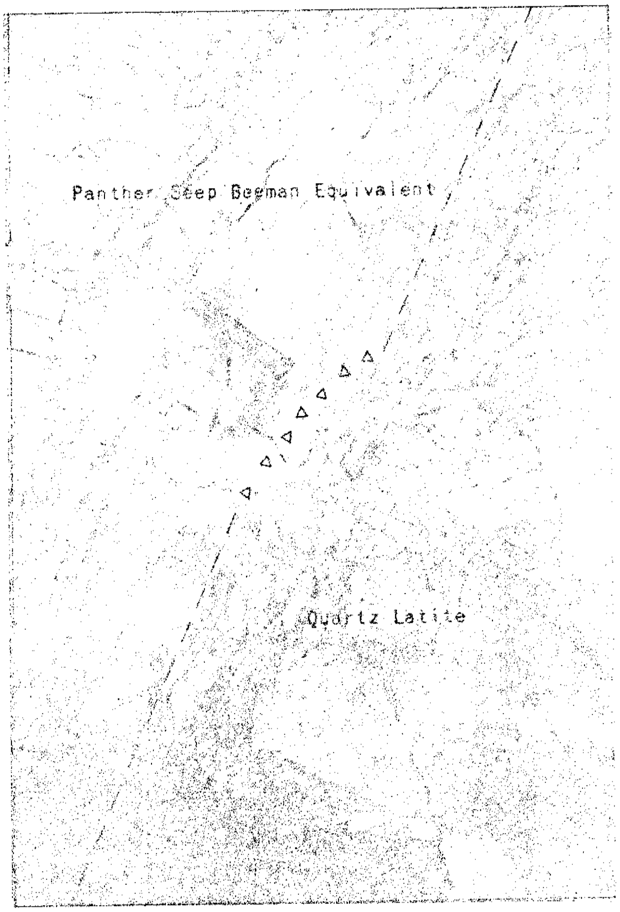
Panther Seep Beeman Equivalent
Quartz Latite

Metamorphic Petrology

The calc-silicate assemblages, discussed heretofor with respect to an idealized calc-silicate zonation in carbonate wallrocks, have been defined on the basis of physical characteristics. Precise compositional determination by optical techniques of calc-silicate phases with variable composition is also desirable; these data may then be employed in mass balance and mass transfer calculations.

Laboratory investigation of twenty thin sections has shown that the predominant calc-silicate, oxide, and carbonate phases characteristic of pyrometasomatic alteration in carbonate wallrock are garnet of the andradite-grossularite binary solid solution, clinozoisite-epidote solid solution, pyroxene (wollastonite-diopside-hedenbergite), quartz, hematite, and calcite. Idocrase and an amphibole of the actinolite-ferrotremolite series are locally important accessory minerals restricted to the endoskarn. Concise but comprehensive documentation of the calc-silicate phases of interest may be found in Appendix C.

Mineralization

Previous investigations of pyrometasomatic deposits (Umpleby, 1916; Burt, 1972) have suggested that multiple hydrothermal fluids are involved in alteration and mineralization. The geometry of mineral distribution in the Jarilla Mountains clearly demonstrates that sulfide mineralization followed calc-silicate alteration. Very few sulfides are present in the calc-silicate zones where cross-cutting sulfide veinlets are absent; limestones adjacent to the calc-silicate zones contain only a few minor sulfide-bearing fractures. Whereas pyrite veinlets extend to the edge of calc-silicate zones, chalcopyrite and magnetite are generally restricted to the immediate area of intrusive contacts. An individual and mobile aqueous phase involved in mass transport during the alteration process would be expected to coprecipitate sulfide minerals and calc-silicates in response to decreasing temperature, progressive compositional variation, etc; this cogenetic relationship has not been observed. The cross-cutting relationships lend credence to an early hydrothermal fluid to which the calc-silicate alteration can be ascribed and a relatively later fluid which precipitated magnetite, pyrite, and chalcopyrite adjacent to intrusive contacts as well as pyrite throughout the calc-silicate zones. Magnetite and chalcopyrite saturated with respect to the aqueous phase at physiochemical parameters still favorable to transport of aqueous species required for iron sulfide saturation.

METASOMATISM

Progressive metamorphism of siliceous carbonate rocks is viewed classically in terms of a generalized sequence of decarbonation reactions which is consistent with the mineral zones observed in metamorphic facies. Most former studies of phase equilibria during the course of progressive metamorphism have stressed solid and gas-phase equilibria influenced by changes in temperature and pressure in a system with chemical potentials fixed by the solid phases. Early investigators documented the naturally occurring mineral assemblages and attempted to determine empirically the nature and order of the chemical reactions required to produce the mineral zonation they observed (Eskola, 1922; Bowen, 1940; Tilley, 1943, 1959). These studies have been supplemented by experimental investigations performed to determine the temperature and pressure dependence of certain reactions in the system $CaO-MgO-SiO_2-H_2O-CO_2$ (Metz, Puhan, and Winkler, 1963; Metz and Trommsdorf, 1968; Gordon and Greenwood, 1970).

In addition to changes in temperature and pressure, compositional variation in an aqueous phase may be responsible for metamorphic mineral assemblages (Brown, 1971). In the presence of a non-circulating aqueous phase (a closed system), the partial pressure of CO_2 increases rapidly as decarbonation proceeds and high temperatures are soon required for reactions to proceed spontaneously. Alternately, in an environment where a relatively large mobile volume of an aqueous phase undersaturated with respect to CO_2 is available, extensive decarbonation may proceed for a long time without significant increase in P_{CO_2} of the system. Thus, the formation of calc-silicate phases may be maintained without significant increases in equilibrium temperatures, and the appearance of solid phases is controlled by the composition of the aqueous phase at fixed temperature and pressure with chemical potentials of components as variables.

Considerable progress has recently been achieved in the application of theoretical solution chemistry to metasomatic processes (Helgeson, 1964, 1967, 1968; Helgeson, Garrels, and MacKenzie, 1969; Helgeson, Brown, Nigrini, and Jones, 1969). These advances have made possible accurate predictions of phase equilibria in metamorphic reactions involving an aqueous phase at elevated temperatures and pressures (Brown, 1971). Brown suggested that the sequence in which minerals appear as stable phases during a progressive compositional change may be interpreted as the mineral zonation in a system in which the aqueous phase flows through, and reacts with the rock. This alternate approach to progressive metamorphism is used herein, but is restricted to a qualitative consideration of compositional variation of the aqueous phase at fixed temperature and pressure. An analogy to the evaluation of Brown is employed by substituting the components Fe_2O_3 and Al_2O_3 for MgO. The conclusions suggest that the classical decarbonation series of progressive metasomatism may in part be replaced with dehydration reactions in the system CaO-Fe_2O_3-Al_2O_3-SiO_2-CO_2-H_2O.

Graphic Representation of Compositional Variation

Diagrams depicting mineral compositions and compatibilities are convenient for the simultaneous consideration of petrology and solution chemistry. Representation of phase relations on triangular composition diagrams enables visual illustration of changes in mineralogy resulting from changes in compositional parameters at fixed temperature and pressure. Calc-silicate phases present in the skarns consist primarily of the components $CaO-Fe_2O_3-Al_2O_3-SiO_2-CO_2-H_2O$. The stoichiometric compositions of the more common minerals in the system expressed in terms of these components are listed in Table 1. The mineral compositions plotted in mole percent of the essential components are illustrated on the triangular composition diagram in the system $CaO-Fe_2O_3+Al_2O_3-SiO_2$ (Figure 9).

Petrographic investigation indicates that the phases in which the FeO component is essential (hedenbergite and ferrotremolite) are subordinate and need not be considered in detail. Phase compositions containing CO_2 and H_2O as essential components are plotted by combining the volatile components. Tie lines connect mineral pairs which exhibit mutual grain boundary relationships in thin section. It is assumed unless petrographic evidence indicates to the contrary, that under the constraint of fixed temperature and pressure, homogeneous and heterogeneous equilibrium obtain in the system.

Continuous solid solution between pure end members in the andradite-grossularite and clinozoisite-epidote series is amenable to representation on the triangular composition diagram in the system $Al_2O_3-Fe_2O_3-CaO+SiO_2$ (Figure 10). The heavier lines indicate the range in composition of garnet and epidote from thin section investigations. Recalling that tie lines connecting equilibrium mineral pairs cannot cross, the clinozoisite-epidote/calcite and andradite-grossularite/hematite tie lines illustrated in Figure 9 appear to be in error. The aforementioned assemblages cannot coexist by assuming garnet compositions over the complete solid

Table 1. Minerals in the System $CaO-Fe_2O_3(-FeO)-Al_2O_3-SiO_2-CO_2-H_2O$

Mineral Name	Stoichiometric Formula	Oxide Formula	Molar Volume (cm^3/mole)	Density (grams/cm^3)
Andradite	$Ca_3Fe_2Si_3O_{12}$	$3CaO + Fe_2O_3 + 3SiO_2$	131.67	3.86
Grossularite	$Ca_3Al_2Si_3O_{12}$	$3CaO + Al_2O_3 + 3SiO_2$	125.32	3.59
Spessartite	$Mn_3Al_2Si_3O_{12}$	$3MnO + Al_2O_3 + 3SiO_2$	118.16	4.19
Ferrotremolite	$Ca_2Fe_5Si_8O_{22}(OH)_2$	$2CaO + 5FeO + 8SiO_2 + H_2O$	285.30	3.40
Epidote	$Ca_2Al_2FeSi_3O_{12}(OH)$	$2CaO + Al_2O_3 + 1/2Fe_2O_3 + 3SiO_2 + 1/2H_2O$	136.20±	3.34±
Clinozoisite	$Ca_2Al_3Si_3O_{12}(OH)$	$2CaO + 3/2Al_2O_3 + 3SiO_2 + 1/2H_2O$	136.20±	3.34±
Prehnite	$CaAl_2Si_3O_{10}(OH)_2$	$CaO + Al_2O_3 + 3SiO_2 + H_2O$		
Anorthite	$CaAl_2Si_2O_8$	$CaO + Al_2O_3 + 2SiO_2$	100.73	2.76
Hedenbergite	$CaFeSi_2O_6$	$CaO + FeO + 2SiO_2$	65.97	3.55
Wollastonite	$CaSiO_3$	$CaO + SiO_2$	39.94	2.91
Calcite	$CaCO_3$	$CaO + CO_2$	36.94	2.71
Quartz	SiO_2	SiO_2	22.69	2.65
Magnetite	Fe_3O_4	$Fe_2O_3 + FeO$	44.53	5.20
Hematite	Fe_2O_3	Fe_2O_3	30.28	5.27

Figure 9 Compositional triangle illustrating coexisting mineral pairs in the system CaO-Fe_2O_3+Al_2O_3-SiO_2-CO_2-H_2O

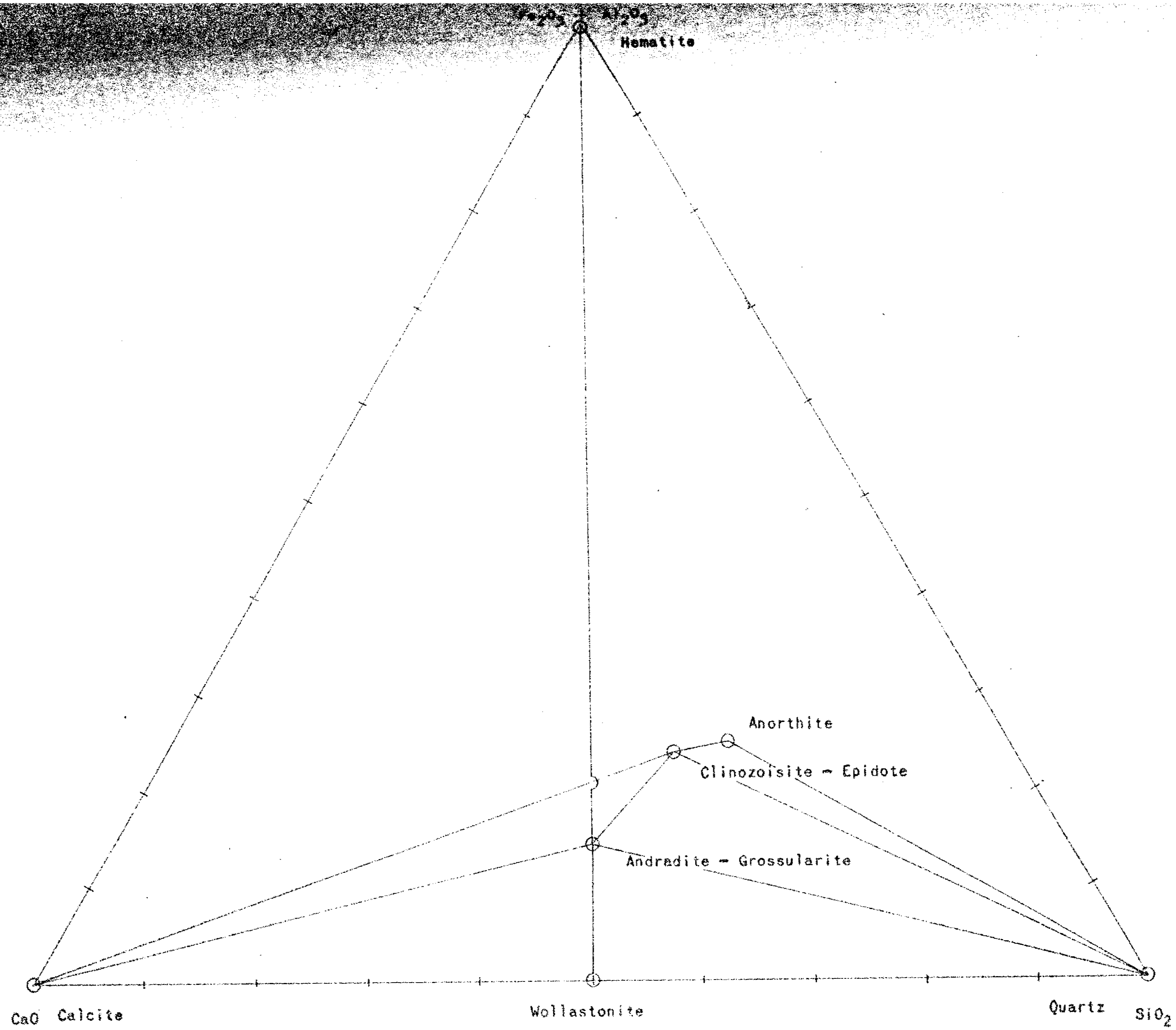Fe2O3 + Al2O3
Hematite
Anorthite
Clinozoisite - Epidote
Andradite - Grossularite
CaO
Calcite
Wollastonite
Quartz
SiO2

Figure 10 Compositional triangle illustrating coexisting mineral pairs in the system $CaO+SiO_2-Fe_2O_3-Al_2O_3-CO_2-H_2O$

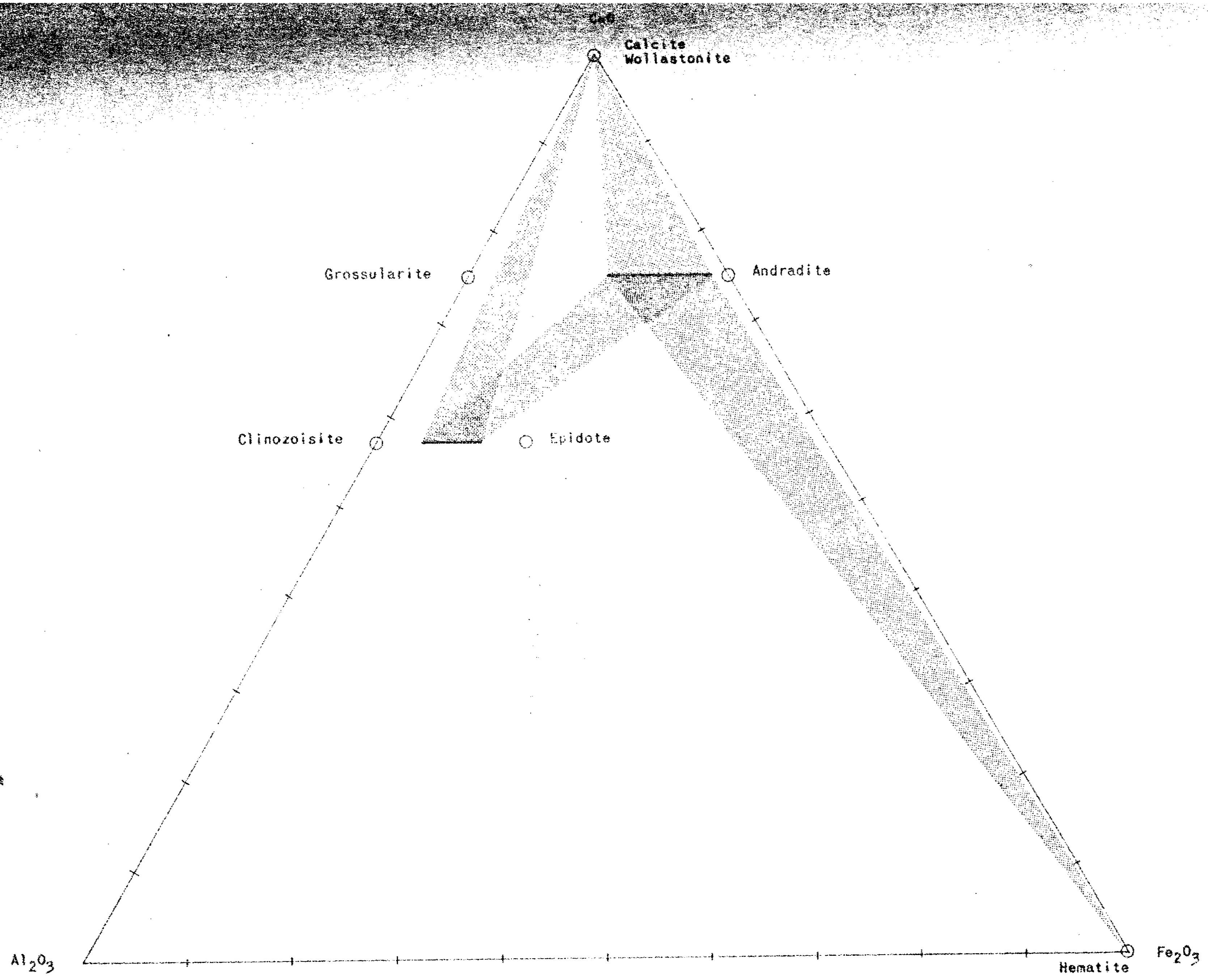
CaO
Calcite
Wollastonite
Grossularite
Andradite
Clinozoisite
Epidote
Al_2O_3
Fe_2O_3
Hematite

solution range; however, hematite may coexist with a garnet of high iron content and still allow the clinozoisite-epidote/calcite tie line to be drawn as illustrated in Figure 10.

Chemical Potential Diagrams

Conventional triangular composition diagrams have found widespread use in petrology as a graphic means of representing composition; however, an alternate procedure applying an orthogonal method of representation affords an important advantage over its triangular counterpart. The slopes of the tie lines on orthogonal composition diagrams are equivalent to the negative reciprocals of the slopes of the corresponding phase stability boundaries on chemical potential diagrams (Korzhinski, 1959). Consideration of equilibrium mineral assemblages from chemical potential diagrams provides the link among geochemical principles, graphic representation of the consequences of compositional variation, and the observed mineral assemblages (Brown, 1971). Triangular composition diagrams in a three-component system may easily be converted to orthogonal coordinates by expressing mineral compositions in terms of two components each referenced to a third component whose chemical potential is held constant. The consequent phase stability boundaries define reversible chemical reactions which occur in the specified system. Lines representing saturation in the aqueous phase of minerals which do not occupy stability fields (phases whose compositions do not contain the reference component) limit the composition of the aqueous phase by specifying an additional parameter such as P_{CO_2} at fixed temperature and pressure.

Burt (1972) represented the principal skarn facies in the system

$CaO-FeO-Fe_2O_3-SiO_2-CO_2-H_2O$ as separate areas on chemical potential (μ) diagrams depicting μO_2 versus $\mu 2CO_2$ and μO_2 versus temperature (Figure 11 and Figure 12, respectively). The slopes of the lines representing univarient equilibria were calculated using the stoichiometric compositions of the participated phases expressed as determinants in a method described by Korzhinski (1959). The relative positions of the lines were justified by documenting the mineral assemblages present at numerous field locations and determining empirically the positions necessary to produce the assemblages. Reference to these figures shows that Burt has approached progressive metamorphism in the traditional manner by expressing phase stabilities in terms of solid- and gas-phase equilibria. Consequently, the diagrams are not directly applicable to the approach employed in this investigation; however, they do serve to demonstrate that low P_{CO_2} and high P_{O_2} are required to eliminate certain phases, particularly hedenbergite, from the mineral assemblages. A model describing pyrometasomatic alteration employing chemical potential diagrams and characterized by an aqueous phase undersaturated in respect to CO_2 will be proposed in a discussion to follow.

Mass Balance

The thermodynamic relations employed to predict the isothermal/isobaric response to changing solution composition as a system proceeds to overall equilibrium require an accurate determination of the original mineral assemblage. Theoretical evaluations of mass transfer have the distinct advantage over investigations emphasizing naturally-occurring assemblages in that they may assume, *a priori*, the relative masses of

Figure 11 Empirical chemical potential diagram in the system $CaO-FeO-Fe_2O_3-SiO_2-CO_2-O_2$ (modified after Burt, 1973)

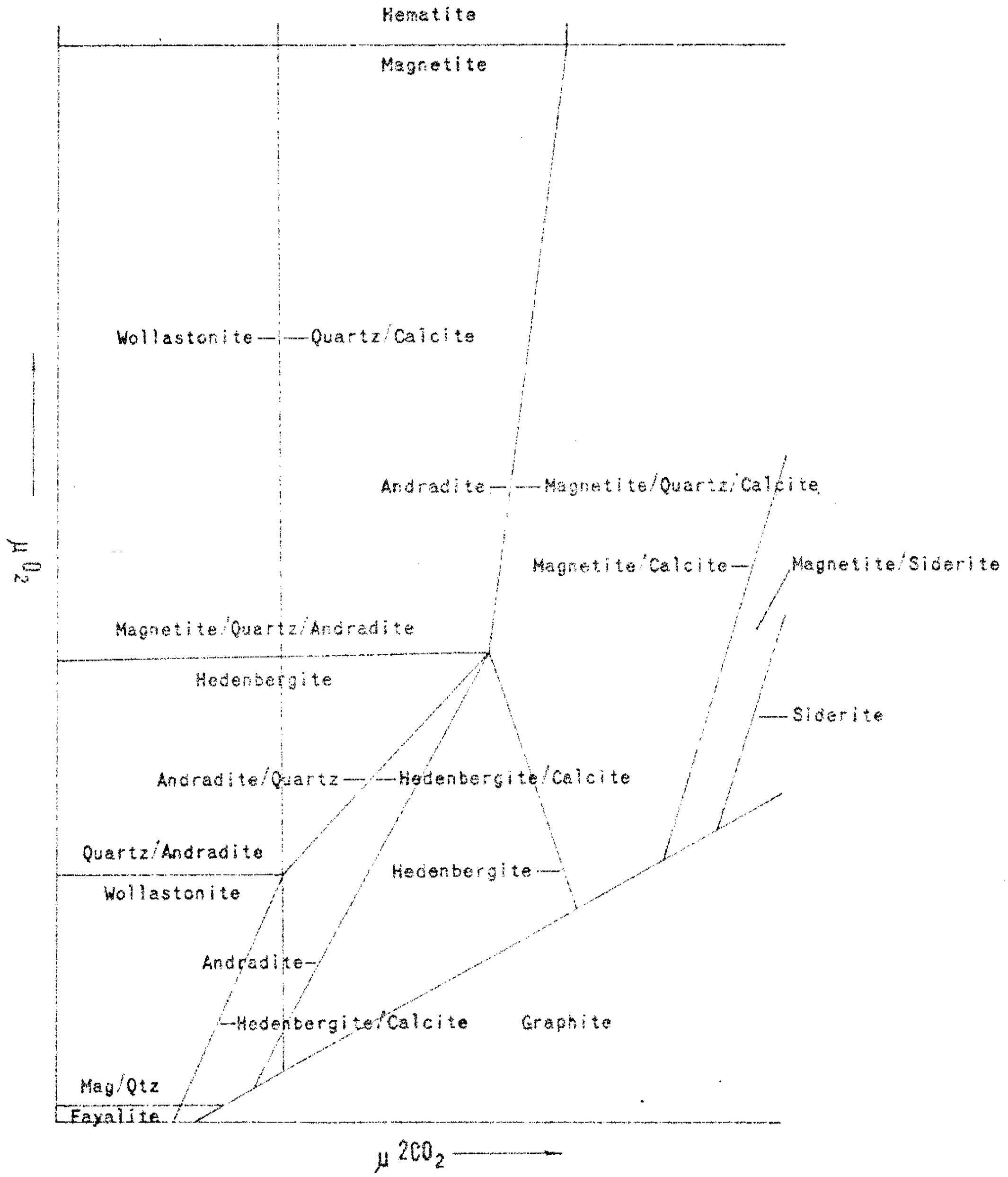
Hematite
Magnetite
Wollastonite — —Quartz/Calcite
Andradite — —Magnetite/Quartz/Calcite
Magnetite/Calcite —
Magnetite/Siderite
μ O2
Magnetite/Quartz/Andradite
Hedenbergite
—Siderite
Andradite/Quartz — —Hedenbergite/Calcite
Quartz/Andradite
Wollastonite
Hedenbergite —
Andradite—
—Hedenbergite/Calcite
Graphite
Mag/Qtz
Fayalite
μ 2CO2

Figure 12 Empirical chemical potential-temperature diagram in the system CaO-FeO-Fe_2O_3-SiO_2-CO_2-O_2 (modified after Burt, 1972)

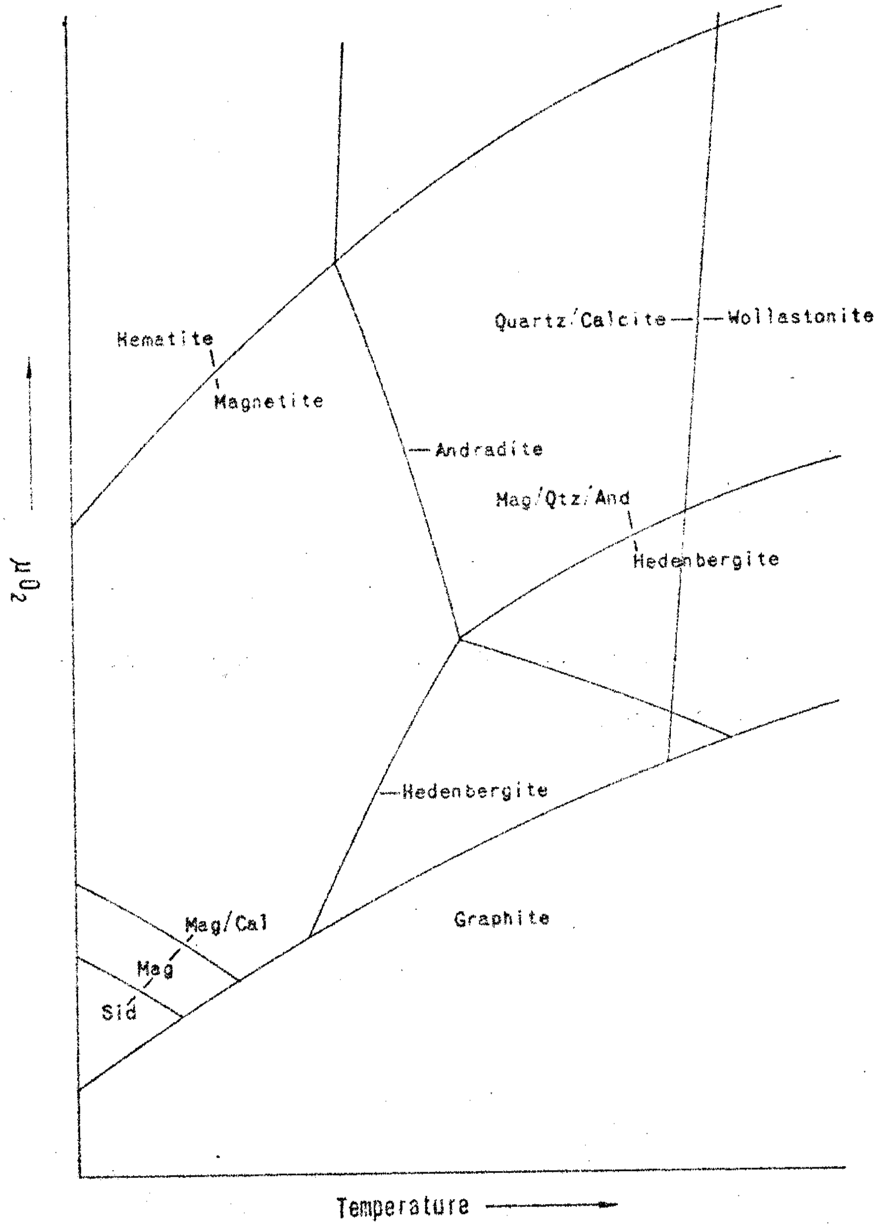
Hematite
Magnetite
Quartz/Calcite
Wollastonite
Andradite
Mag/Qtz/And
Hedenbergite
Hedenbergite
Mag/Cal
Mag
Sid
Graphite
μO_2
Temperature

each phase occurring in a given reaction. Investigations in natural systems must resolve this unknown by simultaneous evaluation of chemical analyses and petrographic information. In this study, oxide components from whole rock analysis are distributed among the phases observed in thin section while conserving mass within the system.

The relation between the stoichiometric composition of a phase and the whole rock chemical analysis defined in terms of the mole percent of oxide components can be described by writing the following mass balance equations where A, B, and C are oxide components and x, y, and z are mineral phases. The oxide components must be reported in moles (M):

$$M_{A,x} + M_{A,y} + M_{A,z} = M_{T,A}$$

$$M_{B,x} + M_{B,y} + M_{B,z} = M_{T,B}$$

$$M_{C,x} + M_{C,y} + M_{C,z} = M_{T,C}$$

The total moles of component A may be defined as the total moles of A summed over the phases x, y, and z, etc. These equations constitute a set of three linear equations in three unknowns, the solution of which distributes a selected component among the phases in which it occurs. The simultaneous solution of linear equations is most easily accomplished by means of determinants. A review of the essential properties of determinants needed for this purpose is beyond the scope of this study but may be found by reference to texts on applied linear algebra.

Rapid solution to a set of simultaneous linear equations using determinants is possible by computor calculation. The raw data required includes total moles of all essential components in each sample, the phases among which the components are to be distributed, and the total moles of the essential components in each phase. Quantitative determination

Table 2A. Examples of Mass Balance in the System $CaO-Fe_2O_3-(FeO-MgO)-Al_2O_3-SiO_2-CO_2-H_2O$ (values in weight percent)

Sample	CS-7	CS-8	CS-10	CS-17
Andradite	27.35	42.65	85.84	29.18
Grossularite	14.55		9.51	12.93
Spessartite	0.54		1.06	
Quartz	15.52	12.22	2.53	
Calcite	23.13	8.15	1.06	57.89
Hematite	18.91			
Epidote		36.98		
Tremolite				
Wollastonite				
Total	100.00	100.00	100.00	100.00

Sample	CS-20	CS-60	CS-81	CS-118
Andradite	82.66			47.61
Grossularite	4.89			
Spessartite	0.54			13.91
Quartz	2.60	6.17		
Calcite	0.65	10.29	40.19	38.48
Hematite	8.65			
Epidote		69.88		
Tremolite		13.90		
Wollastonite			15.59	
Diopside			44.22	
Total	99.99	100.24	100.00	100.00

Table 2B. Examples of Mass Balance in the System CaO-Fe_2O_3-(FeO-MgO)-Al_2O_3-SiO_2-CO_2-H_2O (values in mole percent)

Sample	CS-7	CS-8	CS-10	CS-17
Andradite	7.92	18.64	68.47	5.33
Grossularite	4.75		8.62	2.67
Spessartite	0.16		0.86	
Quartz	38.03	45.20	17.24	
Calcite	31.70	18.08	4.31	0.92
Hematite	17.43			
Epidote		18.08		
Tremolite				
Wollastonite				
Total	99.99	100.00	100.00	100.00

Sample	CS-20	CS-60	CS-81	CS-118
Andradite	58.37			18.52
Grossularite	3.89			
Spessartite	0.39			5.56
Quartz	15.56	27.52		
Calcite	2.33	27.52	46.99	75.93
Hematite	19.46			
Epidote		40.37		
Tremolite		4.59		
Wollastonite			44.58	
Diopside			8.43	
Total	100.00	100.00	100.00	100.01

Table 2C. Examples of Mass Balance in the System CaO-Fe_2O_3-(FeO-MgO)-Al_2O_3-SiO_2-CO_2-H_2O (values in volume percent)

Sample	CS-7	CS-8	CS-10	CS-17
Andradite	24.71	37.14	83.94	15.84
Grossularite	14.12		10.00	7.54
Spessartite	0.45		0.96	
Quartz	20.47	15.51	3.62	
Calcite	27.75	10.09	1.47	76.62
Hematite	12.50			
Epidote		37.26		
Tremolite				
Wollastonite				
Total	100.00	100.00	99.99	100.00

Sample	CS-20	CS-60	CS-81	CS-118
Andradite	88.37			41.34
Grossularite	4.98			
Spessartite	0.51			11.11
Quartz	3.84	7.36		
Calcite	0.93	11.97	42.61	47.55
Hematite	6.37			
Epidote		63.87		
Tremolite		16.81		
Wollastonite			43.70	
Diopside			13.69	
Total	100.00	100.01	100.00	100.00

of the essential components was provided by wet chemical analysis of 20 calc-silicate assemblages; the major element concentrations of Fe_2O_3, FeO, MnO, CaO, K_2O, SiO_2, Al_2O_3, MgO, Na_2O, and CO_2 reported in weight percent and the appropriate analytical procedures are listed in Appendix D. The concentrations in weight percent must be converted to mole percent prior to use in the mass balance calculations; this is accomplished employing the product equation

[weight % (grams)] x [molecular weight (grams/mole)] = mole %

The phases among which the components are to be distributed are determined by petrographic investigation. The total moles of the essential components in each phase involves the conversion of stoichiometric compositions to oxide formulas as listed in Table 1. The observed phases for selected calc-silicate assemblages and results of the computer calculations employing these data are reported in Table 2. Comparison of these data illustrates that the mass of CaO per unit volume remains essentially constant, with the exception of samples collected immediately adjacent to the intrusive contact. CaO may thus be employed as the reference component in the construction of chemical potential diagrams.

Reaction Path

Chemical potential diagrams constructed conserving CaO and considering the mobile components SiO_2, Al_2O_3, and/or Fe_2O_3 may be employed to describe the possible reaction paths suggested in this report as a first approximation of progressive metamorphism in the system $CaO-Fe_2O_3-Al_2O_3-SiO_2-CO_2-H_2O$ as an aqueous phase reacts with carbonate wall rock. The actual reaction path is based not only on observed phases, but also on the relative amount and reaction rate of the phases involved, and initial solution composition. The lengths and positions of the individual segments

Figure 13 Schematic chemical potential diagram illustrating the proposed reaction path in the system $CaO-Al_2O_3-SiO_2-CO_2-H_2O$

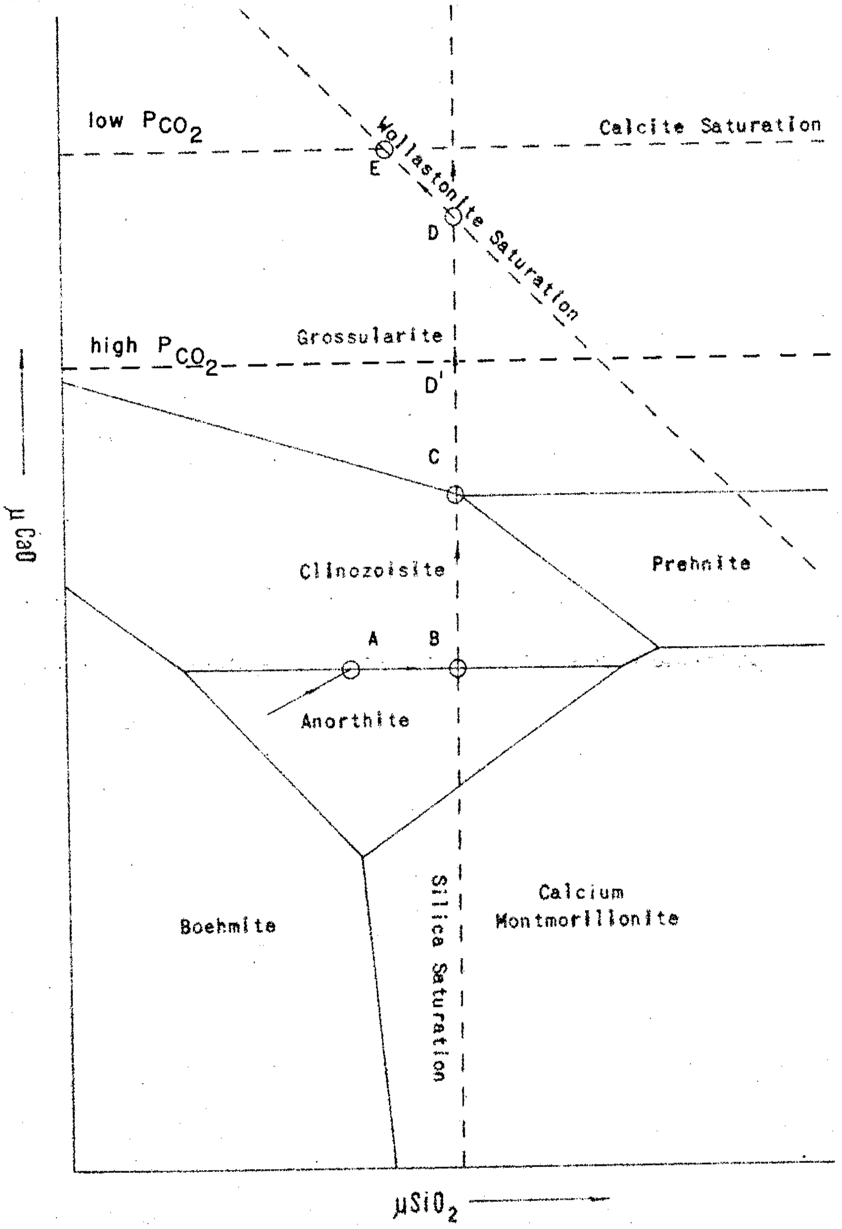
low P_{CO_2}
Calcite Saturation
Wollastonite Saturation
E
D
high P_{CO_2}
Grossularite
D'
C
Clinozoisite
Prehnite
A
B
Anorthite
Boehmite
Silica Saturation
Calcium Montmorillonite
μCaO
μSiO_2

along the proposed reaction path are schematic, implying only relative intensities of mass transfer.

The aforementioned restrictions of low P_{CO_2} and high P_{O_2} (cf. Burt, 1972) are compatible with a model of pyrometasomatic alteration employing an aqueous phase as a transport medium which is undersaturated with respect to CO_2. The CO_2 component must be removed at a rate similar to that at which it is generated during decarbonation reactions to meet these criteria. This precludes a diffusion transport mechanism and infers that a mobile aqueous phase is essential. The flow direction of this aqueous phase may be ascertained by considering a schematic isothermal, isobaric chemical potential diagram in the system $CaO-Al_2O_3-SiO_2-CO_2-H_2O$ (Figure 13). Because pyrometasomatic alteration is initiated when the aqueous phase is introduced into carbonate wallrocks with which it is not in equilibrium, and is terminated when equilibrium has been attained, (i.e., when calcite saturates in the aqueous phase) the transport medium is moving from areas of low μCaO to regions of higher μCaO until it saturates with respect to calcite. The geometry of the diagram is such that calc-silicate zonation documented in the field can only be produced isothermally if the aqueous phase emanates from the intrusive and moves into the carbonate wallrocks. The low P_{CO_2} values restricting the extent of pyrometasomatic alteration and precluding hedenbergite from andradite-stable assemblages are compatible with field observations of narrow calc-silicate zones without hedenbergite.

Predictions of phase equilibria in the five-component system $CaO-Al_2O_3-SiO_2-CO_2-H_2O$ are illustrated by the schematic chemical potential diagram at fixed P_{H_2O}, P_{CO_2} and μAl_2O_3 in figure 13; the Fe_2O_3 component plots normal to the plane of this diagram. The size of the stability fields on any given diagram can change as a result of variations in temperature and/or pressure and solid solution, but the relative positions of the phase boundaries and the slope of the tie lines remain fixed.

The initial composition of the aqueous phase is suggested to be in equilibrium with anorthite (calcic plagioclase in the monzonite as heretofore discussed) and is arbitrarily established in the anorthite field. Points in the following discussion are referenced to points appearing on Figure 13; reactions in the endoskarn are written conserving aluminum. Anorthite reacts with the aqueous phase to form clinozoisite at A:

$$2CaAl_2Si_3O_8 + H_2O \rightleftarrows Ca_2Al_3Si_3O_{12}(OH) + Al_2O_3 + SiO_2.$$

The simultaneous introduction of an aqueous phase containing Fe_2O_3 produces epidote in addition to clinozoisite. Including provision for solid solution between ferric iron and aluminum accomplished through the addition of Fe_2O_3 and SiO_2 in the aqueous phase requires consideration of generalized equations involving both end members of the clinozoisite-epidote series. The reactions are written employing variable Fe_2O_3 and stoichiometric clinozoisite and epidote where x is the amount of introduced Fe_2O_3.

$$(3-x)\ CaAl_2Si_2O_8 + (x+1)\ CaO + (x)\ Fe_2O_3 + (2x)\ SiO_2 + H_2O \rightleftarrows$$
$$(2-2x)\ Ca_2Al_3Si_3O_{12}(OH) + (2x)\ Ca_2Al_2FeSi_3O_{12}(OH),\ \text{where } 0 \leq x \leq 1.$$

The composition of the aqueous phase proceeds along segment A-B corresponding with the extensive zone of stable clinozoisite/anorthite (propylitic alteration); petrographic investigations indicate that secondary quartz is not stable in this region. Quartz saturated in the aqueous phase at B, fixing the composition of the aqueous phase with respect to silica; the saturation line must occur at values of μSiO_2 lower than that necessary for a prehnite-stable assemblage. At C the composition of the aqueous phase crosses the clinozoisite/anorthite boundary; the reaction path proceeds along the fixed-μSiO_2 line within the clinozoisite field along segment B-C. Field relations demonstrating a sharp transition from endoskarn into exoskarn suggest that constant movement of the aqueous phase through point C must be maintained; fixed μSiO_2 precludes an extensive zone of mixed clinozoisite and grossularite in a moving aqueous phase. Segments along the reaction path from A to C represent a series of hydration reactions defining the endoskarn.

The generalized decarbonation reaction conserving CaO below is proposed to define the response to changing solution composition in the exoskarn:

$$3\ CaCO_3 + (x)\ Fe_2O_3 + (1-x)\ Al_2O_3 + 3\ SiO_2 \rightleftarrows$$

$$(x)\ Ca_3Fe_2Si_3O_{12} + (1-x)\ Ca_3Al_2Si_3O_{12} + 3\ CO_2.$$

Petrographic relations demonstrate that the quartz/garnet assemblage is stable beginning at point C and throughout the garnet zone unless wollastonite is present. The reaction path must continue to proceed along the fixed μSiO_2 line until wollastonite or calcite saturate in the aqueous phase at D or D', respectively. Two possible reaction paths are of interest; that which is followed at any given locality is dependent upon P_{CO_2} and/or temperature. If field relations show that if a pyroxene zone is present, the aqueous phase saturates with respect to wollastonite at D. The reaction path proceeds through the pyroxene zone along segment D-E until calcite saturates in the aqueous phase, i.e., the solution equilibrates with the carbonate wallrock. P_{CO_2} is relatively low in this first option. Alternately, if the pyroxene zone is absent in the field, the reaction path proceeds directly to D' where equilibrium with calcite is attained. P_{CO_2} is relatively high in this second option. Additional pyrometasomatic alteration is not possible after calcite has saturated with respect to the aqueous phase.

Mass Transfer

Pyrometasomatic alteration resulting from the introduction of an aqueous phase into wallrock with which it is not in equilibrium requires the introduction or removal of components. Korzhinski (1968) has distinguished two ideal metasomatic processes: infiltration metasomatism in which components are carried by the flow of solution forced by pressure gradients through permeable wallrock and diffusion metasomatism in which components of a solution move under action of the gradients of their chemical potentials through a stagnant pore solution. The introduction of mobile components from external sources and irregular zonation characteristic of phases which demonstrate solid solution are compatible with infiltration metasomatism. Korzhinski (1968) considers characteristic mineral assemblages in a systematic zonal arrangement to be a direct consequence of infiltrational metasomatism.

Quantitative calculations of mass transfer are possible employing the mass balance data as calculated earlier and presented in Table 2. The calc-silicate phases constituting representative endoskarn and exoskarn assemblages must be defined in terms of volume percent. The mass of each component in the system $CaO-Fe_2O_3-Al_2O_3-SiO_2-CO_2-H_2O$ summed over the total mass of all the phases documented in an assemblage which replaces 100 cm^3 of calcite may then be compared to the mass of the components constituting an equal volume of unaltered calcite to demonstrate introduction, conservation, or removal of components.

Figure 14 is a schematic diagram of mass transfer for the components $CaO-Fe_2O_3-Al_2O_3-SiO_2$ illustrating lateral variation in total mass of each component with respect to distance normal to the intrusive contact. SiO_2 and Al_2O_3 show similar mass distributions. The mass of these components on the intrusive side of the contact is independent of the hypogene hydrothermal alteration assemblage. The original Al_2O_3 and SiO_2 ratios are preserved between the reactant and product mineral phases, and chemical reactions occurring among the primary igneous minerals and their alteration products may be balanced conserving either component. The mass of SiO_2 or Al_2O_3 removed from the igneous rock immediately adjacent to the calc-silicates is as much as an order of magnitude less than the mass of SiO_2 added to the carbonate wallrock.

The distribution of CaO and Fe_2O_3 warrants more comprehensive discussion. The mass of CaO in 100 cm^3 of calcite is similar to the mass of CaO in an equal volume of any calc-silicate assemblage from the exoskarn as calculated earlier (Table 2). It remains essentially constant throughout the exoskarn and is similar to SiO_2 and Al_2O_3 from the intrusive in this respect. CaO may be considered as an immobile component, and chemical reactions occurring among calc-silicates in the exoskarn may be balanced conserving CaO.

The saturation of iron-bearing calc-silicates in response to variable chemical potential is reflected in the Fe_2O_3 concentration at

Figure 14 Quantitative diagram illustrating mass transfer in the system $CaO-Fe_2O_3-Al_2O_3-SiO_2-CO_2-H_2O$

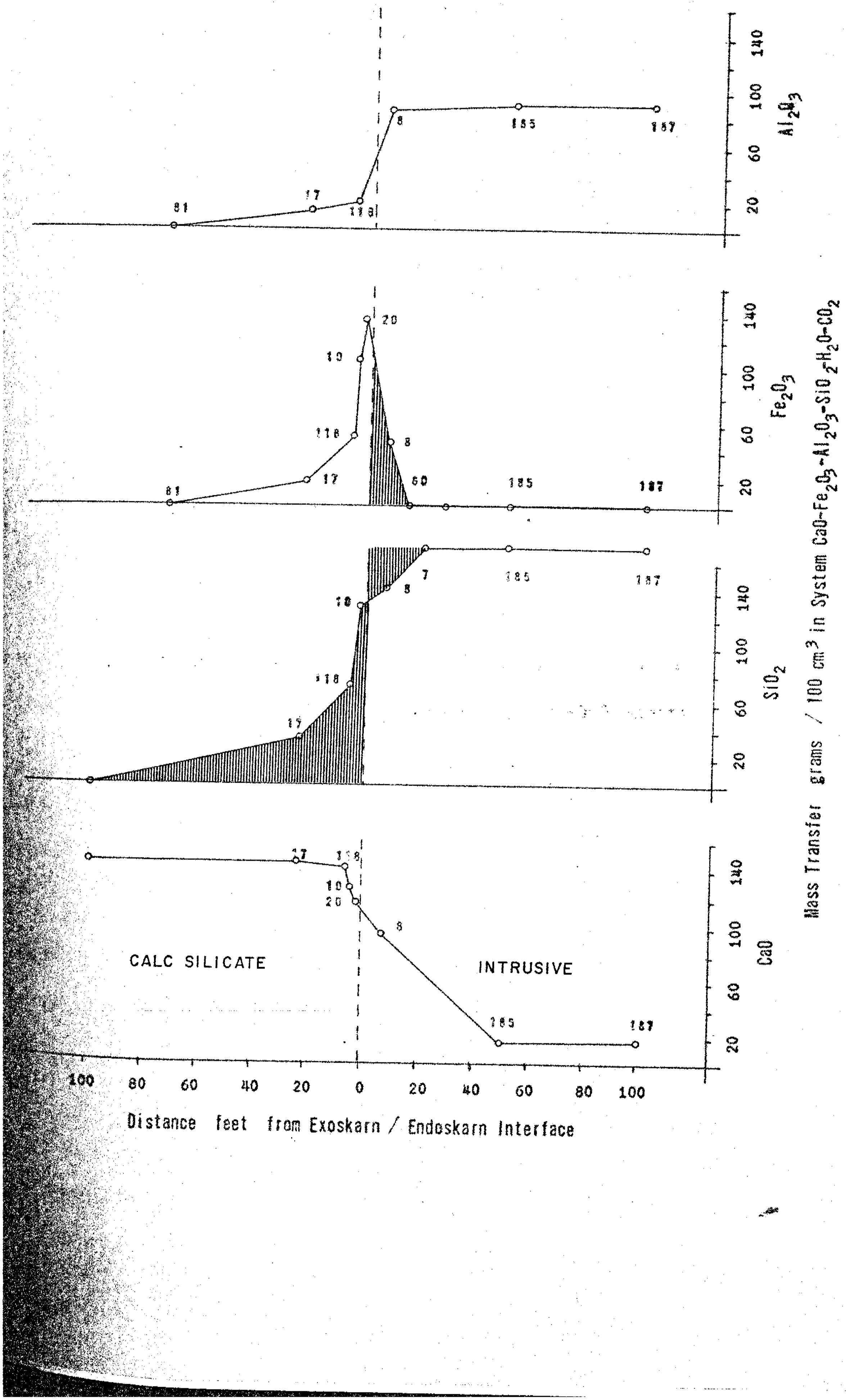
CALC SILICATE
INTRUSIVE
CaO
SiO_2
Fe_2O_3
Al_2O_3
Mass Transfer grams / 100 cm^3 in System $CaO-Fe_2O_3-Al_2O_3-SiO_2-H_2O-CO_2$
Distance feet from Exoskarn / Endoskarn Interface
100
80
60
40
20
0
20
40
60
80
100
20
60
100
140
81
17
118
10
20
8
7
60
185
187

the endoskarn-exoskarn interface. The mass of Fe_2O_3 in the exoskarn is an order of magnitude greater than the mass in either carbonate or intrusive wallrocks; there is no immediately apparent depletion adjacent to the enrichment. Diffusional transport is limited to distances of a few meters for geologically reasonable time periods and alone cannot explain the large mass of Fe_2O_3. Transport must be effected by a mobile aqueous phase which introduces the ferric iron component from an external source.

Three modes of origin for the external Fe_2O_3 source merit consideration. The first option requires the removal of ferric iron from rock units stratigraphically below the Bug Scuffle Limestone, aqueous phase transport up and along the intrusive contact, and localized concentration of iron-bearing calc-silicates in response to reaction of the transport medium with the carbonate wallrock. Similar origins have been proposed for the calc-silicate skarns immediately adjacent to the Hanover-Fierro Stock in Grant County, New Mexico. The Cambrian Bliss sandstone underlies Paleozoic units throughout southwest and south-central New Mexico, and a particularly iron-rich facies is present in the Hanover-Fierro area. This facies has been entirely leached of its iron content beneath the skarns. Extension of this mode of origin to the Jarilla Mountains is at best speculative; the primary weakness of this hypothesis is that, although the stratigraphy of the Jarilla Mountains is not unlike that of the Hanover-Fierro area, the iron-rich facies of the Bliss cannot be established with the data currently available.

The remaining alternatives call upon deuteric or hypogene hydrothermal alteration of the monzonitic intrusive. A well-developed but poorly exposed alteration zoning pattern in the monzonite coincides with the pediment gravels in the center of Section 3, T.22S., R.8E. Buried beneath the gravels is a central zone of orthoclase-quartz veining and matrix replacement, surrounded by a zone of quartz-sericite envelopes which border thick pyrite veins. The center is flanked by fresh to weakly-altered monzonite and pyrometasomatic alteration in roof pendants of carbonate wallrock. Concentric zones of actinolite and chlorite alteration of hornblende in the monzonite may be employed to subdivide the propylitic zone and are the basis for the two remaining modes of origin for the external source of Fe_2O_3.

Jaramillo (1973) documents a systematic variation with respect to hornblende alteration from the monzonite in which magnesian chlorite in the central zone is flanked by iron chlorite adjacent to pyrometasomatic alteration. A similar distribution in which magnesian chlorite and actinolite replace hornblende in intrusive rocks coincident with intense hypogene hydrothermal alteration, and iron chlorite partially replaces hornblende in fresh to weakly altered monzonite. The iron in the calc-silicates may be derived either from partial alteration of the mafics in monzonite adjacent to the pyrometasomatic alteration, or from pervasive alteration of the mafics in monzonite from the central zone. It is difficult to ascribe the source of Fe_2O_3 to assemblages in which iron chlorite is stable. This phase may reflect ferrous iron in transport which begins to saturate with respect to the aqueous phase before reaching the carbonate wallrock, or minimal leaching of ferrous iron from the original hornblende. It is more likely that the ferrous iron was derived from the more intensely altered monzonite where magnesian chlorite is stable. The mechanism for ferric iron saturation may be a ferrous-ferric oxidation-reduction couple induced by rising pH which is the response of the aqueous phase as it encounters carbonate wallrock with which it is not in equilibrium.

SUMMARY AND CONCLUSIONS

The Jarilla Mountains are formed by a complex suite of multiple intrusives flanked by pelitic and carbonate wallrocks of Virgillian and Missourian-DesMoinesian age. Metamorphic equivalents of the Bug Scuffle Limestone Member of the Gobbler Formation (Kottlowski, 1963) and the Beeman and Holder Formations (Pray, 1959) are exposed as xenoliths and roof pendants in the area of investigation.

The spatial and temporal relationships among granodiorite immediately to the north of the area of this study, and of hornblende monzonite and quartz latite within the area are documented by concise but comprehensive consideration of field and laboratory investigations. Jaramillo (1973) reports granodiorite intruded by monzonite immediately to the north, and quartz latite is intruded by monzonite in the area of investigation. Direct geologic relationships between granodiorite and quartz latite were not observed during the course of the field work. Similar fracture patterns in the granodiorite and quartz latite imply a roughly time coincident intrusion which is not shown by the monzonite. These data are compatible with the co-genetic relationship between granodiorite and quartz latite suggested by consideration of the compositional triangle $KAlSi_3O_8$-$NaAlSi_3O_8$-SiO_2. The K-Ar date of 47.1 ± 1.8 million years for the granodiorite is coincident with an advancing front of Laramide magmatic emplacement with progressive decrease in age to the east. Rocks of similar composition and intrusive sequence to the monzonite have been dated at 32 million years and are of mid-Tertiary age.

Pyrometasomatic alteration is extensively developed adjacent to intrusive contacts. Calcic plagioclase is altered to mineral asemblages which conserve the original Al_2O_3 and SiO_2 ratios, and form the endoskarn. Chemical reactions occurring among the igneous mineral phases may be balanced conserving either Al_2O_3 or SiO_2. The exoskarn is the reaction product of carbonate wallrock and an aqueous phase with which it is not in equilibrium. Calc-silicates show well-developed zonation of characteristic mineral assemblages systematically arranged radially away from intrusive monzonite. The calc-silicate zones are 1) clinozoisite-epidote, 2)andradite-grossularite, and 3) pyroxene moving progressively away from the intrusive.

Calc-silicate phase equilibria in compositional space may be documented employing isothermal, isobaric chemical potential diagrams. Chemical reactions occurring among calc-silicate phases in the exoskarn are balanced conserving CaO; similar reactions occurring in the endoskarn are balanced conserving Al_2O_3. The geometry of the chemical potential diagram in the system $CaO-Al_2O_3-SiO_2-CO_2-H_2O$ is compatible with an aqueous phase which emanates from the intrusive and moves into carbonate wallrocks. The possible reaction path in this report is suggested as a first approximation to progressive metasomatism in the system $CaO-Fe_2O_3-Al_2O_3-SiO_2-CO_2-H_2O$. The following series of generalized reactions is proposed to replace, in part, the traditional series of decarbonation reactions determined empirically by previous authors:

1) $2CaAl_2Si_3O_8 + H_2O \rightleftarrows Ca_2Al_3Si_3O_{12}(OH) + Al_2O_3 + SiO_2$

2) $4\ CaAl_2Si_2O_8 + (x)\ Fe_2O_3 + H_2O \rightleftarrows (2-2x)\ Ca_2Al_3Si_3O_{12}\ (OH)$

$+ (2x)\ Ca_2Al_2FeSi_3O_{12}(OH) + 2\ SiO_2 + (x+1)\ Al_2O_3$

and

3) $3\ CaCO_3 + (x)\ Fe_2O_3 + (1-x)\ Al_2O_3 + SiO_2 \rightleftarrows (x)\ Ca_3Fe_2Si_3O_{12}$

$+ (1-x)\ Ca_3Al_2Si_3O_{12} + 3\ CO_2$

where x indicates moles of Fe_2O_3, $0 \leq x \leq 1$.

SiO_2 and Fe_2O_3 must be introduced into the carbonate wallrock from the aqueous phase. These components are introduced from an external source, as evidenced by an absence of depletion adjacent to enrichment. The SiO_2 may be derived from hypogene hydrothermal alteration of the monzonite; however, only tentative suggestions regarding the origin of the Fe_2O_3 may be proposed. The most acceptable mode of origin with respect to the data currently available is leaching of ferrous iron from the potassically- and phyllically-altered hornblende monzonite. The mechanism of ferric iron saturation is a ferrous-ferric iron oxidation-reduction couple induced by rising pH in response to the aqueous phase encountering carbonate wallrock with which it is not in equilibrium.

This alternate approach to the classical decarbonation series in part accounts for the temporal and spacial relationships between the pluton environment and structure, alteration, and fluid flow. The first approximation to progressive metasomatism proposed herein cannot, however, fully describe the systematic and well-developed calc-silicate zonation. Complementary models might be put forth in which the style and duration of fluid flow or the isothermal, isobaric constraints of this investigation do not obtain.

Appendix A: Igneous Petrology

Textural Variations

The texture of typical granodiorite (Plate 8), hornblende monzonite (Plate 9), and quartz monzonite (Plate 10) is holocrystalline hypidiomorphic granular. The texture of typical quartz latite is holocrystalline allotriomorphic granular (Plate 11). The primary mineral phases are discussed below as they occur in a characteristic monzonite.

Plagioclase

Plagioclase occurs as euhedral to anhedral crystals in the groundmass with polysynthetic albite twinning, combined Carlsbad twinning, or albite-pericline twinning; it also occurs as zoned phenocrysts (Plate 12) which have andesine cores grading progressively outward into oligoclase. Anorthite contents are variable among different thin sections but remain internally consistant within the same section. Anorthite contents established by the Fouqué method of plagioclase determination range from An_{24} to An_{34}. Optical properties of plagioclase, a significant phase for which the properties may be regarded as a continuous function of composition, are listed in Table 3. Estimates of total plagioclase content derived from point counts of representative monzonites range from 14 percent to 36 percent and average approximately 30 percent.

Orthoclase

Orthoclase is the predominant potash feldspar, commonly occurring in the groundmass but rarely present as phenocrysts. Anhedral microcrystals range from 4 to 20 percent of the groundmass, but are usually less than 10 percent. Antirapakivi mantling of orthoclase over plagioclase has been

Plate 8 Photomicrograph illustrating holocrystalline hypidiomorphic granular texture of granodiorite

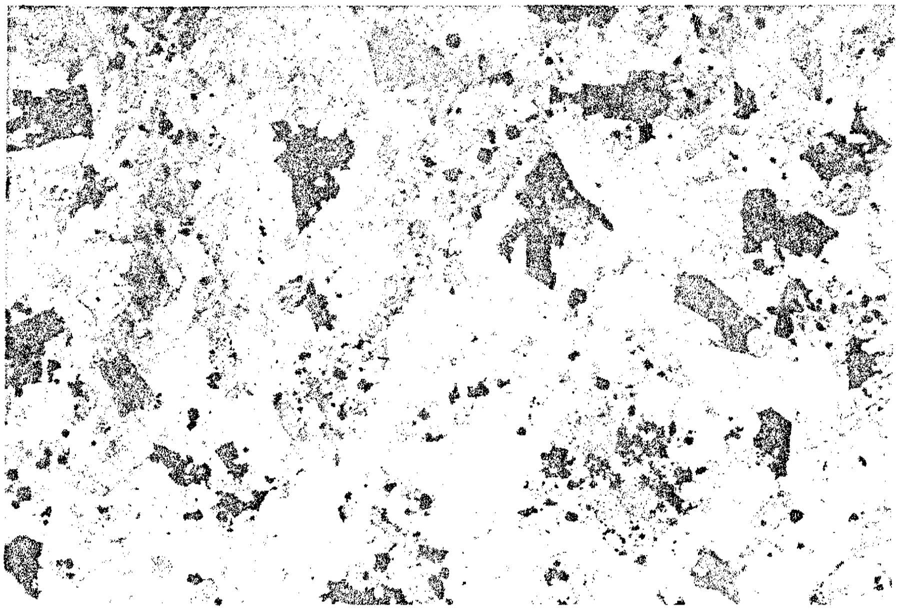

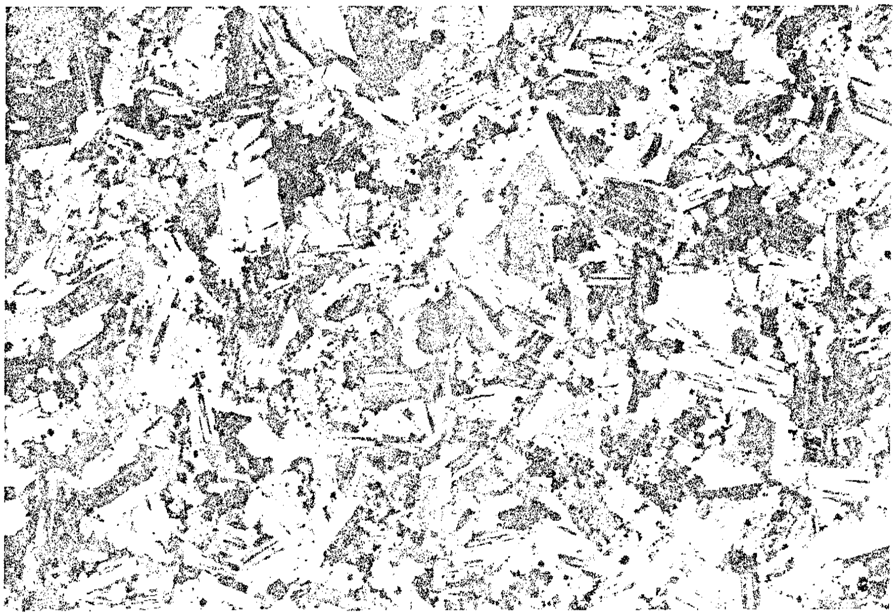

Plate 9 Photomicrograph illustrating holocrystalline hypidiomorphic granular texture of quartz monzonite

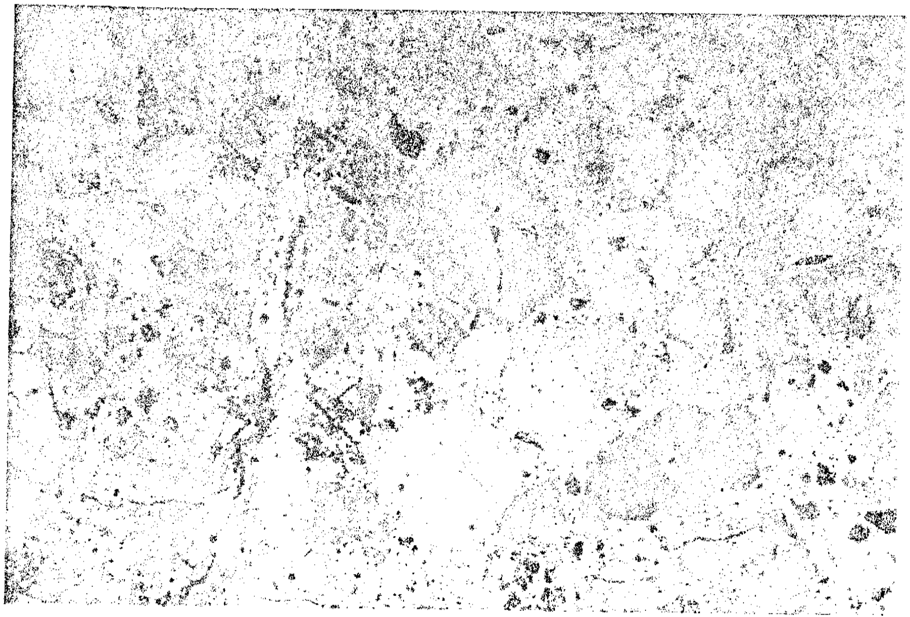

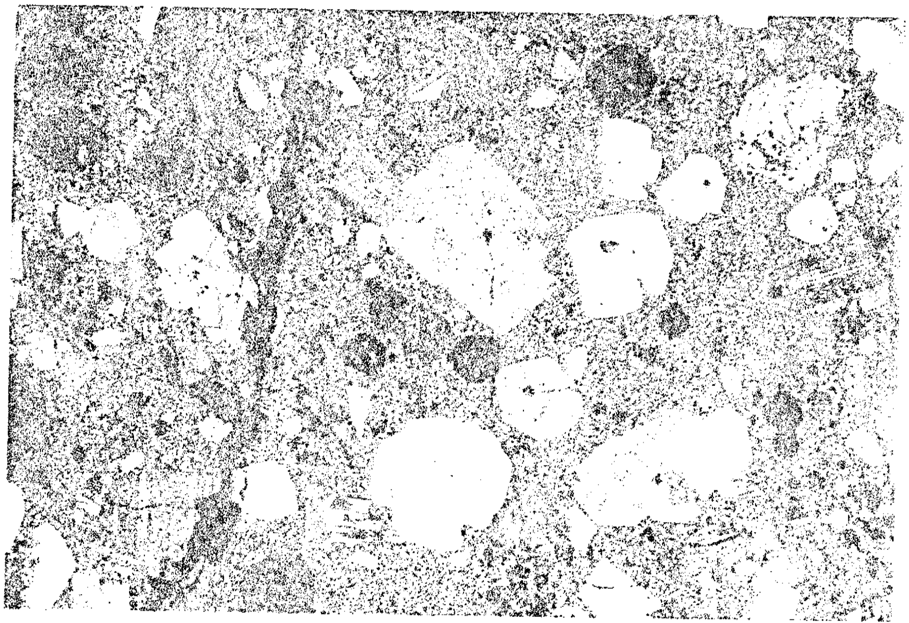

Plate 10 Photomicrograph illustrating holocrystalline allotriomorphic granular texture of quartz latite

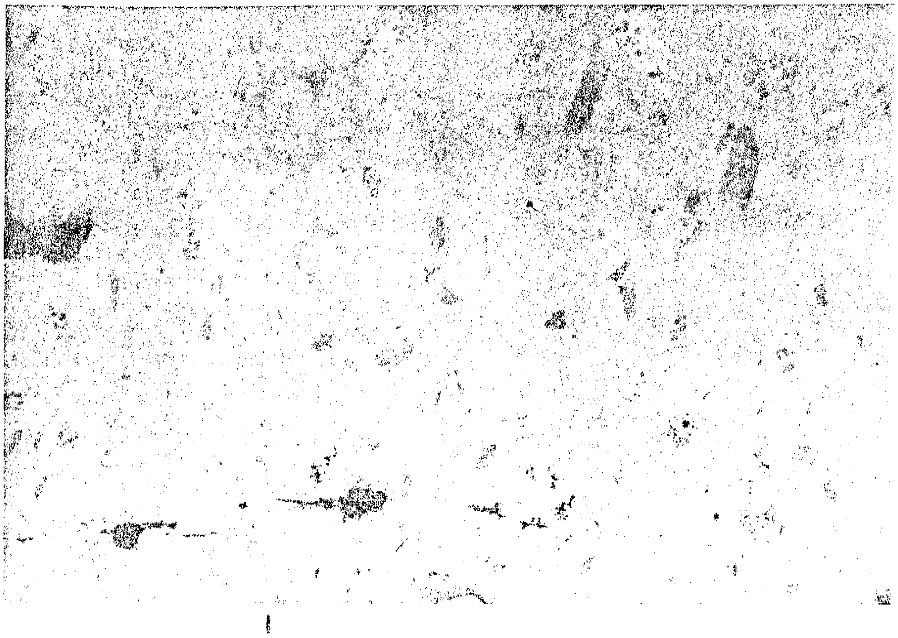

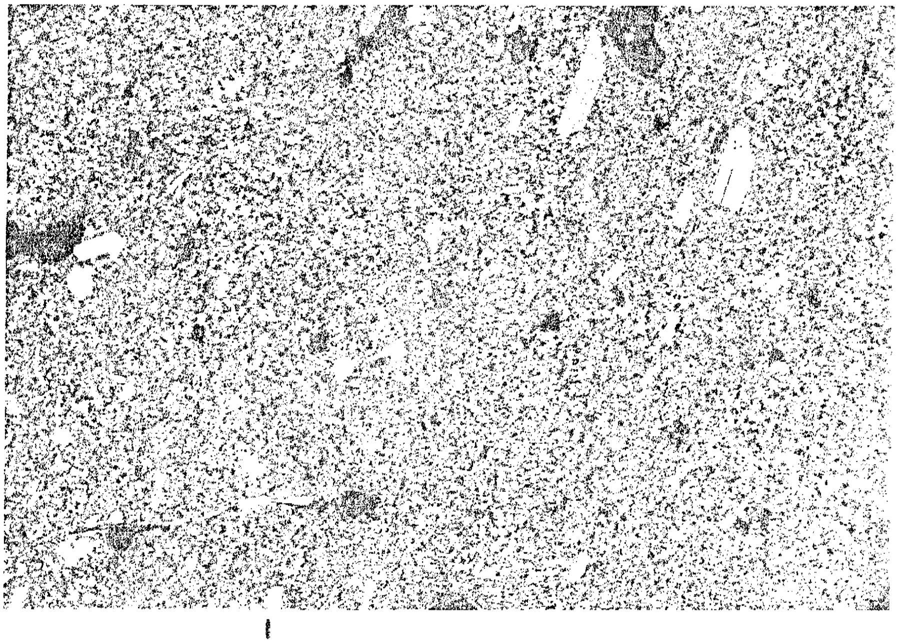

Plate 12 Photomicrograph illustrating plagioclase phenocryst in hornblende monzonite

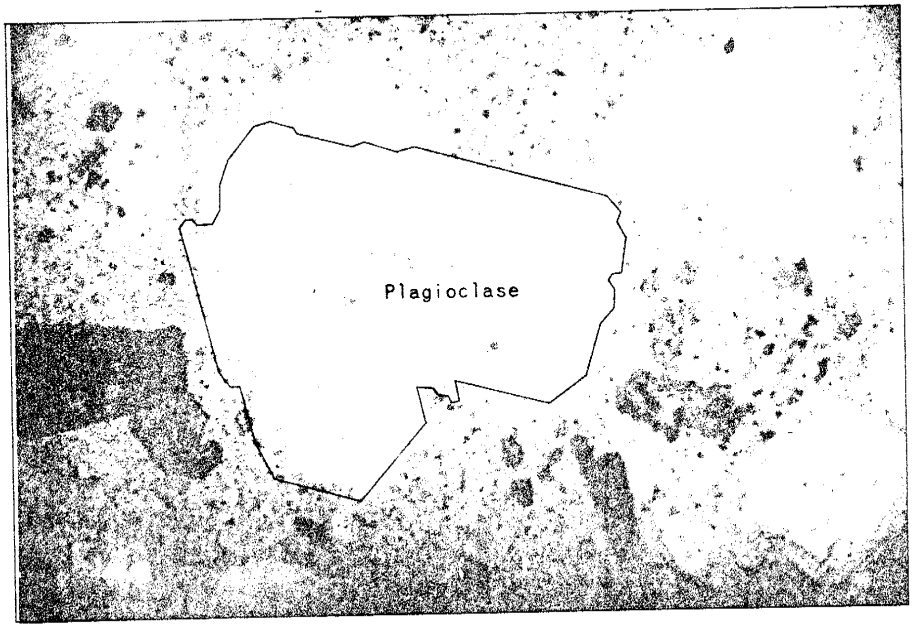

A. PLANE LIGHT × 30

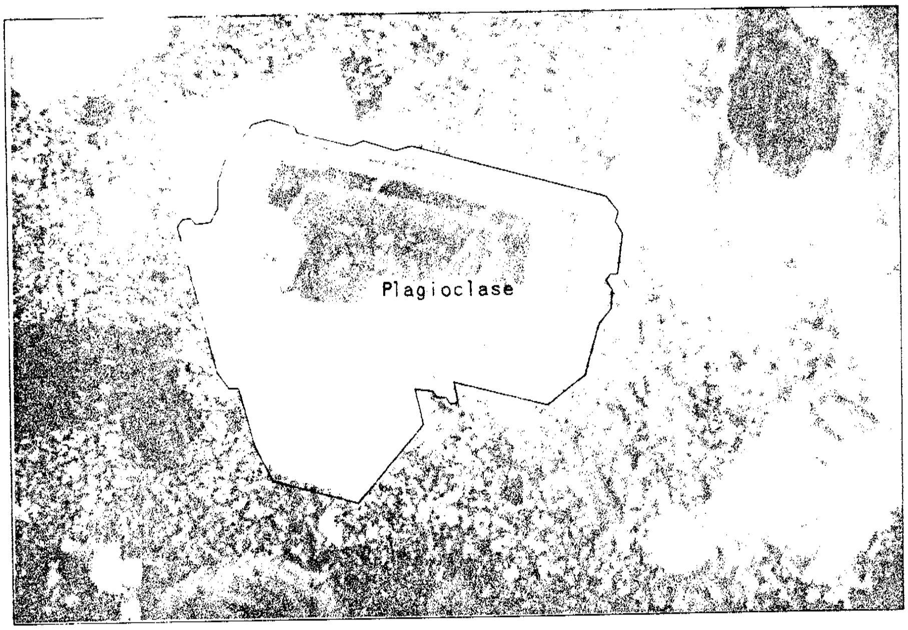

B. CROSSED NICOLS × 30

Plate 12

Appendix A (Table 3). Plagioclase Compositions from Hornblende Monzonite

Sample	Orientation	Measurement	Extinction Angle	An Content
66	z	y 001	+10° to +13°	26
150	z	y 010	+ 5° to +10°	26
153	z	y 001	+ 8° to +14°	28
157	z	y 010	+14° to +16°	32
171	z	y 001	+12° to +16°	30
176	x	y 001	- 2° to + 2°	30
178	z	y 010	+ 5° to + 7°	24
179	z	y 010	+10° to +16°	30
180	z	y 010	+16° to +18°	34
181	x	y 001	+ 4° to + 6°	24
182	x	y 001	- 8° to -10°	28
185	x	y 001	0° to + 3°	27
189	x	y 010	- 2° to - 6°	32
192	z	y 010	0° to +10°	24
193	x	y 001	- 6° to - 8°	35
197	z	y 001	+ 5° to + 9°	24
206	x	y 010	- 4° to - 6°	32

observed, but is rarely a primary igneous texture.

Quartz

Quartz occurs as anhedral microcrystals in the groundmass of all the monzonite facies. Matrix quartz ranges from 6 to 25 percent, but usually constitutes less than 10 volume percent. The quartz monzonite facies is identified on the basis of euhedral to subhedral phenocrysts ranging from 2 to 8 percent (Plate 13).

Hornblende

Hornblende is the most common characterizing accessory mineral. It occurs as prismatic euhedral to subhedral phenocrysts in the hornblende monzonite. Glomeroporphyritic texture with biotite, sphene, and magnetite (Plate 14) is common. Pleochroism is pale green to pale brown. Twinning along the (100) plane is not uncommon. Hornblende normally constitutes approximately 10 percent of a typical monzonite.

Biotite

Biotite is often a subordinate mafic mineral occurring as euhedral to subhedral phenocrysts in the hornblende monzonite facies. It locally appears to be replacing hornblende; however, primary igneous biotite is typical. Magnetite occasionally rims and is usually associated with the biotite. Biotite constitutes from 3 to 5 percent of a representative biotite-hornblende monzonite. The unique identification of secondary biotite versus primary biotite has not been attempted in this study.

Plate 13 Photomicrograph illustrating quartz phenocryst in quartz monzonite

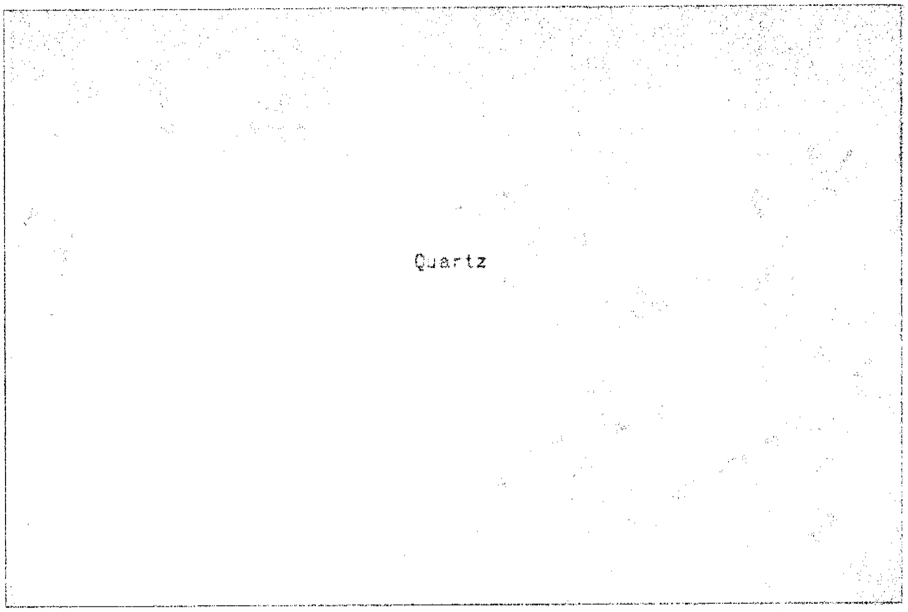

A. PLANE LIGHT × 30

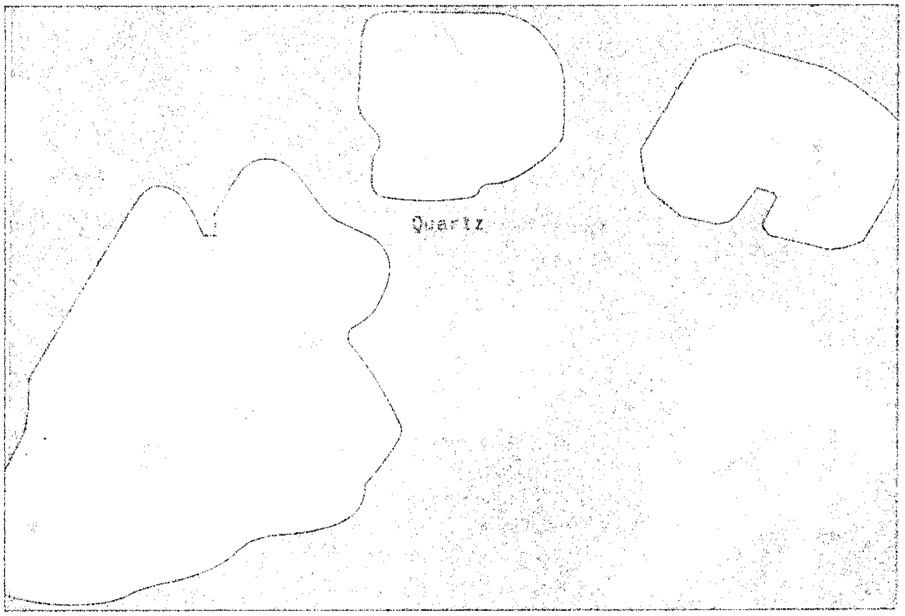

B. CROSSED NICOLS × 30

Plate 13

Plate 14 Photomicrograph illustrating glomeroporphyritic hornblende and biotite in hornblende monzonite

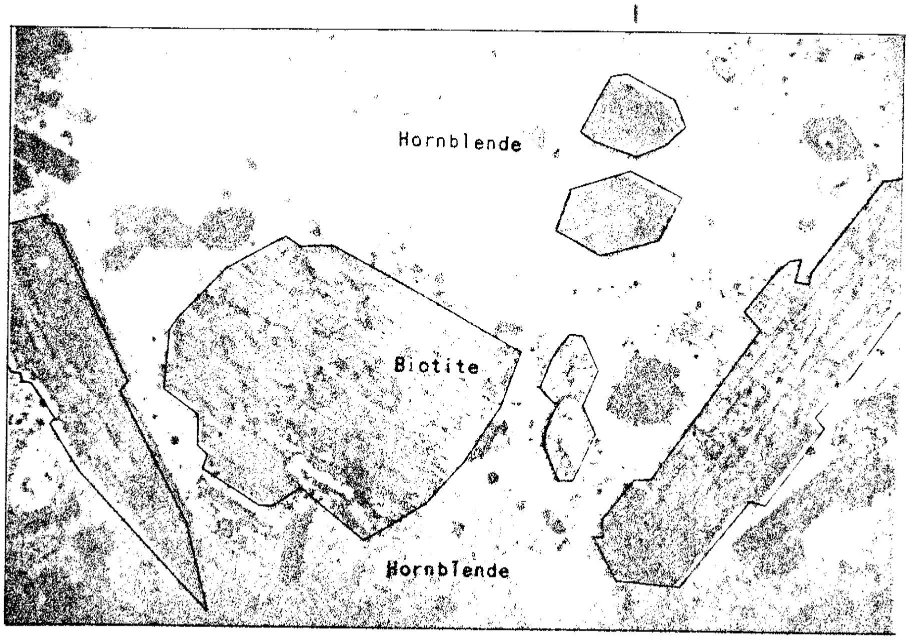

A. PLANE LIGHT x 30

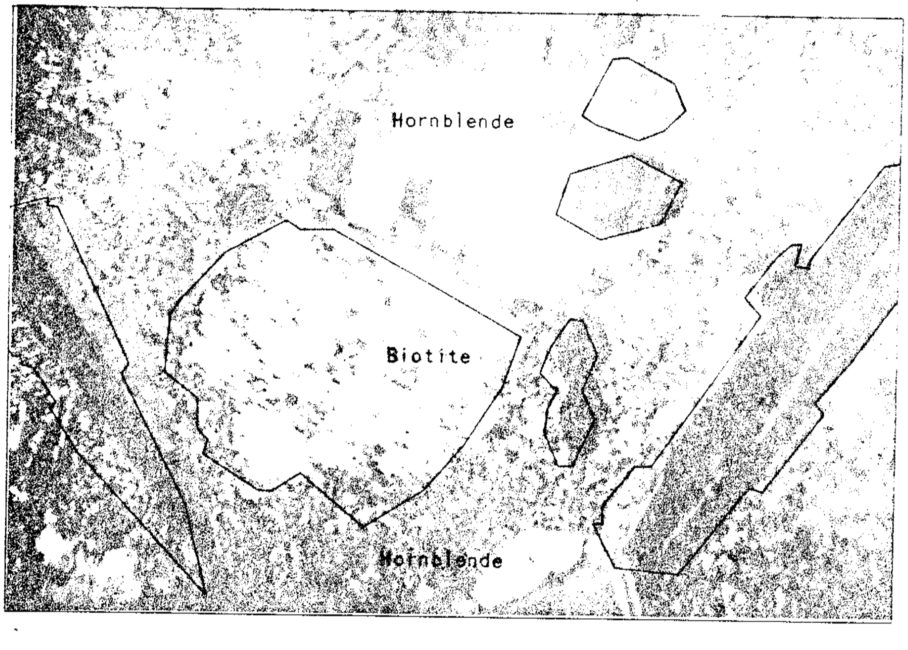

B. CROSSED NICOLS x 30

Plate 14

Appendix B: Analytical Procedures and Results

Igneous rock types collected in the field for geochemical analysis were chosen chiefly on the basis of areal distribution and freshness. Sample locations are shown on the overlay accompanying the geologic map of the area under investigation. At each location samples were taken in duplicate, providing a specimen for thin section and chemical analysis.

Preparation of rock samples for chemical analysis was accomplished by a procedure outlined by Hayslip (1973). The most likely sources of contamination were iron from jaw crushers, alumina from ceramic mixing vials, and silica from an agate morter grinder. Each of these cases involves major elements and very minor contamination; their influence on the analyses was considered negligible.

Analyses were performed by non-destructive X-ray fluorescence (XRF) using methods previously described (Condie, 1967 a,b). Forty-five samples of monzonite and five samples of the quartz latite were selected for complete analysis in order to identify gross trends on the compositional triangle $KAlSi_3O_8$-$NaAlSi_3O_8$-SiO_2. Counting was done entirely in the fixed-time mode. The major elements Si, Ti, Al, Fe, Mg, Ca, Na, and K were analyzed; the results of these analyses are listed in Appendix B, Table 4. U.S. Geological Survey standards W-1, BCR-1, T-1, GSP-1, AGV-1, SY-1, and G-2 and the French granite standards GH and GR were employed to construct major element calibration curves. Instrumental parameters for the XRF analysis and major element calibration curves statistics are listed in Appendix B, Tables 5 and 6, respectively.

Appendix B (Table 4). X-Ray Fluorescence Major Element Concentrations of Intrusive Rocks

Sample	HM-63	HM-75	HM-112	HM-151	HM-152	HM-153
Fe_2O_3	3.03	6.70	5.30	1.96	4.27	4.01
TiO_2	0.55	0.62	0.41	0.46	0.46	0.57
CaO	2.71	6.57	9.40	2.58	5.79	6.46
K_2O	2.87	3.11	5.51	3.72	3.72	2.99
SiO_2	65.32	62.23	61.63	64.41	63.16	63.48
Al_2O_3	17.19	15.52	15.21	15.76	14.78	15.94
MgO	tr	4.36	2.04	2.39	2.24	2.35
Na_2O	4.64	2.92	2.29	6.63	4.90	5.73
Total	96.31	102.03	101.79	97.91	99.36	101.53

Sample	HM-154	HM-155	HM-156	HM-157	HM-160	HM-161
Fe_2O_3	2.40	2.63	5.12	2.99	2.56	3.25
TiO_2	0.56	0.56	0.53	0.42	0.45	0.48
CaO	7.45	3.97	1.02	5.03	7.20	3.81
K_2O	1.69	4.71	2.02	3.61	1.45	2.98
SiO_2	62.70	63.87	64.31	64.51	63.60	64.64
Al_2O_3	12.16	16.12	15.73	15.72	15.10	17.74
MgO	2.87	3.16	3.64	1.36	0.96	0.61
Na_2O	8.83	5.05	7.21	4.36	9.95	4.98
Total	98.66	100.07	99.57	97.99	101.27	98.48

Appendix B (Table 4). X-Ray Fluorescence Major Element Concentrations of Intrusive Rocks (Cont.)

Sample	HM-162	HM-163	HM-164	HM-165	HM-168	HM-169
Fe_2O_3	2.93	5.75	4.40	3.50	4.53	3.67
TiO_2	0.48	0.39	0.48	0.47	0.44	0.49
CaO	7.69	4.25	4.87	3.27	5.01	7.03
K_2O	1.61	2.73	3.85	4.20	2.58	2.97
SiO_2	63.23	64.54	63.95	63.96	64.21	63.33
Al_2O_3	14.65	13.36	14.60	15.89	15.90	16.25
MgO	0.81	1.71	2.77	1.89	1.33	1.63
Na_2O	9.27	5.90	4.84	5.73	6.98	6.51
otal	100.69	98.65	99.76	98.90	100.97	101.98

ample	HM-170	HM-171	HM-172	HM-173	HM-174	HM-175
e_2O_3	3.17	5.96	4.81	3.22	4.27	3.37
iO_2	0.46	0.52	0.45	0.44	0.42	0.45
aO	3.80	4.73	3.56	4.66	5.69	4.53
$_2O$	4.03	3.23	4.12	3.82	3.01	3.05
iO_2	64.20	63.26	63.98	64.22	64.10	64.53
$_2O_3$	16.30	15.73	15.29	15.21	15.58	16.85
O	1.39	3.02	1.63	1.18	1.34	1.28
$_2O$	5.99	3.88	5.04	6.24	5.93	6.27
tal	99.34	100.34	98.89	99.00	100.35	100.33

Appendix B (Table 4). X-Ray Fluorescence Mjaor Element Concentrations of Intrusive Rocks (Cont.)

Sample	HM-176	HM-177	HM-178	HM-179	HM-180	HM-181
Fe_2O_3	5.11	4.62	4.71	2.85	4.29	4.82
TiO_2	0.48	0.44	0.47	0.43	0.53	0.55
CaO	3.37	4.80	4.67	5.53	4.98	4.60
K_2O	3.17	3.00	3.73	3.37	3.30	3.00
SiO_2	64.76	64.06	63.83	64.18	64.49	64.16
Al_2O_3	15.58	16.40	15.54	16.08	16.31	16.23
MgO	1.82	1.45	2.11	1.05	1.23	1.71
Na_2O	4.80	5.45	5.55	5.23	4.82	4.98
Total	99.09	100.21	100.61	98.72	99.95	100.05

Sample	HM-183	HM-184	HM-185	HM-186	HM-187	HM-188
Fe_2O_3	3.72	1.91	5.27	3.51	3.70	3.46
TiO_2	0.49	0.41	0.55	0.35	0.43	0.48
CaO	5.79	4.29	4.28	4.61	5.29	5.50
K_2O	3.20	3.91	2.70	4.42	3.50	3.32
SiO_2	64.13	64.60	64.29	65.16	63.62	63.43
Al_2O_3	15.27	17.27	16.48	14.93	15.65	16.13
MgO	2.49	1.30	1.78	0.45	1.47	1.33
a_2O	4.49	5.94	4.87	3.39	5.11	4.75
otal	99.59	99.62	100.22	96.80	98.77	98.40

Appendix B (Table 4). X-Ray Fluorescence Major Element Concentrations of Intrusive Rocks (Cont.)

Sample	HM-189	HM-190	HM-191	HM-192	HM-193	HM-194
Fe_2O_3	6.75	3.46	0.89	1.11	4.35	2.13
TiO_2	0.59	0.42	0.48	0.47	0.48	0.46
CaO	4.31	4.32	4.89	4.33	5.15	6.08
K_2O	2.76	3.31	4.05	3.88	2.90	3.60
SiO_2	63.88	64.23	64.33	64.16	63.67	63.94
Al_2O_3	11.85	16.41	16.39	16.59	15.75	15.70
MgO	2.29	1.08	1.60	1.21	1.72	1.67
Na_2O	4.86	5.99	6.05	6.08	4.66	4.11
Total	97.30	99.22	98.69	97.74	98.68	97.69

Sample	HM-195	QL-196	QL-197
Fe_2O_3	4.18	0.61	4.90
TiO_2	0.44	0.07	0.08
CaO	3.30	0.20	0.16
K_2O	3.48	3.54	4.16
SiO_2	64.17	73.65	71.75
Al_2O_3	16.35	16.81	16.88
MgO	1.92	tr	tr
Na_2O	4.11	5.51	4.29
Total	97.97	100.39	102.22

Appendix B (Table 5). X-Ray Fluorescence Instrumental Parameters

Line	Tube	KV	MA	Xtal	Pos	Peak	Bgrd	Col[1]	Path	Counter	HV	BL[2]	Wndo[3]	Gain
Fe Ka	Cr	30	15	Qtz	1	33.68	34.68	F	Scint	Air	950	0.11	0.32	16
Ti Ka	Cr	35	15	Qtz	1	48.50	47.50	F	Scint	Air	960	0.12	0.30	20
Ca Ka	Cr	20	10	Qtz	1	60.35	59.35	F	Vac	P-10	1720	0.04	0.28	32
K Ka	Cr	40	20	Qtz	1	69.25	72.50	F	Vac	P-10	1690	0.06	0.52	32
Si Ka	Cr	50	35	Gyp	2	25.65	26.65	C	Vac	P-10	1780	0.04	0.44	20
Al Ka	Cr	40	20	Gyp	2	36.40	37.35	C	Vac	P-10	1780	0.08	0.38	20
Mg Ka	Cr	50	35	Gyp	2	51.00	52.00	C	Vac	CH_4	2800	0.02	0.20	20
Na Ka	Cr	50	25	Gyp	2	73.10	74.20	C	Vac	CH_4	2900	0.08	0.34	12

[1] Col = Collimator

[2] BL = Base Line

[3] Wndo = Window

Fixed Time = 10 second counts

Appendix B (Table 6). X-Ray Fluorescence Calibration Curve Statistics

Element		Equation	Accuracy
Fe	=	(ratio - 0.1317)/0.3348	4.02% RMS error
Ti	=	(ratio - -0.0636)/1.0329	5.76% RMS error
Ca	=	(ratio - -0.0278)/0.2056	4.78% RMS error
K	=	(ratio - 0.0652)/0.1967	1.78% RMS error
Si	=	(ratio - -0.5046)/0.0254	0.80% RMS error
Al	=	(ratio - 0.0169)/0.0698	2.70% RMS error
Mg	=	(ratio - 0.3016)/0.4536	3.13% RMS error
Na	=	(ratio - -1.7280)/0.6738	5.10% RMS error

Appendix C: Metamorphic Petrology

Andradite-Grossularite-Spessartite

Garnet occurs as idioblastic porphyroblasts and in idioblastic to xenoblastic aggregates. The composition is variable, falling within the andradite-grossularite binary solid solution. Index of refraction measurements using thallium-arsenic oils calibrated in steps of 0.02 yielded "n" values between 1.82 and 1.88 ± 0.01 indicating, when combined with cell edge data (Sriramadis, 1957), relatively pure andradite (Ad_{60} - Ad_{95}). Unit cell volumes were obtained from Bragg's equation, generally using the (642) reflection of the garnet; the diffraction peaks proved to be broad, indicating slightly variable composition zoning). Calculated mean cell edge measurements ranged from 11.969 Å o 12.037 ± 0.05 Å. The spessartite molecule ($Mn_3Al_2Si_3O_{12}$) locally ubstitutes for as much as 5 percent of the grossularite molecule $Ca_3Al_2Si_3O_{12}$).

Many of the garnets are anisotropic. This is especially true of ne porphyroblastic garnets which are often significantly birefringent; wever, the fine-grained garnet hornfels are generally isotropic. The llowish-colored, high index andradite is generally isotropic, whereas e green to colorless grossularite of relatively low indices tends to anisotropic. This anomalous birefringence could possibly be related the grossularite content. Recent work by Ito and Arem (1970) nonstrates limited solid solution of idocrase and grossularite. The stal structures of these phases are similar (Deer, et al., 1962); imited distortion of the grossularite structure towards idocrase could result in a strained garnet lattice and birefringence in an isotropic phase. Plate 15 illustrates anomalous birefringent andradite-grossularite garnet.

Clinozoisite-Epidote

Epidote solid solution is discussed herein as the product of pyrometasomatic alteration of calcic plagioclase from the monzonite; however, epidote-bearing assemblages are not precluded in the exoskarn where there are interbedded pelitic sediments.

Zoning is a common feature of epidote solid solution; small changes in composition are reflected by significant differences in the optical properties. Ferric iron and aluminum substitution is accompanied by an increase in the optic axial angle, but this optical property is particularly sensitive to compositional variation and cannot be used as a precise indication of ferric iron to aluminum ratios. A satisfactory linear relationship between refractive indices and composition of high-iron epidotes has not been established; therefore, mass balance calculations employing analysis of epidote concentrates from the endoskarn afford the only reasonable estimates of composition. These data indicate that the composition is variable within a fixed range near the clinozoisite-epidote boundary. Plate 16 illustrates idioblastic clinozoisite-epidote porphyroblasts from the epidote zone (endoskarn).

Pyroxene, variety Wollastonite

Wollastonite is restricted to marbles peripheral to the garnet zone. Radiating masses are as much as two millimeters in diameter set in a matrix of very-finely-matted wollastonite crystals; idioblastic porphyroblasts from these aggregates are on the order of 0.02 millimeters

Plate 15 Photomicrograph illustrating anomalous birefringent andradite-grossularite from the garnet zone (exoskarn)

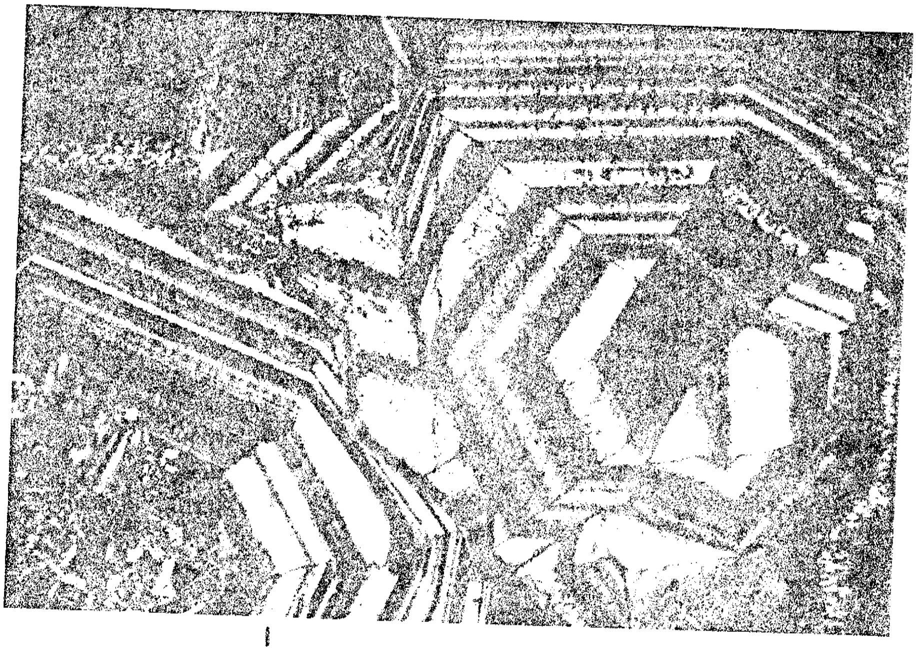

Plate 16 Photomicrograph illustrating idioblastic clinozoisite-epidote from the epidote zone (endoskarn)

in length (Plate 17). The minute size of individual wollastonite crystals precludes detailed petrographic investigation.

Pyroxene, variety Diopside-Hedenbergite

Pyroxene of the diopside-hedenbergite series commonly accompanies wollastonite in small quantities and is associated with massive magnetite replacements in carbonate units of the Panther Seep equivalent. Examination of thin sections indicates that they contain no pyroxene of idioblastic or sub-idioblastic character suitable for extinction angle measurement. Brownish-green color in thin section and weak pleochroism from pale-green or yellowish-green to light-bluish-green suggest a pyroxene rich in the hedenbergite end member.

Chlorite

Two members of the chlorite group, tentatively identified as delessite and penninite, were observed as alteration products of the calc-silicates. The exceedingly fine grain size renders determination of the optical properties difficult and inaccurate. The nomenclature in this report is based upon observable physical characteristics such as norphology.

Delessite is an alteration product of garnet-bearing assemblages. t is pleochroic from green to nearly colorless. The interference olors are weak and not appreciably anomalous. Delessite is most asily distinguished from penninite by the characteristic spherulitic exture (Plate 18).

Penninite is also an alteration product of calc-silicates, but t is usually associated with clinozoisite-epidote. Pleochroism is eaker than that of delessite; the interference is a distinctive

Plate 17 Photomicrograph illustrating fine-grained pyroxene (wollastonite-hedenbergite) from the pyroxene zone (exoskarn)

A. PLANE LIGHT x 30

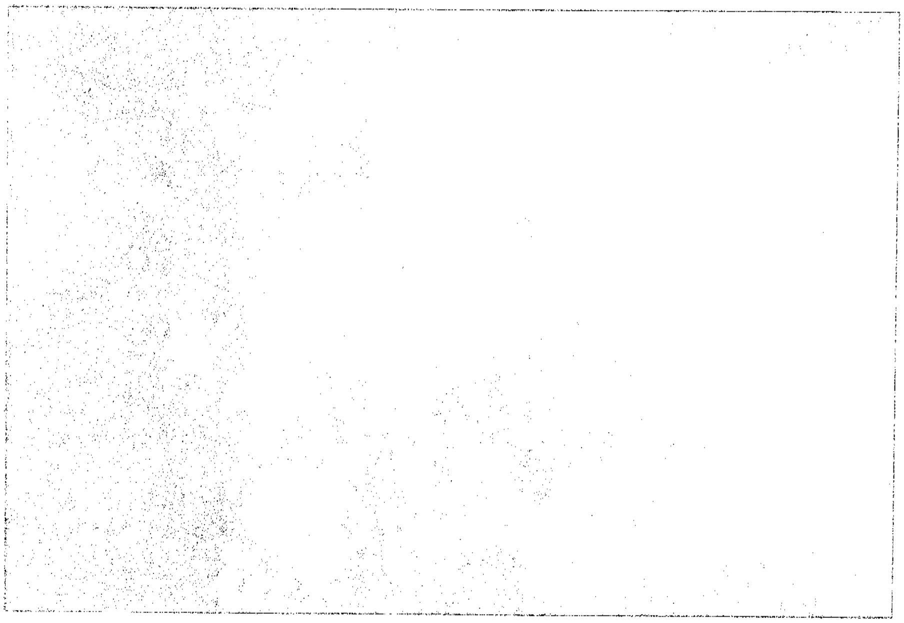

B. CROSSED NICOLS x 30

Plate 17

Plate 22 Photomicrograph illustrating chlorite, variety delessite, from the garnet zone (exoskarn)

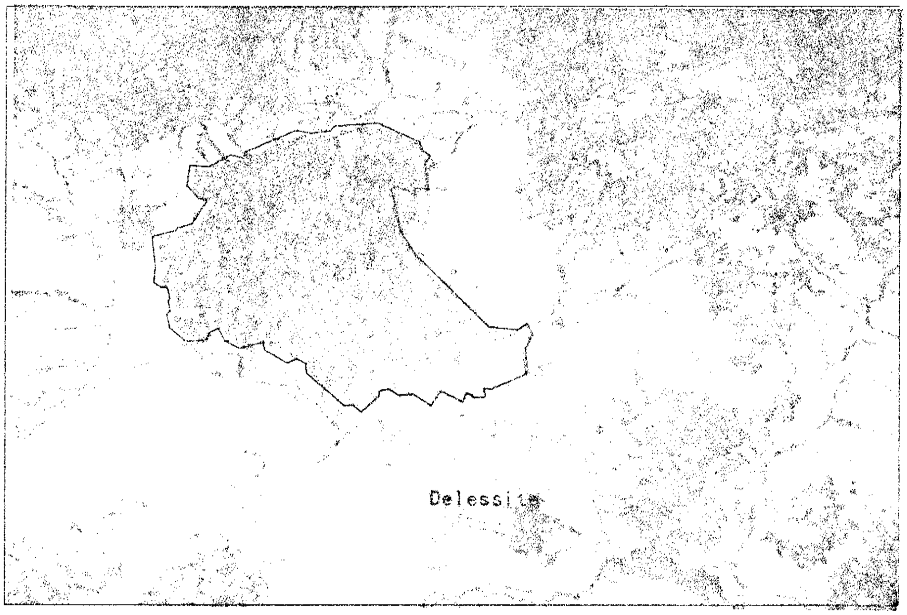

A. PLANE LIGHT x 30

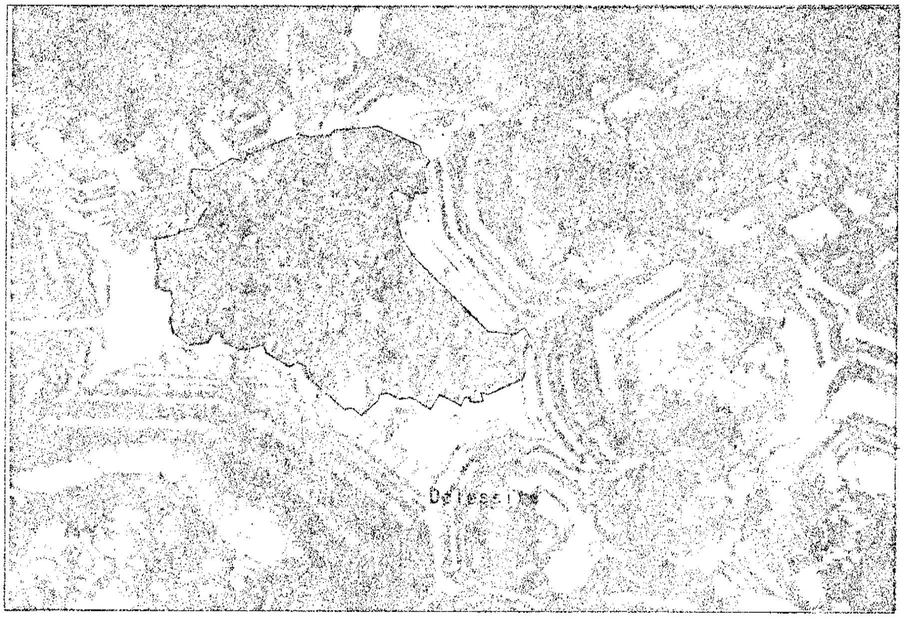

B. CROSSED NICOLS x 30

Plate 22

anomalous "Berlin Blue". The morphology is also different from that of delessite, occurring as fan-shaped aggregates occupying interstices among idioblastic epidote porphyroblasts. Where alteration has been particularly intense, skeletal epidote crystals are set in penninite and exhibit grain boundaries embayed by penninite.

Quartz

Quartz is a subordinate phase common to all the calc-silicate zones. It is invariably xenoblastic, occurring interstitially with clinozoisite-epidote and grossularite-andradite. Idioblastic clinozoisite-epidote often poikiolitically engulfs xenoblastic quartz grains. Quartz is also associated with specular hematite and calcite in late-stage veins in the garnet zone (Plate 19). Mosaics of equant quartz grains are common in veins as much as 10 millimeters in width; the grains frequently exhibit undulatory extinction with intergranular hematite blades.

Calcite

Calcite is the most frequently encountered xenoblastic phase, usually present as large, optically continuous masses and mosaics of fine-grained intergrowths. It is easily recognized by its distinctive birefringence and variable relief.

Tremolite-Ferrotremolite

An amphibole of the tremolite-ferrotremolite series is locally present in clinozoisite-epidote rocks of the endoskarn. Grayish green, fibrous porphyroblasts of this amphibole as much as 2 millimeters in length occur in a matrix of granoblastic clinozoisite-epidote (Plate 20). Quartz, calcite, and epidote are frequently poikiblastically enclosed in the amphibole, and relict plagioclase may often be spatially

Plate 18 Photomicrograph illustrating specular hematite blades and quartz with undulatory extinction from the garnet zone (exoskarn)

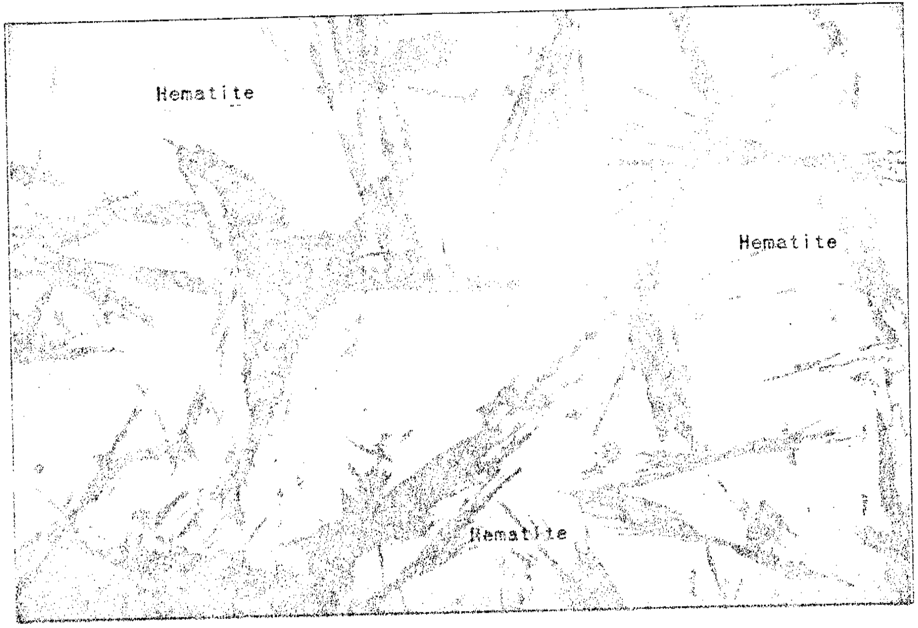

A. PLANE LIGHT x 30

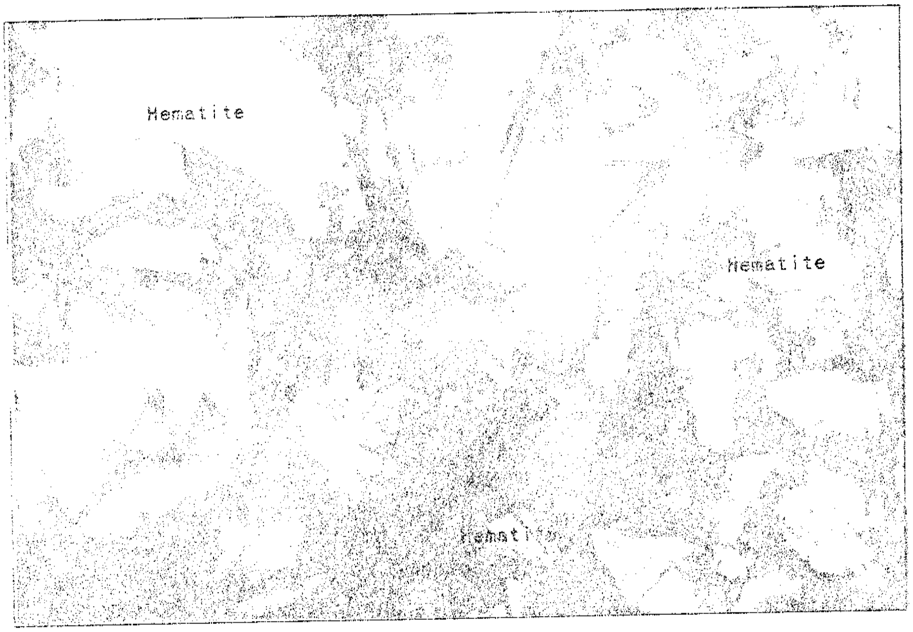

B. CROSSED NICOLS x 30

Plate 18

Plate 19 Photomicrograph illustrating amphibole of the actinolite-ferrotremolite series from the epidote zone (endoskarn)

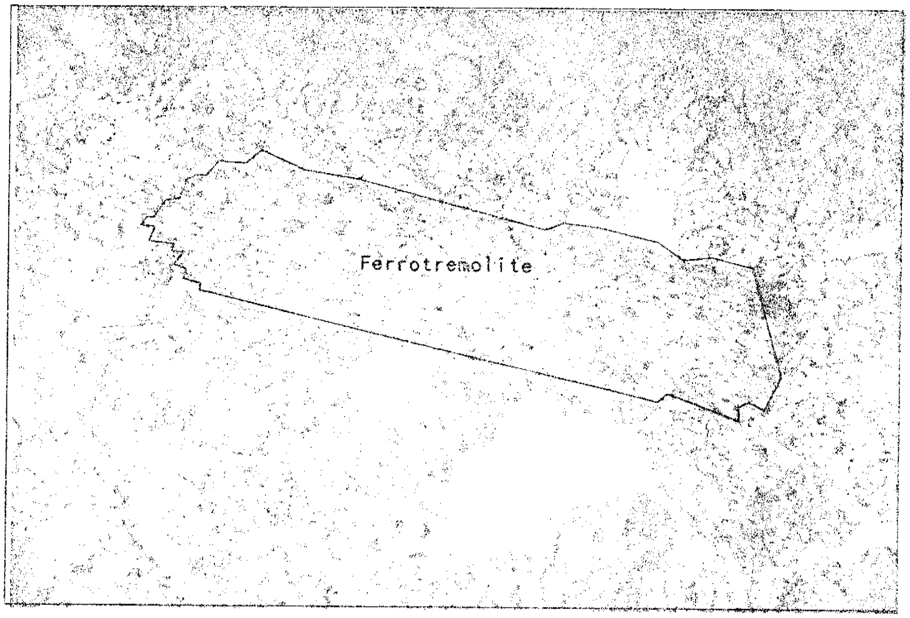

A. PLANE LIGHT x 30

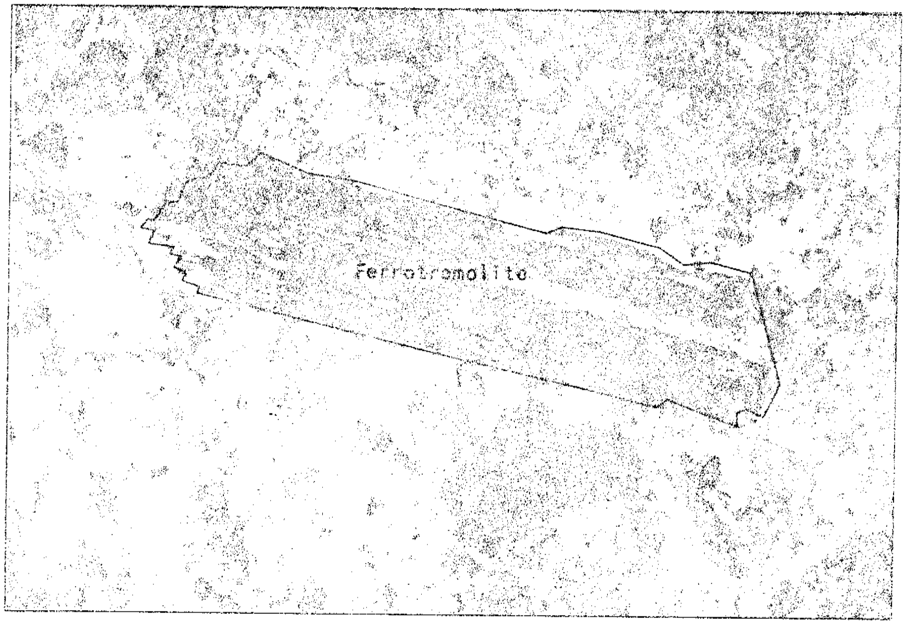

B. CROSSED NICOLS x 30

Plate 19

associated (Plate 21). Burt (1972) suggests that amphiboles are products of a late hydrothermal stage of calc-silicate growth in which the original anhydrous skarn minerals undergo retrograde reactions to hydrous mineral phases. The texture observed in this petrographic investigation does not warrant such a conclusion; the amphibole appears to be a primary calc-silicate phase.

Major variations in the optical properties of the tremolite-ferrotremolite series are related to the replacement of magnesium by ferrous iron. Reliable correlations between iron content and extinction angles are not currently available (Deer, et al., 1962); the amphibole is not amenable to a unique determination of composition employing optical techniques. Pleochroism is a quantitative property proportional to iron content. Tremolite and low-iron actinolite are non-pleochroic, whereas this amphibole is moderately to strongly pleochroic from light-olive-gray to greenish-gray, suggesting that this phase has a significant iron content.

Idocrase

With the exception of the possible solid solution with grossularite, isocrase is restricted to the endoskarn. The typical assemblage is clinozoisite-epidote-quartz-calcite±idocrase. The idocrase is xenoblastic, occurring interstitially among idioblastic to xenoblastic clinozoisite-epidote. Idocrase strongly resembles, and may be difficult to distinguish from, the epidote; the higher relief, lower birefringence, and absence of pleochroism aid in the identification. Basal sections of idocrase may show four diagonal sectors with the optic axial plane perpendicular to the edge of each sector (Deer, et al., 1962).

Plate 20 Photomicrograph illustrating relict plagioclase from the epidote zone (endoskarn)

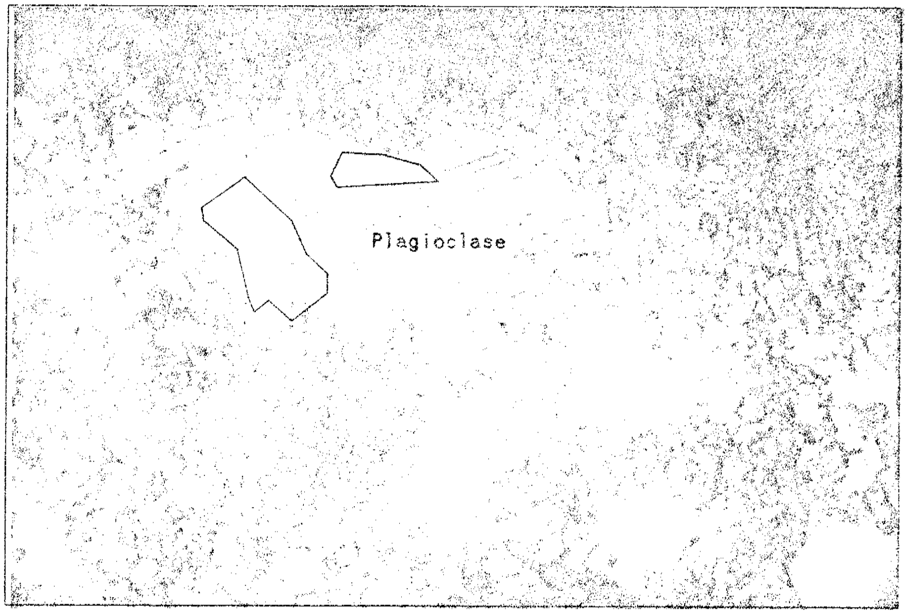

A. PLANE LIGHT x 30

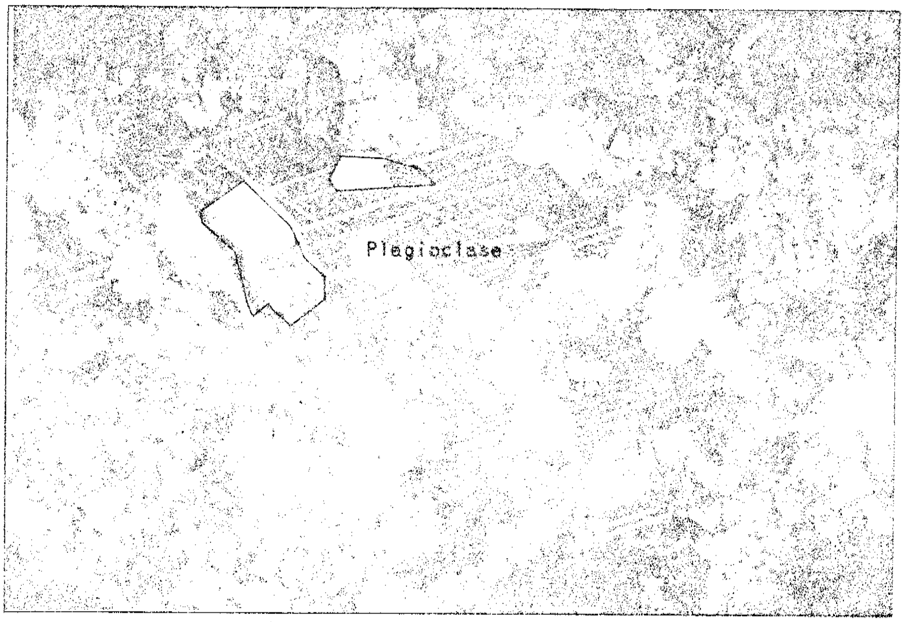

B. CROSSED NICOLS x 30

Plate 20

The variation from ideal idocrase caused by ionic replacements in the structure are often significant; consequently, the physical and optical characteristics are irregular and not amenable to precise compositional determination by optical techniques.

Appendix D:. Wet Chemical Analyses - Analytical Procedures and Results

Calc-silicate rock samples collected in the field for wet chemical analysis were chosen chiefly on the basis of characteristic mineral assemblages with respect to areal distribution. Sample locations are shown on the overlay accompanying the geologic map of the area under investigation. At each location samples were taken in duplicate, providing a specimen for both petrographic and chemical analysis.

Preparation of rock samples for chemical analysis was accomplished by a procedure outlined by Hayslip (1973). Contaminant sources are similar to those described for X-ray fluorescence.

Analyses were performed using methods previously described by the U.S. Geological Survey. Comprehensive descriptions of the procedures employed are available in the references below. SiO_2, H_2O and S were determined gravimetrically. Al_2O_3, MgO, Na_2O, K_2O, and TiO_2 were determined by atomic absorption. Colorimetric procedures were employed for P_2O_5 and MnO analyses. Fe_2O_3 and CaO were determined by atomic absorption and verified by titration. FeO analyses were performed by titration. Gas evolution (thermogravimetric) techniques were employed for CO_2 analyses.

References cited for silicate analyses

Peck, L.C., 1964, Systematic analysis of silicates: U.S. Geol. Survey Bull. 1170, 89 p.

Shapiro, L. and Brannock, W. W., 1956, Rapid analysis of silicate rocks: U.S. Geol. Survey Bull. 1036-C, 56 p.

Appendix D (Table 7). Wet Chemical Major Element Concentrations of Calc-Silicate Rocks Reported in Weight %

Sample	CS-2	CS-7	CS-8	CS-10	CS-17
Fe_2O_3	9.70	25.60	10.60	26.10	4.60
FeO	0.64	2.60	3.20	1.10	0.26
MnO	0.20	0.19	0.10	0.31	0.09
CaO	18.30	25.50	21.60	30.60	52.40
K_2O	1.32	0.84	0.56	0.06	0.06
SiO_2	46.40	29.70	33.20	34.80	5.60
Al_2O_3	10.20	3.50	9.80	2.00	0.75
MgO	4.40	0.71	2.04	0.56	0.20
Na_2O	2.72	1.44	0.06	0.02	0.007
CO_2	0.50	8.80	5.90	0.60	27.00
Total	97.98+	98.88+	87.06+	96.15+	90.97+

Sample	CS-20	CS-22	CS-25	CS-49	CS-60
Fe_2O_3	32.60	12.10	2.0	7.40	11.00
FeO	0.51	0.90	3.80	1.40	0.77
MnO	0.23	0.18	0.05	0.11	0.10
CaO	28.30	24.20	2.30	17.70	21.60
K_2O	0.06	0.26	3.80	0.09	1.10
SiO_2	35.60	32.60	62.50	57.50	37.60
Al_2O_3	1.60	14.40	14.20	3.60	13.20
MgO	0.23	0.18	0.05	0.11	2.91
Na_2O	0.007	0.03	3.20	1.70	0.16
CO_2	0.30	5.00	1.60	8.00	3.70
H_2O	0.11		0.09		
Total	99.55	89.85+	93.59	97.61+	92.14+

Appendix D (Table 7). Wet Chemical Major Element Concentrations of Calc-Silicate Rocks (Cont.)

Sample	CS-66	CS-69	CS-71	CS-81	CS-113
Fe_2O_3	5.60	26.10	12.40	0.71	12.40
FeO	1.30	1.70	1.10	0.51	0.77
MnO	0.15	0.15	0.22	0.06	0.14
CaO	15.60	14.80	24.20	43.70	21.80
K_2O	0.43	0.05	0.09	0.38	1.00
SiO_2	44.60	44.20	36.00	30.10	34.20
Al_2O_3	14.50	0.85	11.70	0.94	12.30
MgO	1.59	0.79	1.39	1.84	2.32
Na_2O	5.20	0.02	0.67	0.13	0.13
CO_2	5.00	9.60	7.70	21.4	5.90
H_2O	0.16	0.05		0.07	0.13
Total	94.13	98.31	95.47+	100.50	91.09

Sample	CS-118	CS-128	CS-129	CS-130	CS-135
Fe_2O_3	15.70	3.70	26.60	16.30	9.00
FeO	1.00	0.39	12.00	3.30	3.20
MnO	0.24	1.31	0.10	0.31	0.26
CaO	33.70	23.20	5.30	30.00	17.30
K_2O	0.06	0.09	0.12	0.09	0.16
SiO_2	30.60	51.40	27.80	27.80	41.30
Al_2O_3	1.20	0.75	tr	2.50	11.10
MgO	3.20	16.70	20.20	1.95	1.22
Na_2O	0.02	0.08	0.04	0.007	0.48
CO_2	23.00	0.20	tr	12.00	3.50
Total	108.9	97.82+	92.16+	94.26+	87.52+

REFERENCES CITED

Anderson, T.H. and Silver, L.T., 1974, Late cretaceous plutonium in Sonora, Mexico, and its relationship to Circum-Pacific magmatism [abstr.]: in Rocky Mountain Section, 27th Annual Meeting, Geol. Soc. Am., Abstr., vol. 6, no. 5, p. 484.

Beane, R.E., 1974, Biotite stability in the porphyry copper environment: Econ. Geol., v. 69, p. 241-256.

Bowen, N.L., 1940, Progressive metamorphism of siliceous limestone and dolomite: J. Geol., v. 48, p. 225-274.

Brown, T.H., 1971, Theoretical predictions of equilibria and mass transfer in the system $CaO-MgO-SiO_2-H_2O-CO_2-NaCl-HCl$: Ph.D. thesis, Evanston, Ill., Northwestern University, 135 p.

Burt, D.M., 1972, Mineralogy and geochemistry of Ca-Fe-Si skarn deposits: Ph.D. thesis, Cambridge Mass., Harvard University.

Condie, K.C., 1967a, Geochemistry of early Precambrian graywackes from Wyoming: Geochim. Cosmochim. Acta, v. 31, p. 2135-2149.

__________, 1967b, Petrology of the late Precambrian tillite association in northern Utah: Geol. Soc. America Bull., v. 78, p. 1317-1344.

Deer, W.A., Howie, R.A., and Zussman, J., 1962, Rock-forming minerals, 4 vols.: London, Longmans, Green and Co.

Dunham, K. C., 1935, The geology of the Organ Mountains: N. Mex. Inst Min. and Tech., State Bur. Mines and Mineral Res., Bull. 11, 272 p.

Ehlers, E.G., 1972, The interpretation of geological phase diagrams: San Francisco, W.H. Freeman and Company, 280 p.

Eskola, P., 1922, On contact phenomena between gneiss and limestone in western Massachusetts: Jour. Geol., v. 30, p. 265-294.

Garrels, R.M., and Christ, C.L., 1965, Solutions, minerals and equilibria: New York, Harper and Row, 450 p.

Gordon, T.M., and Greenwood, H.J., 1970, The reaction: dolomite + quartz + water = talc + calcite + carbon dioxide: Am. Jour. Sci., v. 268, p. 225-242.

Hayslip, D.L., 1973, Geochemistry of the bimodal Quaternary volcanism in the Medicine Lake Highlands, northern California: M.S. thesis, Socorro, New Mexico, N. Mex. Inst. Min. and Tech.

Helgeson, H.C., 1967b, Solution chemistry and metamorphism, in Abelson, P., ed., Researches in geochemistry, v. 2: New York, John Wiley and Sons, p. 362-404.

__________, 1969, Thermodynamics of hydrothermal systems at elevated temperatures and pressures: Am. Jour. Sci., v. 267, p. 729-804.

__________, 1970a, Description and interpretation of phase relations in geochemical processes involving aqueous solutions: Am. Jour. Sci., v. 268, p. 415-438.

Helgeson, H. C., Brown, T.H., Nigrini, A., and Jones, T.A., 1970, Calculations of mass transfer in geochemical processes involving aqueous solutions: Geochim. Cosmochim. Acta, v. 34, p. 569-590.

Helgeson, H.C., Garrels, R.M., and MacKenzie, F.T., 1969, Evaluation of irreversible reactions in geochemical processes involving minerals and aqueous solutions: II. Applications: Geochim. Cosmochim. Acta, v. 33, p. 455-481.

Hidden, W.E., 1893, Two new localities for turquoise: Am. Jour. Sci. (3), v. 46, p. 400-402.

Ito, J., and Arem, J., 1970, Idocrase: Synthesis, phase relations, and crystal chemistry: Am. Mineral., v. 55, p. 880.

Jaramillo, L., 1973, Alteration and mineralization in the Jarilla Mountains, Otero County, New Mexico: M.S. thesis, Socorro, New Mexico, New Mexico Institute of Mining and Technology, 45 p. → see ERRATA

Kelly, V.C., 1949, Geology and economics of New Mexico iron ore deposits: Univ. New Mexico Pub. in Geol. no. 2, p. 181-193.

Korzhinski, D.S., 1959, Physiochemical basis of the analysis of the paragenesis of minerals: New York, Consultants Bureau, 142 p.

Kottlowski, F., 1963, Paleozoic and Mesozoic strata of southwestern and south-central New Mexico: N. Mex. Inst. Min. and Tech., State Bur. Mines and Mineral Resources, Bull. 79, 100 p.

Lasky, S.G., and Wootton, T.P., 1933, The metal resources of New Mexico and their economic features: New Mexico Bur. Mines and Mineral Res., Bull. 7, 178 p.

Lindgren, W., Graten, L.C., and Gordon, C.H., 1910, Ore deposits of New Mexico: U.S. Geol. Survey Prof. Paper 68, p. 184-187.

Livingston, D. E., 1973, A plate tectonic hypothesis for the genesis of porphyry copper deposits of the southern Basin and Range Province: Earth and Planetary Sci. Letters, vol. 20, p. 171-179.

ERRATA

Jaramillo, L., 1973, Alteration and mineralization in the Jarilla Mountains, Otero County, New Mexico: independent study, Socorro, New Mexico, New Mexico Institute of Mining and Technology, Geology Department, 45 p.

Lowell, J.D., and Guilbert, J.M., Lateral and vertical alteration-mineralization zoning in porphyry ore deposits: Econ. Geol. v. 65, p. 373-408.

Metz, P., Puhan, D., and Winkler, H.G.F., 1968, Equilibrium reactions on the formation of talc and tremolite by metamorphism of siliceous dolomite: Naturwissenschaften, Heft 5, p. 225-226.

Metz, P., and Trommsdorf, V., 1968, On phase equilibria in metamorphosed siliceous dolomites: Contr. Min. and Petr., v. 18, p. 305-309.

Pray, L.C., 1959, Stratigraphy and structural features of the Sacramento Mountain escarpment, New Mexico: in Guidebook to the Sacramento Mountains, Permian Basin Section, Soc, Econ. Paleontologists and Mineralogists and Roswell Geological Society, p. 87-130.

Reynolds, C.B., and Craddock, J.C., 1959, Geology of the Jarilla Mountains: in Guidebook to the Sacramento Mountains, Permian Basin Section, Soc. Econ. Paleontologists and Mineralogists and Roswell Geol. Soc., p. 279-283.

Schmidt, P.G., and Craddock, C., 1965, The geology of the Jarilla Mountains, Otero County, New Mexico: N. Mex. Inst. Min. and Tech., State Bur. Mines and Mineral Res., Bull 81.

Schmitt, H.A., 1965, The porphyry copper deposits in their regional setting, in Titley, S.R., and Hicks, C.L., eds., Geology of the porphyry copper deposits, South-western North America: Tucson, The University of Arizona Press, p. 17-33.

Seager, W., 1961, Geology of the Jarilla Mountains, Tularosa Basin, New Mexico: M.S. thesis, Albuquerque, New Mexico, University of New Mexico, 80 p.

Sriramadas, A., 1957, Diagrams for the correlation of unit cell edges and refractive indexes with chemical composition of garnets: Amer. Mineral., v. 42, p. 294-298.

Tilley, C.E., 1925, Contact-metamorphic assemblages in the system $CaO-MgO-Al_2O_3-SiO_2$: Geol. Mag, v. 62, p. 363-367.

__________, 1948, Earlier stages in the metamorphism of siliceous dolomites: Mineralog. Mag., v. 28, p. 272-276.

__________, 1951b, A note on the progressive metamorphism of siliceous limestones and dolomites: Geol. Mag., v. 88, p. 175-178.

Travis, Russell B., 1955, Classification of rocks: Quarterly of the Colorado School of Mines, vol. 50 no. 1.

Turner, F.J., 1967, Thermodynamic appraisal of steps in progressive metamorphism of siliceous dolomitic limestones: Neues Jb. Miner. Mh., v.I, p. 1-22.

__________, 1968, Metamorphic petrology, mineralogical and field aspects: San Francisco, McGraw-Hill Book Company, 403 p.

Umpleby, Joseph B., 1916, The occurrence of ore on the limestone side of garnet zones: University of California Bull. of the Dept. of Geology, v. 10, no. 3, p. 25-37.

Weeks, W.F., 1956, A thermochemical study of equilibrium relations during metamorphism of siliceous carbonate rocks: J. Geol., v. 64, p. 245-270.

Williams, H., Turner, F.J., and Gilbert, C.M., 1954, Petrography, an introduction to the study of rocks in thin sections: San Francisco, W.H. Freeman and Co., 406 p.

Zharikov, V.A., 1970, Skarns (parts II and III): Int. Geol. Rev. v. 12, p. 619-647 and p. 760-775.

This thesis is accepted on behalf of the faculty of the Institute by the following committee:

Richard E. Blane

Date 12 July, 1976